MODELING AND CONTROL STRATEGIES FOR AUTONOMOUS VEHICLES AND TRUCK PLATOONS IN MIXED TRAFFIC SCENARIOS

TOMMY CHAANINE

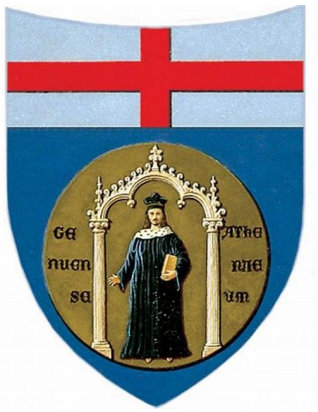

DEPARTMENT OF INFORMATICS, BIOENGINEERING, ROBOTICS AND SYSTEMS ENGINEERING

PH.D. IN **COMPUTER SCIENCE AND SYSTEMS ENGINEERING**
CURRICULUM OF **SYSTEMS ENGINEERING**

UNIVERSITY OF GENOVA

Supervisors:
SILVIA SIRI
CECILIA PASQUALE

XXXVII CYCLE

Abstract

Since the dawn of civilization, people started to move around and transport goods. The more in time we move forward, the more we find bigger cities and therefore bigger economies, and that is thanks to human creativity and inventions, all the way from the wheel to the transportation industry nowadays. Technology advanced and a person's well-being and comfort became more and more important. Unfortunately, the infrastructure and the environment could not keep up with all these advancements; problems could not be foreseen, so that is what led us to the challenges that we face today: pollution and environmental disasters, traffic congestion and accidents, energy resources scarcity and high price, etc. Every day, the challenges posed by economic globalization and climate change become more pressing for institutions and governments to tackle. In this scenario, the role of the transport sector, particularly the road network, is undeniably significant. The increasing demand for both passenger travel and goods transportation has contributed to the ongoing deterioration of quality of life. In addition, both routine and unexpected traffic jams continue to frustrate citizens, eroding public trust in the reliability of transportation systems. Researchers and institutions tried and succeeded in solving, even if partially, some of these problems, at least in some parts of the world: emission reduction in more effective fuel engines, traffic control methods, upgrade of infrastructure, campaigns of information and teaching to the public, etc. Like mentioned before, technology keeps advancing and the world keeps witnessing new inventions, like electric vehicles, autonomous driving and platooning. These advancements not only promise individual comfort but also solutions to the problems. For example, electric cars powered by renewable resources can reduce significantly green house emissions and pollution in cities. Autonomous electric vehicles present a great potential to optimize energy consumption; that's why their trajectories need to be carefully planned taking advantage of their regenerative brakes to get optimized speed profiles. Autonomous vehicles (AVs) in general can improve traffic flow and prevent congestion from forming, of

course apart from the other benefits of more comfort, less travel time, energy efficiency and so on. They have as well the potential to significantly improve traffic flow around signalized intersections by leveraging real-time communication and advanced control systems. Equipped with Vehicle-to-Infrastructure (V2I) technology, AVs can receive traffic light timing information and adjust their speed accordingly to minimize stops and optimize fuel efficiency. This coordination reduces the formation of queues and prevents sudden acceleration or deceleration, leading to smoother traffic flow. This concept along with the vehicles being electric, fall in the domain of eco-driving, a sustainable concept in the automotive sector. The problem is that not all traditional cars can be immediately, or at least fast enough, be replaced by AVs; this creates mixed traffic scenarios that are not studied enough and do not completely provide the promised solution to congestion. Moreover, some challenges arise from the unpredictable behavior of human-driven vehicles (HVs) and the lack of vehicle-to-vehicle (V2V) and V2I communication. Modelling and controlling the interaction between the two types of vehicles is crucial, especially in the absence of real life experiments. Another subject related to mixed traffic is the travel of autonomous truck platoons on freeways. Platooning, especially for trucks, can reduce significantly the air drag for the vehicles traveling within the platoon. Other than fuel efficiency, autonomous truck platooning can improve traffic flow compared to when each truck travels alone; this is thanks to better use of road space, less lane changes, synchronous acceleration and deceleration among the trucks and less sudden braking. All the previous is possible thanks to the autonomous functionality and the V2V communication of the trucks. The ultimate goal is to form as many truck platoons per day as possible, but that presents a big number of difficulties and challenges. Competition among carriers, lack of V2I communication, absence of traffic prediction based trajectory planning, etc. all delay the accomplishment of this ultimate goal. This thesis provides control schemes and control-oriented models that aim to improve the usage of networks and infrastructure, reduce traffic congestion, and ultimately minimize travel times and energy/fuel consumption. To achieve these goals, the research presents a real-time planning framework for platoon coordination decisions based on traffic prediction, enabling autonomous vehicle groups to dynamically adapt to changing road conditions while optimizing efficiency. Additionally, a control-oriented highway traffic model is introduced, incorporating multiple clusters of connected autonomous vehicles

to better capture the interactions between AVs and HVs and enhance traffic management strategies. Furthermore, the thesis addresses the minimization of energy consumption for electric autonomous vehicles by formulating optimal trajectory planning methods that leverage regenerative braking, ensuring sustainable and energy-efficient operations. By integrating these approaches, the proposed methodologies facilitate the safe and efficient coexistence of AVs and HVs while promoting sustainability in modern transportation systems.

Acknowledgements

First and foremost, I would like to express my deepest gratitude to my family for their unconditional love, support, and encouragement throughout this journey. Their belief in me has been my greatest source of strength and motivation.

I extend my deepest appreciation to my supervisors for their invaluable guidance, patience, and continuous support. Their expertise and advice have been instrumental in shaping my research, and I am incredibly fortunate to have had the opportunity to learn from them.

I am also sincerely grateful to my friends and colleagues, who have stood by my side, offering both companionship, insightful discussions and much-needed moments of laughter during this challenging yet rewarding process.

I am also thankful to the professors and faculty members at the University of Genova, whose knowledge and mentorship have played a crucial role in my academic development. Their dedication to teaching and research has been truly inspiring.

Additionally, I am profoundly grateful to the professors at the Technical University of Crete for warmly welcoming me during my period abroad. Their hospitality, support, and the enriching academic environment they provided made my experience there both meaningful and memorable.

Finally, I would like to thank everyone who, in one way or another, has contributed to this work. This thesis is not only the result of my efforts but also of the encouragement, guidance, and support I have received from many along the way.

Borsa di dottorato cofinanziata con risorse del Programma Operativo Nazionale Ricerca e Innovazione 2014-2020 (CCI 2014IT16M2OP005), risorse Fondo Sociale Europeo REACT-EU, Azione I.1 “Dottorati Innovativi con caratterizzazione industriale”, Azione IV.4 “Dottorati e contratti di ricerca su tematiche dell’innovazione” e Azione IV.5 “Dottorati su tematiche Green”

Contents

List of Figures

List of Abbreviations

ACC	Adaptive Cruise Control
AI	Artificial Intelligence
AIMSUN	Advanced Interactive Microscopic Simulator for Urban and Non-Urban Networks
ARZ	Aw-Rascle-Zhang
AV	Autonomous Vehicle
CACC	Cooperative Adaptive Cruise Control
CAV	Connected Autonomous Vehicle
CTM	Cell Transmission Model
DP	Dynamic Programming
EV	Electric Vehicle
FDA	Feasible Direction Algorithm
GHG	Green House Gases
GLOSA	Green Light Optimal Speed Advisory
GPS	Global Positioning System
HV	Human-driven Vehicle
ICE	Internal Combustion Engine
IMU	Inertial Measurements Unit
LWR	Lighthill-Whitham-Richards
METANET	Modèle d'Ecoulement du Traffic Autoroutièr NETwork
NLP	Non-Linear Programming
PMP	Pontryagin's Maximum Principle

SUMO	Simulation of Urban MObility
TTS	Total Time Spent
V2V	Vehicle-to-Vehicle
V2I	Vehicle-to-Infrastructure
VISSIM	Verkehr In Städten - SIMulationsmodell

Chapter 1

INTRODUCTION

1.1 Paths of Progress: Advances in Traffic and Transportation

The idea of doing trades and transporting materials, products and people started since ancient civilizations. In fact, it is what made it possible for these civilizations to grow and become stronger in all aspects. Paved roads go back all the way to the Roman empire which laid the foundation for modern road networks. Since then, the idea of transportation evolved from just doing trades, wars and politics into an essential part of almost every individual's life. Globalization made that crucial as the world became virtually one village, connecting people from all corners of the Earth. Economies became more interconnected and international trade was expanded; trade agreements and economic liberalization made it easier for raw materials, goods and people to cross borders between countries. That made the building of mega cities possible, which allowed for these cities on the other hand to demand more and more. Moreover, the right of every person to access their work, educational and health institutions or travel either inside their country or to another one for any other reason, and their right to do so comfortably, increased incredibly the demand on transportation modes and networks. Competitiveness between technological and automotive industries skyrocketed, increasing pressure to always provide the best and most comfortable solutions for customers. As the quality of life improved, the number of people on Earth increased leading to more demand on cars, international trade, services and goods delivery; that kept putting pressure on industries to innovate and find better solutions.

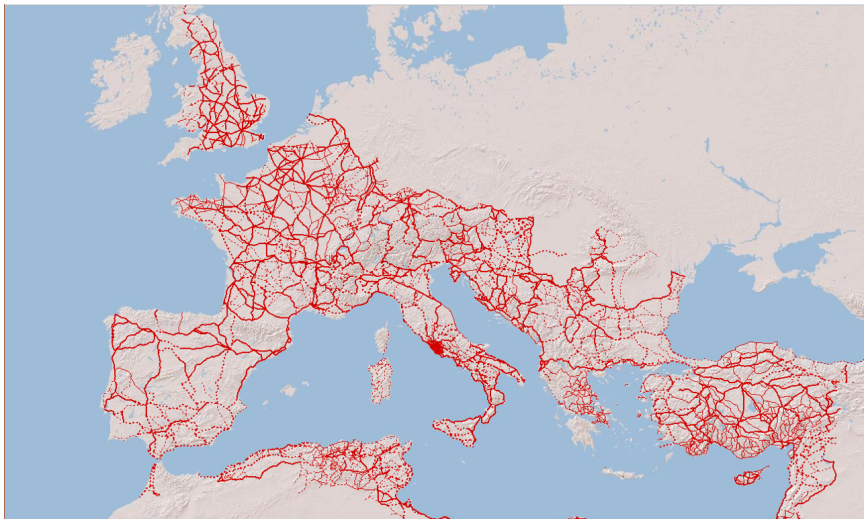

FIGURE 1.1: "All roads lead to Rome" - Map showing the complex road network of the Roman empire *(Source:* ***Newsbeezer - BBC News****)*

1.2 Confronting the Costs and Challenges of Mobility and Transportation

Unfortunately, everything has limits and in this case they were reached: the huge, and still increasing, number of cars and trucks surpassed what the infrastructure could handle. That led to a complex problem called congestion and it is very common nowadays in many urban areas, where road networks struggle to handle the big number of vehicles, especially in peak hours. The imbalance between road capacity and traffic demand affects millions of people and reduces the quality of life that was promised, causing reduced speeds (sometimes no movement at all), higher travel times, more toxic gas emission resulting in more polluted air in small areas, noise pollution, etc. Other than the previously mentioned cause, congestion can be triggered by one or a combination of the following:

- Lack and poor coordination of traffic signals: traffic lights can be badly synchronized, leading to cars stopping more often and for longer times, especially for higher demand directions and lanes. The absence of these lights cause human driven cars to act in a way that might lead to accidents, slower speeds and higher stopping times. Moreover, lack of traffic signs or their misplacement lead to less coordination and control of traffic.
- Poor design of road networks: number of lanes, off-ramps, on-ramps,

intersections and roundabouts are all very essential for a smooth traffic flow. Designing them badly and not taking into consideration all conditions and situations lead to both recurrent and non-recurrent congestion.

- Accidents and incidents: when an accident happens, one or more lanes are blocked, depending on the severity of the accident and the debris resulting from it. Consequently, traffic flow is interrupted on the accident lanes and probably reduced in all other lanes in both directions as drivers might slow down to watch the accident or the rescue mission.
- Bad weather conditions: road pavements become more slippery in rain and snow conditions, and vision is reduced greatly in fogs, that is why drivers become more cautious during bad weather. They start to reduce their speed, leave a bigger space gap from the vehicle in front of them and change lanes less frequently. In addition to that predicted behavior, accidents occur more often in those conditions, leading to congestion that is unexpected and difficult to resolve in that weather.
- Human driving behavior: driving and changing lanes aggressively or hesitantly can cause disruptions in traffic flow, reducing the overall efficiency.
- Lack of public transport: if there are not enough vehicles or modes of public transport in a city or region, people tend to use more their private cars, causing the demand on the network to increase, especially in peak hours. Besides the size of the fleets, lack of trust in the public transport can cause the same effect.
- Road works and special events: these are temporary events that reduce the capacity of the road and cause non-recurrent congestion.

The increase in the use of all modes of road transport not only caused more congestion but also more pollution. Figure 1.2 shows that the transportation sector is accountable for almost 17% of the global GHG emission. The scariest effect on the environment is global warming that is caused by greenhouse gases, mainly carbon dioxide CO_2, nitrous oxide N_2O and hydro fluorocarbons $HFCs$. These gases trap heat coming from the sun within the atmosphere, causing the global temperature average to rise, climate to change and a lot of catastrophic environmental events to happen. Moreover, high

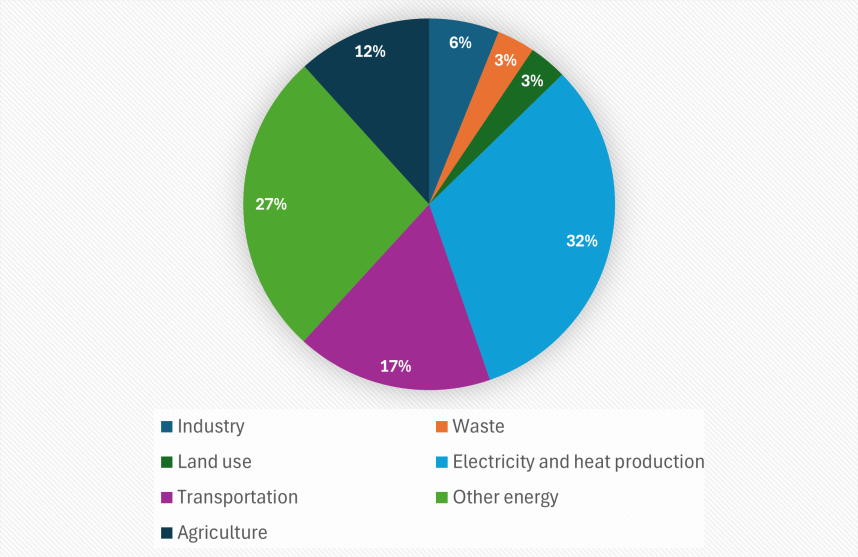

FIGURE 1.2: Global *GHG* emissions in 2021 by sector *(Source: **World Resources Institute**)*

concentration of these gases in urban areas cause a localized greenhouse effect, turning the city or an area of it into a heat bubble, leading to an increased use of energy for climate conditioning.

Pollution has been worrying the world for decades, and despite all the technological advancements to make combustion engines more fuel efficient and less polluting, road transport stays on top of the transport sectors in terms of toxic gases emission, especially CO_2 as shown in Figure 1.3, with 74% of the global emission. These pollutants contribute to the degradation of the air quality and the health of humans; respiratory and cardiovascular diseases and increased premature death rates and cancer risk (heart and lungs) are direct consequences of their high concentration in the air, especially in urban areas. Humans are not the only ones affected by this pollution as it has a huge environmental impact. Biodiversity is suffering immensely, not only directly but also indirectly through acid rains that cause damage to the soil and water bodies.

Other than environmental and health consequences, traffic congestion and pollution from road transport have significant economic impacts. In 2021, traffic congestion alone costs the U.S. trucking industry around 94.6 billion, due to lost productivity and additional fuel expenses. This includes over 1.27 billion hours of delays and the waste of 6.7 billion gallons of fuel, contributing to higher operational costs for the sector [8]. For the general economy, congestion cost the U.S. nearly 87 billion in 2018, with major cities like

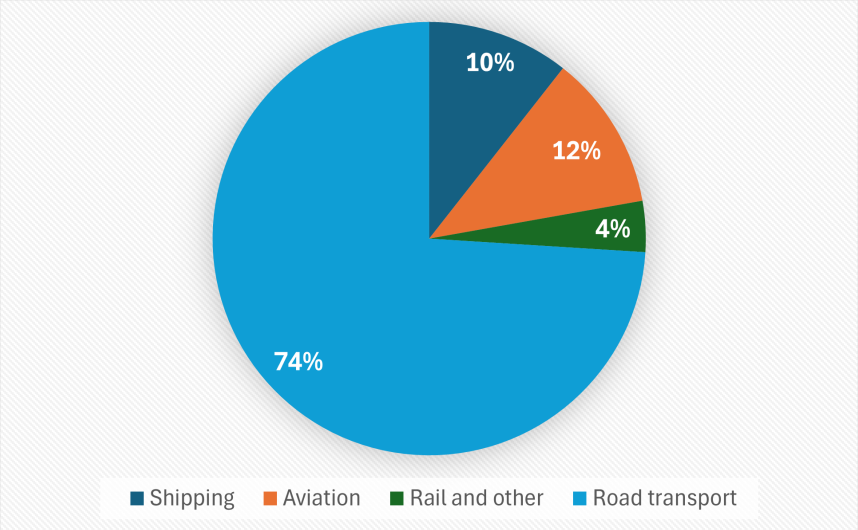

FIGURE 1.3: Global CO_2 emissions by transport mode in 2018 *(Source: **Our World in Data**)*

Boston, Chicago, and Washington, D.C., facing the highest economic losses due to time wasted in traffic [70][144]. Air pollution further compounds these losses. Globally, around 1.2 billion workdays are lost annually due to pollution-related illnesses, which could reach 3.8 billion by 2060. This affects productivity, healthcare costs, and the environment, with the economic costs of pollution-related ecosystem damage exceeding 5 trillion per year [98]. Together, the combined effects of congestion and pollution present a major economic burden on society, highlighting the need for sustainable solutions in transport and urban planning.
The main goal of this thesis is to suggest methods and control schemes to reduce congestion and increase energy/fuel efficiency. Despite not addressing pollution directly, these models and schemes contribute indirectly to a reduction in pollutants emission, by reducing travel times and high accelerations/decelerations.

1.3 Navigating a Greener Future: Sustainable Transport Innovations

To help reduce all the problems mentioned, sustainability emerged as part of the plan. It aims to reduce the negative effects of transportation systems on humans and the environment, while making sure they remain efficient, accessible and affordable to everyone. The problem to fix is a complex one

because it depends on the availability of resources, the advancements of technology and infrastructure, and the mindset of people. That being said, sustainability can be divided into three main aspects: technological, managerial and informative.

1.3.1 Technological aspects

A logical approach to reduce the high emissions of road transport is to improve the technology that powers the vehicles. Improving the engine's efficiency seems to be a good idea until it is not enough, that's why more modern solutions as the electrification of cars and their automation emerged:

Improvements to the conventional engines
With road transport contributing significantly to resources depletion and pollution, the need for technological advancements had to be part of the pavement of the sustainable path. It started with the improvement of the already very popular type of vehicles, the ICE vehicles. Fuel efficiency and reduction of toxic gas emission are the main goals and it is achieved through different ways: better vehicle aerodynamics, lighter body materials, more efficient and advanced engine components and systems, turbocharging, variable valve timing, etc. The next step was the introduction of the hybrid engine, a combination of an ICE and an electric motor, allowing for reduction of fuel consumption and the use of advantages offered from both engines: the clean and calm functioning of the electric motor and the torque provided from the ICE when needed on slopes and high accelerations.
Other improvements include the introduction of bio-fuels, like ethanol and bio-diesel, which are blended with the commonly used fossil fuels. These additives are produced from renewable biological sources (crops, waste, etc.) and help reduce GHG emissions. A zero-emission alternative to conventional fuels is hydrogen fuel cells that emit only water vapor, but this solution is challenging, especially for producing and storing hydrogen.

Electrification of vehicles
Recent years showed a transformative shift from ICE vehicles to ones with electric powertrain, relying fully on electricity. The goal is to lower pollution and greenhouse gas emissions and to improve air quality, especially in cities, as fully EVs do not emit tailpipe gases. These vehicles are powered only

by large battery packs which are charged by external electric sources. When these sources are renewable, EVs have a very low carbon footprint but there are still some challenges that face this transformation; high costs, difficulties in investments and building charging infrastructure that can satisfy the demand are delaying the increase in number of electric vehicles in the markets. The life cycle emissions of EVs in the United States are now approximately 60% lower than ICE vehicles; this translates to nearly 50 tons of CO2 equivalent saved over the vehicle's lifespan [2][37].

Autonomous driving

Self-driving technology, or autonomous driving in other words, is the next level of driving that allows the vehicles to drive from point A to point B without the need for human intervention, including navigation, operation and any necessary action required to arrive on time, while of course respecting the rules, safety and comfort of the passengers. This technology was and still is a hot topic during this last decade, but the concept dates back to about a century ago. Nowadays, it has come a long way, allowing for real-world applications, with some AVs on few markets. Autonomous driving is categorized into different levels, organized by the Society of Automotive Engineers (SAE) [126], from Level 0 (no automation) to Level 5 (full automation with absolutely no need for any human intervention) and the self-driving vehicles currently on the market are either of Levels 2 or 3, meaning partial automation. AVs use a combination of different technologies in order to percept, interpret and navigate:

- Perception: through sensors like Lidar, cameras, radar and ultrasonic sensors.
- Mapping and localization: through high detailed maps, GPS and Inertial Measurements Units (IMUs).
- Path planning: either short term (for example lane change, acceleration, deceleration) or long term (for example optimal routing, traffic prediction).
- Vehicle-to-vehicle (V2V) or Vehicle-to-infrastructure (V2I) communication: which enables AVs to prevent potential accidents and gather real-time information that can help with finding the optimal route.

Platooning
Thanks to vehicle automation and V2V communication, the formation of group of connected autonomous vehicles (CAV) that travel with a short inter-vehicular distance on highways is possible. These vehicles are able to coordinate their speed and acceleration with little to no human intervention. Platooning, especially for trucks, presents several benefits like fuel/energy consumption reduction, increased road capacity and more safety thanks to very short reaction times.

1.3.2 Managerial aspects

In order to ensure that technological solutions are effective as much as possible, some changes are done on the managerial level, providing policy changes, infrastructure improvements and other:

Public transport
Buses, trams, trains, metros, etc., transport a great number of people, reducing the number of private vehicles on the road, which helps to minimize congestion and pollution, especially if they are powered by electricity. Increasing their numbers, making them affordable and ensuring they stay in good conditions encourage people to use them more often, ensuring their efficient usage.

Shared mobility
Car-sharing and bike-sharing, like Uber and Lyft, can reduce congestion and emissions by reducing private vehicles on the roads.

Micro mobility
Scooters and bikes, electric or conventional, stationed all around the city can provide a sustainable alternative for citizens who have short trips.

Intelligent transportation systems (ITS)
These are smart traffic management systems, technologies and applications with the aim of managing traffic flow, reducing congestion and optimizing travel routes. By integrating real-time information processing, ITS promote an optimized road network and an efficient and sustainable transportation. They include, but not limited to: dynamic traffic signal control, ramp metering, incident detection and management, eco-driving assistance, etc.

Stricter emission regulations and fuel economy standards
Governments worldwide are enforcing stringent emission standards (e.g., Euro 6, CAFE standards) to reduce NOx, PM, and CO2 emissions from vehicles. These standards push automakers to innovate and develop cleaner engines.

Zero-Emission Zones (ZEZs)
Some cities have implemented ZEZs, where only electric or very low-emission vehicles are allowed. These zones help reduce air pollution in densely populated areas.

1.3.3 Informative aspects

This part of the sustainability plan focuses on the individual level, raising awareness and ensuring that people understand the gravity of the situation and the need to improve our behavior in order to make sure the world remains in good conditions for future generations:

Eco-driving
As the behavior of drivers impacts the energy/fuel efficiency of their vehicles, teaching them eco-driving techniques, such as smooth acceleration, proper tire inflation, and minimizing idling, can reduce fuel consumption and emissions.

Increased Awareness
Public awareness campaigns about the environmental impact of vehicle use and the benefits of a modal shift to more sustainable transport options (e.g., carpooling, public transport, EVs, cycling, etc.) can encourage more environmentally friendly transportation choices.

1.4 Objectives and structure of the thesis

In this section, an elaboration of the objectives and chapters of the thesis is presented. The focus of this work in general is on autonomous vehicles in traffic: defining control schemes and control-oriented models to reduce congestion, improve energy efficiency and reduce travel times. More specifically, Chapter 2 presents traffic modeling theory and its different categories, based

on the point of view of the traffic and the predicted output. It provides detailed formulation of two well known macroscopic models, METANET and CTM; the latter is the base of the work presented in the same chapter, while the former is used to predict traffic speeds in Chapter 3. Chapter 2 discusses HVs and CAVs coexistence, modeling of mixed traffic flow and vehicle-based control. The last section presents a contribution of this thesis that is a control-oriented highway traffic CTM with clusters of CAVs along with case studies and simulation results. This contribution is based on the work published and presented in the 26th IEEE International Conference on Intelligent Transportation Systems that was held in September 2023 in Bilbao, Spain.

Chapter 3 focuses on platooning, specifically for trucks. Truck platoon trips, from initial phases of planning until arrival to destination, will be addressed with the emphasis on the effect of traffic conditions. The contribution to the thesis in this chapter is real-time planning of platoons coordination decisions based on traffic prediction. These decisions include the merge and split of platoons, while taking into consideration improving the travel of truck platoons in freeways with the goal of arriving on time to their destinations. METANET is used to predict traffic conditions for the mentioned work and case studies and simulation results are presented, showing the effectiveness of the proposed scheme. This contribution is based on the work published and presented in the 22nd of the EUCA Series of European Control Conferences, which was held in June 2024 in Stockhol, Sweden.

Finally, Chapter 4 addresses eco-driving techniques and algorithms applied to vehicles. The work of the thesis related to this part focuses on trips from an initial state of position and speed to a final one for electric autonomous vehicles that are equipped with regenerative breaking. Its speed is controlled to ensure a smooth and energy-efficient trip, without brut acceleration or deceleration. An extension of this work takes into consideration a traffic signal with fixed switching time on the way of the vehicle; this application is called GLOSA and allows the EV to cross the signal with minimal to no waiting time, making sure that energy efficiency and smooth speed profiles are achieved. The contribution in this chapter was submitted to a scientific journal and is still under review.

Chapter 2

Traffic modeling

2.1 Introduction

As discussed in Chapter 1, population growth and rapid urbanization, along with the improvement of the individual well-being, increased the number of vehicles and the complexity of traffic systems. Simple solutions were enough and helped reduce congestion until they could not anymore; in the early 20th century, improving traffic flow was done by simple observations and rules-of-thumb which increased the efficiency of the overall network. Unfortunately, by the middle of the 20th century, they weren't enough. Inspired by fluid dynamics, mathematical modeling introduced itself as the new age solution: vehicles flow was compared to fluid flow and the first models were revealed. This revolutionized how traffic is observed and predicted and allowed for planning of future infrastructure and policy projects. Models even allowed testing the introduction of new traffic systems and control strategies. This was all thanks to mathematical equations and relations that described real traffic systems and allowed traffic flow theory to flourish in the last century. Autonomous vehicles, truck platoons and mixed traffic are few examples of modern introductions and modifications to traditional traffic, and models are always updated to take into consideration these changes.
This chapter is organized as follows: Section 2.2 gives an overview of approaches for HVs traffic flow modeling and its importance, Section 2.3 gives a detailed description of the well known METANET that will be used in the thesis work of Chapter 3, and Section 2.4 introduces the CTM model in details. Section 2.5 presents the state of the art in modeling of mixed traffic of CAVs and HVs while Section 2.6 introduces the contribution to the state of the art that is a control-oriented version of the CTM for mixed traffic and

is based on the work published in the 2023 IEEE 26th International Conference on Intelligent Transportation Systems (ITSC), held in Bilbao, Spain [31]. The aim of this work is to model the presence of multiple clusters of CAVs that, if properly controlled, can positively influence traffic behavior by acting as actuators of specific control strategies. The cells of a highway stretch are divided into two categories: cells with no clusters of CAVs and cells with a cluster of CAVs. For the first type of cells, the model is the same as the classical CTM. For the second type, we model the presence of a cluster as a moving bottleneck that divides the cell into different parts corresponding to the part of the cell in front of the cluster (downstream cell), and the part of the cell behind the cluster (upstream cell). The proposed control-oriented traffic model has been tested on a case study based on real traffic data, showing the effectiveness of grouping the CAVs in clusters to improve the traffic flow.

2.2 Traffic flow modeling

As road networks kept growing and became more and more complex, scientists made sure that models kept up as they are very important and crucial for modern world mobility:

Congestion simulation and prediction
With input traffic data, models are able to predict potential congestion points in the network. This allows traffic monitoring centers to identify bottlenecks and causes for congestion before they occur. The models can also help identify appropriate solutions like re-routing of vehicles, ramp metering, visual warnings and speed recommendations, variable maximum speed, etc., and this helps improve the overall efficiency of the network.

Environmental impact
Thanks to helping in congestion reduction, traffic models already assist to the reduction of toxic gases emission. But their contribution does not end here as some models also estimate emission from vehicles, which gives a more accurate number to deal with.

Infrastructure planning
Traffic models provide an understanding of traffic patterns and identification of high risk and high congestion areas, which allows officials to make better policies and push for the improvement of infrastructure. Models also allow

the prediction of future demands, helping planners to design appropriate future infrastructure and public transportation projects serving the growth in population and mobility needs.

Multi-modal/multi-class traffic modeling
In order to represent the interaction between different classes of vehicles (cars, buses, trucks, motorcycles, etc.), models are expanded to become multi-class, allowing a more detailed study of traffic flows. Moreover, as part of sustainability, multi-modal models incorporate pedestrians, bicycles, public transport and others into traditional traffic. This helps better planning of sustainable areas and cities.

Mixed traffic modeling
Mixed traffic implies to the integration of AVs in traffic, and traffic models are needed more than ever to study their impact on flow, safety and overall efficiency. As real world experiments and scenarios are very limited, interactions between HVs and AVs need to be simulated, allowing for control strategies and infrastructure plans to be tested and studied. The limited numbers of AVs can play a crucial role in controlling traffic as part of the vehicle-based traffic control; AVs have the possibility to force a speed reduction or a lane change of the traffic behind them which helps reducing congestion downstream. One goal of this thesis is to propose a mixed traffic model that represents AVs as clusters and allows for traffic control strategies.

Traffic modeling has evolved into a vital tool that supports the sustainability of urban development, the protection of the environment and the efficiency and safety of road networks. When it started in the 1950s, it was mainly macroscopic that represented mathematically the vehicles flow as a flow of fluids. Then in the late 20th century, advances in computing power allowed more complex models to exist, that work from a microscopic point of view and simulate individual vehicle behavior, or work with a mesoscopic perspective, combining macroscopic and microscopic characteristics.

2.2.1 Macroscopic traffic modeling

As the name suggests, this type of modeling is best suited for large-scale analysis and traffic flow management. It is useful to model congestion and evaluate impacts on emissions, mainly in highways and arterial roads, where the

individual behavior of vehicles is less relevant compared to their collective behavior. Macroscopic models consider traffic flow as a continuous fluid-like entity, analyzing its aggregated properties for a position x and time t such as density ($\rho(x,t)$ described as the number of vehicles per unit of length [veh/km]), flow rate ($q(x,t)$ defined as number of vehicles passing through a location in a specific time instant [veh/h]) and average speed ($v(x,t)$ expressed in [km/h]). The conservation of mass, one of the fundamental principles of conservation, presents the continuity equation in traffic flow theory: the number of vehicles must be conserved over time. In fact, a small segment of the road is considered as a closed system and the number of vehicles entering, leaving and remaining withing this segment over a period of time must be balanced; in other words, the vehicle density in this segment increases or decreases during a time period depending on how many vehicles enter and leave. This conclusion is based on that the traffic flows in one direction, there is no dispersion of vehicles and the road segment has no entrances or exits, like shown in Figure 2.1.

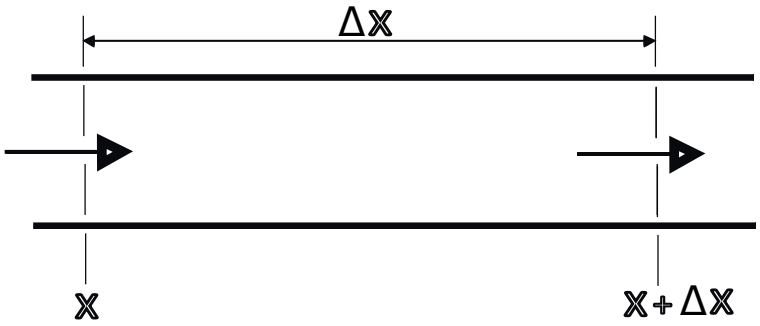

FIGURE 2.1: Road segment of length Δx

Assuming that the density is uniform and continuous on the whole segment, the number of vehicles in a small segment of the road Δx is given by:

$$N(x,t) = \rho(x,t)\Delta x. \tag{2.1}$$

As the number of the vehicles is conserved, its rate of change is equal to:

$$\frac{\partial N(x,t)}{\partial t} = \frac{\partial}{\partial t}\left(\rho(x,t)\Delta x\right) = \Delta x \frac{\partial \rho(x,t)}{\partial t}. \tag{2.2}$$

As $q(x,t)$ is the flow entering the road segment at x at time t, $q(x+\Delta x,t)$ is the flow exiting it at $x+\Delta x$ at time t, and the net flow is approximately:

$$q(x+\Delta x,t) - q(x,t) \approx \frac{\partial q(x,t)}{\partial x}\Delta x. \tag{2.3}$$

By conservation of the number vehicles in the segment Δx:

$$\Delta x \frac{\partial \rho(x,t)}{\partial t} = -\frac{\partial q(x,t)}{\partial x} \Delta x. \tag{2.4}$$

Dividing by Δx and simplifying gives the continuity equation:

$$\frac{\partial \rho(x,t)}{\partial t} + \frac{\partial q(x,t)}{\partial x} = 0. \tag{2.5}$$

As the flow is assumed to be dependent on speed and density:

$$q(x,t) = \rho(x,t) \cdot v(x,t), \tag{2.6}$$

the continuity equation is written as follows:

$$\frac{\partial \rho(x,t)}{\partial t} + \frac{\partial \rho(x,t) v(x,t)}{\partial x} = 0. \tag{2.7}$$

This formulation is the focus of mainly some of the most known macroscopic models, like the LWR model which was proposed by M.J. Lighthill and G.B. Whitham in 1955 [88] and independently by P.I. Richards in 1956 [122] and introduces the fundamental diagram of traffic flow, linking density to traffic flow. This model is classified as a first-order model because it considers that the traffic speed depends only on the density:

$$v(x,t) = V(\rho(x,t)) = v^{free}\left(1 - \frac{\rho(x,t)}{\rho^{max}}\right). \tag{2.8}$$

As shown in Equation (2.8), traffic speed decreases as density increases and vice-versa, based on empirical observations as vehicles can travel at free-flow speed when densities are low and their speed tends to zero at high densities, like for example in traffic jams. The problem with this relation is that it assumes that the speed at location x depends only on the density in this position and not also the density downstream and that each value of density corresponds to a specific speed. Another non realistic assumption is that drivers do not have a reaction time, which breaks the limits for accelerations and decelerations, taking unrealistic values.

Then in 1971, H.J. Payne develops an extension of Whitham's model [113] by adding a second differential equation (shown in Equation (2.9)) that captures the dynamics of the speed of vehicles; this marked the introduction of

second-order models:

$$\frac{\partial v(x,t)}{\partial t} + v(x,t)\frac{\partial v(x,t)}{\partial x} = \frac{1}{\tau}\left(V((x,t)) - v(x,t)\right) - \frac{1}{\rho(x,t)}\frac{\partial p(x,t)}{\partial x}, \quad (2.9)$$

where τ is a relaxation time parameter reflecting the reaction time of drivers (smaller τ means less reaction time) and $p(x,t)$ represents traffic pressure reflecting interactions between vehicles. The particular terms of this speed dynamics equation are:

- $v(x,t)\frac{\partial v(x,t)}{\partial x}$: a convective term that shows spatial rate change of the speed and models how the speed of a vehicle is influenced by the traffic speed approaching a certain position x.
- $\frac{1}{\tau}\left(V((x,t)) - v(x,t)\right)$: a relaxation term that represents the will of drivers to adjust their speed towards the equilibrium speed $V(x,t)$, based on the current density.
- $\frac{\partial p(x,t)}{\partial x}$: a pressure gradient term that shows the influence of traffic pressure on the speed of the vehicles. It accounts for driver reactions to the density of nearby vehicles as he will accelerate if he notices a decreasing density downstream and vice-versa.

Thanks to these new terms in the speed equation, a more accurate representation of traffic dynamics was established. Further improvements were made in the METANET model [95], that will be detailed in one of the following sections. Another improvement to the Payne-Whitham model is the ARZ model, which has a new velocity equation. This work came as the results of Cassidy and Windover [30] and Daganzo [38] showing that disturbances in PW model travel faster than traffic velocity and as a result, a vehicle on the freeway is influenced from both behind and front, indicating that traffic flow is isotropic. Zhang [156] however explained that traffic flow is anisotropic because drivers are mostly influenced by the traffic in front of them. To fix this, Aw and Rascle [11] and Zhang [157] separately introduced the traffic momentum concept which consists of a desired speed that drivers aim to maintain and contains itself a traffic pressure component, which is a more flexible and realistic approach to capture stop-and-go phenomena and sharper transitions in congested traffic while avoiding negative speeds. Going back to first-order models, the Cell Transmission Model (CTM) [39] is a discretized model but its continuous form resembles the one of the LWR. In the CTM, the flow depends on the density and is bounded by the road capacity. It will also be shown in details later on in this chapter. These macroscopic models

are foundational in traffic modeling and are suitable for large networks and control strategies thanks to their low computational effort.

2.2.2 Microscopic traffic modeling

Instead of describing traffic flow from a high point of view with dynamics of traffic as a whole (density and flow) like in macroscopic models, microscopic ones represent each vehicle and its characteristics are calculated and studied, such as position, speed and acceleration, to track its precise trajectory over time. This detailed modeling also represents the drivers behaviors, such as reaction time and preferred speed, and the interactions between them at a very fine level. Microscopic modeling is used widely in traffic simulators like PARAMICS [28], VISSIM [48], AIMSUN [13] and SUMO [80] (Figure 2.2) to represent complex scenarios on highways and urban roads.

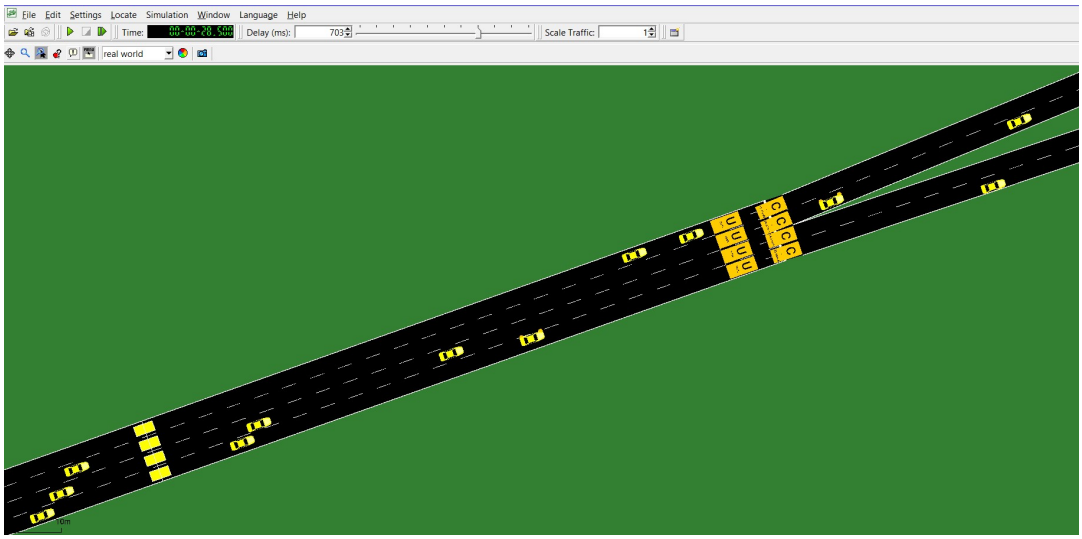

FIGURE 2.2: A microscopic simulation of a highway using the tool SUMO [139]

Car-following

This component describes the longitudinal movement of the vehicles, either forwards or backwards, showing that a driver accelerates/decelerates to adjust their speed in response to the speed of the vehicle directly ahead and the distance between them. Car-following models evolved throughout the years from just ways to understand the dynamics of individual vehicles and their interaction with others to crucial parts of traffic simulation and autonomous vehicles development. Their theory dates back to the 1950s, specifically in [115], [121] and [34] and in that last work specifically, Chandler, Herman,

and Montroll introduced the concept the acceleration of a vehicle depending on the speed difference (or "stimulus") between itself and the preceding vehicle. Some of the most notable models in car-following are:

- **The Gazis-Herman-Rothery model (General Motors Model)**: the GHR model [55] described a driver's acceleration as dependent on both their current speed and the speed difference between their vehicle and the vehicle in front.
- **Gipps' model**: Gipps introduced the safe braking distance from the vehicle in front [57], assuming that every driver adjusts their speed, according to their reaction time and maximum braking capability, in order to avoid colliding with the vehicle in front of them.
- **Helly's model**: Helly calculated the acceleration of the vehicle based on the speed difference with the vehicle ahead and the distance between them, while considering a desired minimum spacing [62].
- **The intelligent driver model**: Treiber, Hennecke, and Helbing developed the IDM in [140] to reproduce realistic traffic phenomena, like and stop-and-go waves. It represents the acceleration as depending on a desired speed, a safe time headway, a maximum acceleration, a comfortable deceleration and a minimum spacing. Thanks to its suitability for capturing realistic congested traffic, the IDM is used as a standard in autonomous vehicles studies.
- **Newell's car-following model**: this model [102] is a simplified version of the other models that calculates the position of each vehicle with the assumption that the driver maintains a constant time and distance lag behind the vehicle in front.

A more detailed history of car-following models is shown in [24] and [54]. With the increase in number of AVs, car-following models present a powerful tool to represent mixed traffic, addressing heterogeneous driver behaviors and complex traffic management systems. In fact, adaptive ones represent how AVs can interact with HVs to optimize traffic flow and safety, taking into consideration driver profiles, real data and V2V communication.

Lane changing

This component of microscopic modeling describes the lateral movement of vehicles as a decision to change lanes and a gap acceptance, which is the willingness of a driver to merge into a gap in the adjacent lane. This behavior is

very important to model as it impacts safety and congestion, and representing it is one of the most difficult problems to solve. The earliest lane-changing models appeared in the 1960s and 1970s, and were qualitative representing basic principles and rules of when and why to change lanes. The most notable work back then is the Gipp's model [58] that established simple rules for decision-making, like determining if the other lane has a large enough gap to move to while taking into account the motivation of the driver (moving into a faster lane, etc.) and opened the door for later models to be created. Models proposed in the late 1980s and 1990s were decision-based and they involved evaluating a certain criteria before making a lane change like in [3]. Later models studied the lane changing process more in details and categorized it into three levels:

- **Strategic level**: this level consists of high level choices like routing of vehicles to arrive to their destinations.
- **Tactical level**: this level focuses on short term goals and the decision to change lane is influenced by the surroundings of the driver, like in a congestion or approaching the desired exit from a highway.
- **Operational level**: lane changing in this level is influenced by avoiding collisions and failure to maintain safe distance from the vehicle ahead, taking into account speed and headway.

Examples of works presenting these models are [78], [142] and [127].

Cellular Automata Models

They are grid-based mathematical models that use simple rules to represent complex systems, like traffic flow modeling where they combine both the longitudinal and lateral movement concept of the vehicles. The road is divided into discrete cells, with a length enough for contain one vehicle, or to stay empty. Vehicles move from one cell to another based on pre-defined rules, which makes these models simple and suitable for simulating large traffic systems. Time is discretized into steps and vehicle positions are updated at each step. The first concept in traffic flow was proposed in 1992 as the Nagel-Schreckenberg model for freeway simulation [100] which established the basic rules and structure that are still used today. Vehicle speed is updated based on the cell ahead: the vehicle increases its speed by one cell per time step up to a maximum speed as long as there is space ahead, and decreases it if another vehicle is detected to avoid collision that will be caused by the current speed. Lane changing occurs based on the occupancy

and speed of adjacent cells, and of course rules that deem it beneficial or necessary. Cellular automata (CA) models have a high computational efficiency, are able to model complex phenomena and are presented in several works and studies like [52, 36, 76, 20]. CA modeling represents as well the base for agent-based models where each vehicle is treated as an agent with decision-making capabilities, opening the way for simplified AVs simulation in mixed traffic, in which they use behavior-based and real-time data for decisions [141, 16].

2.2.3 Mesoscopic traffic modeling

Combining detail and computational efficiency, mesoscopic models are a middle ground between microscopic and macroscopic models. They represent traffic by modeling aggregate and individual characteristics: they track for example density and average speed, while representing all or some vehicles as clusters or platoons. This allows them to capture detailed vehicle interactions while simplifying some individual vehicle dynamics, which makes them suitable for large-scale simulations with moderated computational effort. One of the approaches that made this idea possible is comparing the behavior of gases to that traffic thanks to many similarities like density and flow rates, stop-and-go waves compared to shock waves, pressure-like effects and others. Different modeling approaches are shown in [68]. Among the latest works, we can find the one in [67] where a multi-lane and multi-class framework inspired by gas kinetics is designed. Away from the behavior of gases, some researchers proposed other types of methodologies. For example, using head-way distribution for traffic modeling is considered essential for capturing interactions between vehicles while estimating flow characteristics and traffic density. Using different probability distributions, different models were proposed, like in [101] and [145]. Another methodology is clustering models, where groups of vehicles are represented as single entities that move and interact on the road. Vehicles can be grouped based on distance/speed [68] and different clusters can interact with each other, like merging or splitting [59]. Both head-way distribution and clustering techniques are used for representing AVs in mixed traffic, as will be shown later in Section 2.5. Other than lacking the fine detail of individual vehicle behavior, limitations of mesoscopic models consist of non-suitability for real-time applications as they have a large number of variables.

2.3 METANET Model

2.3.1 Introduction

Modèle d'Ecoulement du Traffic Autoroutier NETwork, or METANET for short, was first introduced by Albert Messmer and Markos Papageorgiou in 1990 [95]. It builds on the principles of the macroscopic point of view of traffic modeling, notably the Lighthill-Whitham-Richards (LWR) model, but extends it to a system of ordinary differential equations that can handle multi-segment networks and represent them through an acyclic graph made of freeway stretches with uniform characteristics, freeway ramps and branching. The equations also incorporate detailed traffic dynamics, like flow, speed and density, that can be modeled continuously over space and time. METANET also incorporates a speed adaptation to model how vehicles adjust their speed based on density in their segment and downstream, inflows from ramps and closing of some lanes. Freeway traffic networks are its primary application [79] and it helps understand overall traffic evolution, as well as congestion patterns and shockwave effects. Thanks to its deterministic and discrete nature, it is well-suited and widely applied in traffic control systems like route guidance, dynamic speed regulation, lane control and ramp metering [61, 107, 108, 29]. Moreover, METANET can model freeway traffic behavior in two different ways like explained in [79]: the first way is the non destination-oriented mode when the traffic assignment problem is not taken into account, and the second way is the destination-oriented mode when the road users can choose from different alternative paths to plan their travel, which can be used to solve routing issues. The first way will be presented in this section resulting in the equations being independent from the destination of the vehicles. Only origin and freeway links will be considered in this model (no on-ramps or off-ramps) as it will be used in the work shown in Section **??**.

2.3.2 Formulation of METANET

In METANET, the freeway network is represented with an oriented graph composed of O origin links and M freeway links. In turn, each freeway link M is divided into N_m sections of equal length length L_m and λ_m is the number of its lanes. Time as well is discretized into K time steps of sample time interval equal to T, which is normally equal to 10 $[s]$ for freeways. In the following, $k = 0, ..., K$ denotes the temporal stage, $o = 1, ..., O$ represents

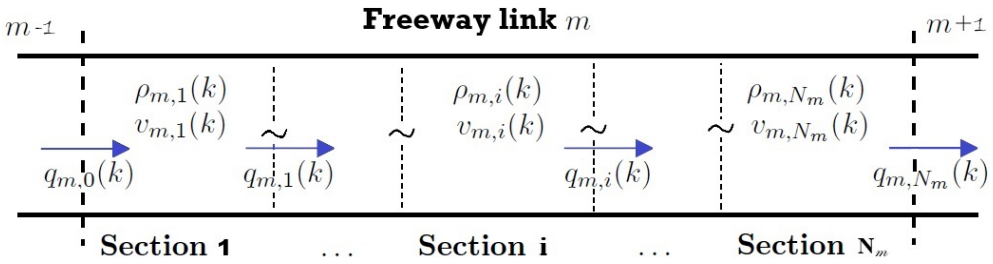

FIGURE 2.3: METANET freeway link variables

origin link, $m = 1, ..., M$ indicates freeway link, $i = 1, ..., N_m$ indicates section i of the freeway link m. Taken all that into account, a condition is required to be fulfilled for achieving numerical stability:

$$L_m > v_{m,i}^{free} T, \tag{2.10}$$

where $v_{m,i}^{free}$ is the average speed of the traffic in free-flow conditions. To describe the dynamic traffic evolution in origin and freeway links, the main aggregate variables are: (like shown in Figure 2.3):

- $\rho_{m,i}(k)$ is the traffic density in section i of link m at time instant kT (expressed in vehicles per kilometer per lane);
- $v_{m,i}(k)$ is the mean traffic speed in section i of link m at time instant kT (expressed in kilometer per hour);
- $q_{m,i}(k)$ is the traffic flow leaving section i of link m during time interval $[kT, (k+1)T)$ (expressed in vehicles per hour);
- $d_o^O(k)$ is the the traffic demand of vehicles requiring to access the mainstream from the origin link o at time instant kT (expressed in vehicles per hour);
- $l_o^O(k)$ is the queue length of vehicles waiting at origin link o at time instant kT (expressed in vehicles);
- $q_o^O(k)$ is the outflow traffic volume from the origin link o during time interval $[kT, (k+1)T)$ (expressed in vehicles per hour).

The density, speed and flow represent the traffic dynamics (Figure 2.3) and are described for freeway links in the following equations:

$$\rho_{m,i}(k+1) = \rho_{m,i}(k) + \frac{T}{L_m \lambda_m}\Big[q_{m,i-1}(k) - q_{m,i}(k)\Big]$$
$$m = 1,\dots,M, \quad i = 1,\dots,N_m, \quad k = 0,\dots,K-1 \quad (2.11)$$

$$v_{m,i}(k+1) = v_{m,i}(k) + \frac{T}{\tau}\Big[V(\rho_{m,i}(k)) - v_{m,i}(k)\Big] + \frac{T}{L_m} v_{m,i}(k)\big(v_{m,i-1}(k) - v_{m,i}(k)\big) - \frac{\nu T\big(\rho_{m,i+1}(k) - \rho_{m,i}(k)\big)}{\tau L_m\big(\rho_{m,i}(k) + \chi\big)}$$
$$m = 1,\dots,M, \quad i = 1,\dots,N_m, \quad k = 0,\dots,K-1 \quad (2.12)$$

$$q_{m,i}(k) = \rho_{m,i}(k) v_{m,i}(k) \lambda_m$$
$$m = 1,\dots,M, \quad i = 1,\dots,N_m, \quad k = 0,\dots,K-1 \quad (2.13)$$

where τ, ν, χ are suitable model parameters, that in a real application have to be properly tuned with specific identification procedures. Derived from the conservation equation 2.7, Equation 2.11 describes the dynamics of the density $\rho_{m,i}(k+1)$ for each section i of link m and is calculated by summing the density at the previous time step k and the difference between the flow $q_{m,i-1}(k)$ entering the segment (m,i) from upstream and the flow $q_{m,i}(k)$ exiting it. The flow described in Equation 2.13 is the outflow of each section (m,i) and is calculated as the product of the density $\rho_{m,i}(k)$, the speed $v_{m,i}(k)$ and the number of lanes in this section λ_m. As physical accurate relations, Equations 2.11 and 2.13 are the only ones presented by the model because the speed described in Equation 2.12 is calculated based on heuristics analysis. As explained in Section 2.2.1, second-order models improved the LWR model by adding a a convective term that models how the speed of a vehicle is influenced by the traffic speed, a relaxation term which expresses the will of the driver to obtain the desired speed $V\left(\rho_{m,i}(k)\right)$ and an anticipation term that shows the influence of traffic pressure on the speed of the vehicle.

METANET proposed two further adjustments for the speed to take into consideration its decrease due to the merging of on-ramps and origin links (2.14) and due to lane drops in the mainstream (2.15):

$$-\delta^{\text{on}} T \frac{v_{m,1}(k) q_o^O(k)}{L_m \lambda_m (\rho_{m,1}(k) + \chi)} \tag{2.14}$$

where δ^{on} is a constant parameter and m represents the leaving link;

$$-\phi T \Delta\lambda \frac{v_{m,N_m}(k)^2 \rho_{m,N_m}(k)}{L_m \lambda_m \rho_{m,i}^{\text{cr}}} \tag{2.15}$$

with $\rho_{m,i}^{\text{cr}}$ the critical density, ϕ a constant parameter and $\Delta\lambda = \lambda_m - \lambda_{m+1}$ is the lane drop. The steady-state speed-density relation present in the relaxation term in Equation 2.12 can be expressed as

$$V\left(\rho_{m,i}(k)\right) = v_{m,i}^{\text{free}} \cdot \left[1 - \left(\frac{\rho_{m,i}(k)}{\rho_{m,i}^{\max}}\right)^l\right]^m$$
$$m = 1, \ldots, M, \quad i = 1, \ldots, N_m, \quad k = 0, \ldots, K-1 \tag{2.16}$$

where $v_{m,i}^{\text{free}}$ is the free-flow speed in section i of link m, $\rho_{m,i}^{\max}$ is the jam density in section i of link m, while l, m, are other model parameters.

Origin links on the other hand need to be modeled by calculating the length of the queue of vehicles waiting to enter the mainstream (Figure 2.4). The dynamic evolution of the queue length $l_o^O(k+1)$ at the origin link, denoted by $o = 1, ..., O$, may be calculated by adopting a simple queue model and its equal to the state of the queue length at the previous time step k, plus the traffic demand $d_o^O(k)$, requiring to access in the mainstream, and minus the origin outflow $q_o^O(k)$

$$l_o^O(k+1) = l_o^O(k) + T\left[d_o^O(k) - q_o^O(k)\right]$$
$$o = 1, \ldots, O, \quad k = 0, \ldots, K-1 \tag{2.17}$$

The outflow $q_o^O(k)$ in Equation 2.17 is basically the flow allowed to enter the mainstream and is equal to the minimum of three terms: the sum of the origin traffic demand and the origin queue length at the time step k, the level of density of the primary downstream leaving link m, and the origin link

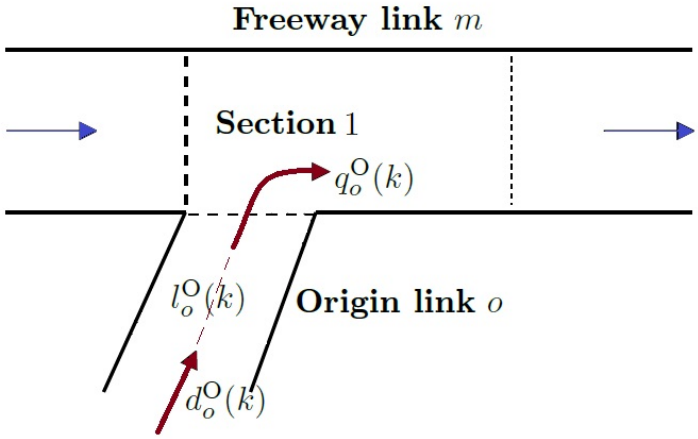

FIGURE 2.4: METANET origin link variables

capacity $q_o^{O,\max}$, as shown in Equation 2.18:

$$q_o^O(k) = \min\left\{ d_o^O(k) + \frac{l_o^O(k)}{T}, q_o^{\max},\ q_o^{O,\max} \cdot \frac{\rho_{m,1}^{\max} - \rho_{m,1}(k)}{\rho_{m,1}^{\max} - \rho_{m,1}^{\mathrm{cr}}} \right\}$$
$$o = 1, \ldots, O, \quad k = 0, \ldots, K-1 \quad (2.18)$$

As METANET accounts for a network of highways, it includes a model node equation that accounts for bifurcations or change in link characteristics. It consists of flow balance equations between flows entering and exiting the nodes and does not provide information about the traffic dynamic behavior. The total flow that enters node $n = 1, ..., N$ is denoted as $Q_n(k)$, I_n^M and I_n^O are the sets of freeway and origin links respectively and O^n is the set of links leaving node n. An illustration of a node model is shown in Figure 2.5. For each network node n, the incoming traffic flow is the sum of the flows coming from the freeway and origin links:

$$Q_n(k) = \sum_{\mu \in I_n^M} q_{\mu,N_\mu}(k) + \sum_{o \in I_n^O} q_o^O(k)$$
$$n = 1, \ldots, N \quad k = 0, \ldots, K-1, \quad (2.19)$$

where N_μ refers to the last section of incoming link μ, whereas o is the incoming origin link. For the same node, the outgoing traffic flow using link

m, $q_{m,0}(k)$, is calculated as follows:

$$q_{m,0}(k) = \beta_{n,m}(k) \cdot Q_n(k)$$
$$m = 1, \ldots, M, \quad n = 1, \ldots, N \quad k = 0, \ldots, K-1, \quad (2.20)$$

where $\beta_{n,m}(k)$ represents the turning rate, i.e the portion of traffic flow $Q_n(k)$ that leaves node n through link m. As the sum of the outgoing flows has to be equal to the sum of the incoming flow, for each node n and for each time step k the following condition must be fulfilled:

$$\sum_{m \in O_n} \beta_{n,m} = 1$$
$$n = 1, \ldots, N \quad k = 0, \ldots, K-1, \quad (2.21)$$

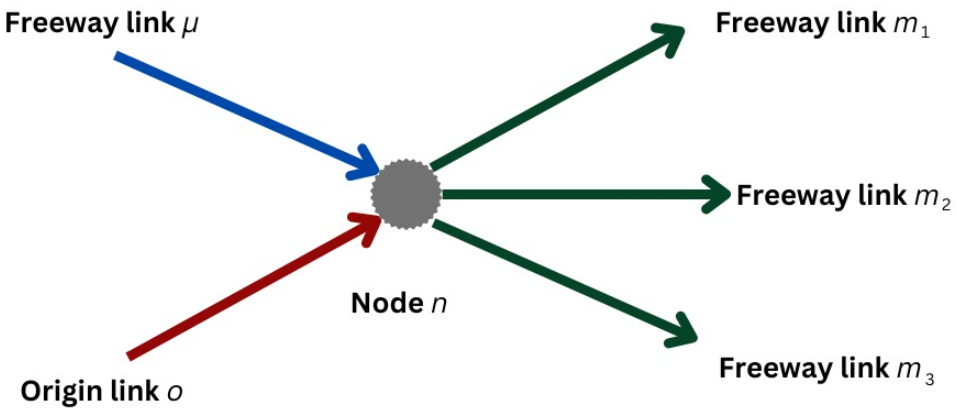

FIGURE 2.5: Flow balance of the METANET node model

In order to calculate the upstream influence of the density in case the node n has more than one leaving link, the following equation is used:

$$\rho_{m,N_m+1}(k) = \frac{\sum_{m \in O_n} (\rho_{m,1}(k))^2}{\sum_{m \in O_n} \rho_{m,1}(k)}$$
$$m = 1, \ldots, M, \quad n = 1, \ldots, N \quad k = 0, \ldots, K-1, \quad (2.22)$$

where $\rho_{m,N_m+1}(k)$ is the virtual density used for the last section in Equation 2.12. Now in the case where the node n has more than one entering link, the downstream influence of speed is calculated through the virtual speed

$v_{m,0}(k)$ that is used in Equation 2.12:

$$v_{m,0}(k) = \frac{\sum_{\mu \in I_n^M} v_{\mu,N_\mu}(k) q_{\mu,N_\mu}(k)}{\sum_{\mu \in I_n^M} q_{\mu,N_\mu}(k)}$$
$$m = 1, \ldots, M, \quad n = 1, \ldots, N \quad k = 0, \ldots, K-1, \quad (2.23)$$

2.4 CTM

2.4.1 Introduction

The Cell Transmission Model (CTM) is a macroscopic traffic flow model introduced in the early 1990s as a computationally efficient and robust method for modeling traffic dynamics on road networks. It was developed by Carlos Daganzo in [39] and [40] and it was inspired by the LWR theory as it discretizes the model into a grid of cells, enabling it to represent traffic dynamics using simple update rules for density and flow. Each cell has a capacity and a flow rate based on fundamental diagrams and it uses a conservation equation to update vehicle densities over time. The equations will be shown in details later in this section. The model is a first-order model so it models traffic flow and density without explicitly considering vehicle acceleration or speed, so it does not capture velocity oscillations or heterogeneous driver behavior. CTM is widely used in dynamic traffic assignment to optimize routes in real time, as well in ramp metering and traffic control systems. Another use of the CTM is in simulation-based studies of highway and arterial networks. Many studies modified it and upgraded it, like in [132] where the authors modified the model to incorporate realistic queue discharge behaviors at signalized intersections. Another example is [72] that proposed an expansion to the CTM to make it a multi-class model. Modeling mixed traffic of CAVs and HVs is also part of the upgrades that the CTM got, like shown in Section 2.5. The model described in Section 2.4.2 is derived from the original version proposed by Daganzo, with different mathematical notation and nomenclature.

2.4.2 Formulation of CTM

As mentioned before, CTM divides the freeway stretch into N cells and time into K time intervals. Let T denote the sample time [h]. Moreover, on-ramps and off-ramps are assumed to be present at the interface between two subsequent cells. The quantities described in the model showing the dynamic

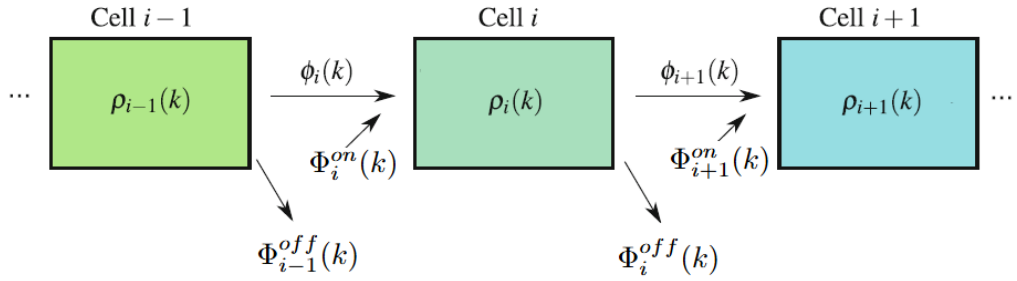

FIGURE 2.6: CTM variables of each cell of the freeway stretch

traffic evolution over time and space for each cell $i = 1, ..., N$, and for each time step $k = 0, ..., K$ are:

- $\rho_i(k)$ is the traffic density of cell i at time instant kT, in [veh/km];
- $\Phi_i(k)$ is the traffic flow entering cell i during time interval $[kT, (k+1)T)$, in [veh/h];
- $D_i(k)$ is the demand of cell i during time interval $[kT, (k+1)T)$, in [veh/h];
- $S_i(k)$ is the supply of cell i during time interval $[kT, (k+1)T)$, in [veh/h].
- $\Phi_i^{off}(k)$ is the flow exiting cell i through the off-ramp during time interval $[kT, (k+1)T)$, in [veh/h].
- $\Phi_i^{on}(k)$ is the flow entering cell from the on-ramp during time interval $[kT, (k+1)T)$, in [veh/h].
- $\beta_i(k) \in [0, 1)$ is the split ratio of cell i during time interval $[kT, (k+1)T)$;
- $D_i^{ramp}(k)$ is the demand of the on-ramp of cell i during time interval $[kT, (k+1)T)[veh/h]$.

The main variables of the CTM in each cell of the stretch are shown in Figure 2.6. The parameters that represent characteristics of the highway and of individual cells are:

- v_i^f is the free-flow speed of cell i [km/h];
- w_i is the congestion wave speed of cell i [km/h];
- q_i^{max} is the capacity of cell i [veh/h];
- ρ_i^{max} is the jam density of cell i [veh/km];
- Δ_i is the length of cell i in [km];

- $p_i^{ramp} \in [0,1]$ is the priority of the on-ramp flow with respect to the mainstream flow in cell i , $p_i \in [0,1]$ is the priority of the mainstream flow with respect to the on-ramp flow in cell i , such that $p_i^{ramp} + p_i = 1$ for $i = 1, ..., N$.

The equations describing the state variable which is the traffic density are given by:

$$\rho_i(k+1) = \rho_i(k) + \frac{T}{\Delta_i}\left[\Phi_i(k) + \Phi_i^{on}(k) - \Phi_{i+1}(k) - \Phi_i^{off}(k)\right]$$
$$i = 1, \ldots, N \quad k = 0, \ldots, K-1. \quad (2.24)$$

The flow exiting through the off-ramp is calculated as

$$\Phi_i^{off}(k) = \frac{\beta_i(k)}{1-\beta_i(k)}\Phi_{i+1}(k)$$
$$i = 1, \ldots, N \quad k = 0, \ldots, K-1, \quad (2.25)$$

since $\Phi_i^{off}(k) = \beta_i(k)[\Phi_{i+1}(k) + \Phi_i^{off}(k)]$ because the off-ramp flow is equal to part of the total exiting flow from cell i.

Going back to Equation 2.24, in order to calculate the flows entering and exiting cells i, CTM presents two important aspects of traffic: the demand and supply of each cell. Moving from cell $i-1$ to cell i, the demand $D_{i-1}(k)$ is the flow that cell $i-1$ could send to cell i during one time step, i.e. $[kT.(k+1)T)$. On the other hand, the supply of cell i, $S_i(k)$, is the flow that cell i is able to receive from cell $i-1$ in the same time interval. They are computed as in the following:

$$D_{i-1}(k) = \min\left\{(1-\beta_{i-1}(k)) \cdot v_{i-1}^{f} \cdot \rho_{i-1}(k), q_{i-1}^{\max}\right\}$$
$$i = 1, \ldots, N \quad k = 0, \ldots, K-1, \quad (2.26)$$

$$S_i(k) = \min\left\{w_i \cdot (\rho_i^{\max} - \rho_i(k)), q_i^{\max}\right\}$$
$$i = 1, \ldots, N \quad k = 0, \ldots, K-1, \quad (2.27)$$

and they are shown graphically as functions of the density in Figures 2.8 and 2.7.

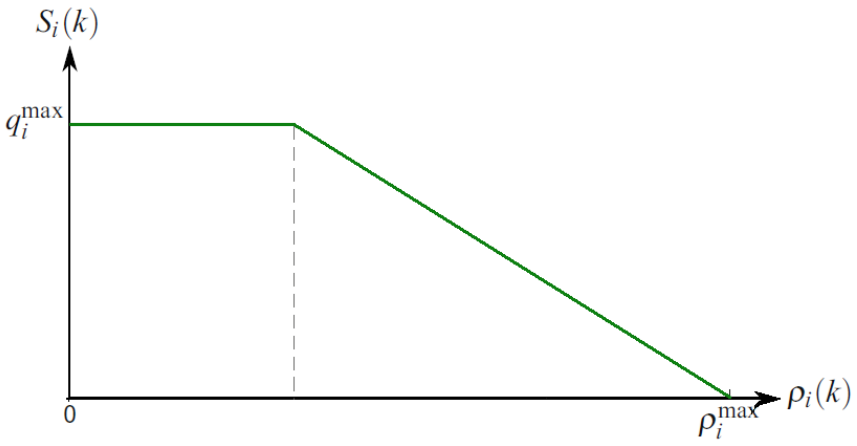

FIGURE 2.7: CTM supply as function of the density

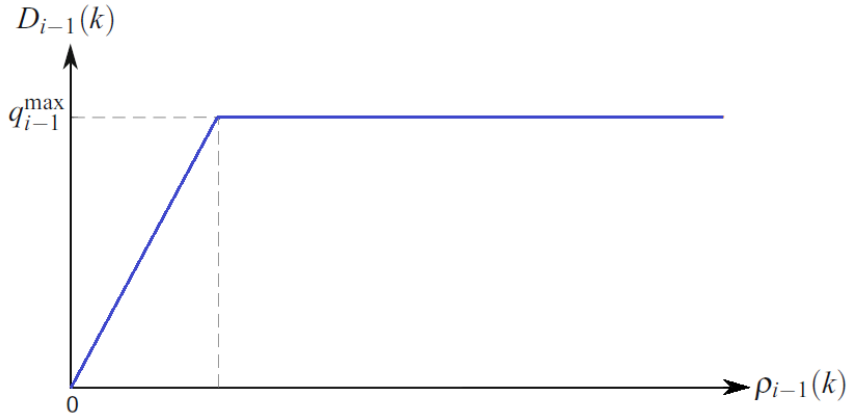

FIGURE 2.8: CTM demand as function of the density

Concerning on-ramps, they merge with the mainstream in the same way two consecutive cells do. In this case we have two sending cells, one on-ramp cell and one mainstream cell $i-1$ and each with its own demand, and one receiving mainstream cell $i+1$ with its proper supply. Two scenarios can be distinguished:

- Free-flow case where the receiving cell has enough space to accommodate for the flow from both sending cells:

$$D_{i-1}(k) + D_i^{\text{ramp}}(k) \leq S_i(k), \tag{2.28}$$

  which gives that $\Phi_i(k) = D_{i-1}(k)$ and $r_i(k) = D_i^{ramp}(k)$,

- Congested case, which is the opposite to the free-flow one and cell i cannot receive the total sum of the flows that want to enter it:

$$D_{i-1}(k) + D_i^{\text{ramp}}(k) > S_i(k), \tag{2.29}$$

which gives that:

$$\Phi_i(k) = \text{mid}\left\{D_{i-1}(k), S_i(k) - D_i^{\text{ramp}}(k), p_i S_i(k)\right\} \tag{2.30}$$

and

$$r_i(k) = \text{mid}\left\{D_i^{\text{ramp}}(k), S_i(k) - D_{i-1}(k), p_i^{\text{ramp}} S_i(k)\right\}, \tag{2.31}$$

where the function mid returns the middle value.

The merge models consists in reserving or guaranteeing a flow $p_i S_i(k)$ for the mainstream demand $D_i - (k)$ and a flow $p_i^{\text{ramp}} S_i(k)$ for the on-ramp demand $D_i^{\text{ramp}}(k)$.

For the cells that do not have any on-ramps or off-ramps, the flow entering cell i is calculated as the minimum between the demand of cell $i-1$ and the supply of cell i:

$$\Phi_i(k) = \min\left\{D_{i-1}(k), S_i(k)\right\} \qquad i = 1, \ldots, N \quad k = 0, \ldots, K-1, \tag{2.32}$$

considering that $\beta_{i-1}(k) = 0$, $D_i^{\text{ramp}}(k) = 0$ and $p_i^{\text{ramp}} = 0$.

2.5 Mixed traffic modeling

Coexistence of HVs and AVs is a reality nowadays more than ever and the penetration rate of AVs in traffic will keep increasing in the future until 100% of the traffic will consist of this type of vehicles. This future is not near though, and mixed traffic will exist for many years to come. Since the 1990s, the integration of AVs into traffic systems has been theorized but early studies did not consider the interactions between AVs and HVs as they only examined the isolated effects of AVs on car-following and lane-changing behaviors. Throughout the years, countless technological advancements were made and autonomous driving became more tangible; at the same time, intensive studies were made to examine their impact on mixed traffic, and the effect of adaptive cruise control [146, 97] and lane merging. Moreover, V2V and V2I benefited AVs and enabled them to be connected, becoming CAVs, and to form platoons with a very short inter-vehicular distance, which increases road capacity. A lot of works found that CAVs could improve traffic flow, efficiency and safety: even a small percentage of CAVs can be used to

regulate traffic movement and reduce the conditions that lead to congestion [153, 152]. This is thanks to the behavior of the CAVs and their driving characteristics compared to HVs, like predictable acceleration/deceleration and lane-changing patterns. Moreover, due to the fact that they process information instantly, their reaction times are shorter which leads to smoother traffic flow and potentially higher capacity [137]. Of course with higher penetration rate, CAVs have more impact on traffic flow and safety, and this is due to the fact that at low levels of penetration, CAVs adjust to HVs behavior. Research examines how traffic flow, congestion and several other traffic scenarios are affected by different CAVs penetration rate [27, 10].

As this rate nowadays is still very low, and with the lack of real life experiments, there is a need for models that represent CAVs in traffic. Mixed traffic presents unique challenges and dynamics that differ from traditional traffic and need to be simulated very well and as close as possible to real life scenarios. Microscopic models are the best suited for this task, as they analyze individual vehicle behaviors. In car-following models, it is taken into consideration that CAVs generally exhibit smoother acceleration and deceleration patterns than HVs. One example that is often adapted for mixed traffic is the Intelligent Driver Model (IDM) that incorporates parameters specific to CAVs and can model different levels of automation [141]. Another example is the Wiedemann model [147] that is used in the software SUMO [89] and VISSIM [48]; it allows for different driving behavior parameters in mixed traffic thus differentiating between CAVs and HVs. Concerning lane-changing, CAVs perform it more strategically and conservatively than HVs. A normally adapted model for CAVs is the Minimizing Overall Braking Induced by Lane Changes (MOBIL) [77] that accounts for smoother and more predictable lane-changing behavior. Many traffic simulation tools are used to represent mixed traffic scenario like shown in [119], where VISSIM, SUMO and AIMSUN are analyzed and their performance is tested in the cases of CAVs research applications and their impact on traffic. VISSIM is a commercial simulator, known for its realistic modeling of individual driver behaviors and lane-changing maneuvers, supports microscopic simulations for interaction between CAVs and HVs, particularly for intersection management and lane-changing [137] [10]. AIMSUN offers tools for simulating CAVs and their impact on traffic flow as it combines microscopic and mesoscopic capabilities to examine strategic management systems [99]. SUMO on the other hand, does not offer specific features for CAVs but it is an open-source software and is widely used for mixed traffic simulation. For example in [128], SUMO is used to

model driver behavior and analyze traffic performance in mixed traffic conditions, focusing on the influence of AV penetration on traffic flow. Another work using SUMO is [161] where cooperative CAVs in mixed traffic are simulated, showing their effect on traffic efficiency and safety. Mesoscopic models are as well used in representing mixed traffic. For example in [93], the authors use a multi-class, simulation-based traffic assignment model to analyze mixed traffic of connected autonomous vehicles (CAVs) and human-driven vehicles (HVs). This model incorporates distinct behaviors for each vehicle type, such as system-optimized routing for CAVs and user-equilibrium for HVs and allows the observation of how increasing the CAV penetration rate affects overall travel time and road efficiency. Another study in [71] focuses on mesoscopic traffic behavior at freeway off-ramps. By incorporating both adaptive cruise control (ACC) and cooperative adaptive cruise control (CACC) models, they simulate the car-following and lane-changing interactions between human-driven, ACC, and CACC vehicles. Other works that use mesoscopic modeling for mixed traffic are [85] and [153]. Models like in [35] and [137], combine multiple distributions (e.g., a mixture of exponential and normal distributions) to represent diverse driver behaviors and mixed traffic conditions, such as human-driven and autonomous vehicles. Mixed distributions are particularly valuable for mesoscopic models because they capture a broader range of vehicle interactions and adapt to varied traffic densities. The CTM holds a very high place among the models used in the mixed traffic modeling domain. For example in [118], the authors propose a mixed CTM taking into consideration different CAV penetration rates. They define that a CAV following an HV uses only ACC and uses CACC when following another CAV, benefiting from V2V communication and allowing for a shorter head-way and higher capacity. Then they simulate an accident and find that the vehicle queue that forms behind it gets shorter when the CAVs penetration is higher. A similar work was done in [148] with focus on congestion. On the other hand, the work in [135] takes into consideration the headway distributions and variations in the fundamental diagram with respect to different penetration rates of CAVs, then the mixed flow and roadway capacity are derived. Lane changing was also taken into consideration based on drivers' anticipation, and it was found as in the other works that CAVs can improve traffic flow and reduce traffic speed oscillation.

All the advantages of CAVs offer the opportunity of controlling them, allowing the development of vehicle-based traffic control schemes that use CAVs as actuators. These strategies can enforce human drivers to take a certain

speed or change lanes to benefit the traffic state and reduce a current congestion or prevent a future one. In [150], a control strategy that depends on cooperation between CAVs to make traffic flow smoother is presented and microscopic simulations using cellular automata were used to evaluate it. On the other hand, macroscopic simulations were used to evaluate the method proposed in [136]. Taken into consideration both the benefits and inconveniences of truck platoons traveling with HVs on highways, some works propose schemes to control them, either for reducing traffic congestion [114] or for improving their travel performance [124]. In particular, A hybrid model, called the Micro-Macro METANET model, was proposed in [111] and it aims to model traffic density dynamics while taking into consideration the platoon's occupancy of the highway. This work also proposes a speed control scheme for the platoon, taken into consideration traffic density ahead. As an extension, [23] upgrades the scheme to a hierarchy of two levels, a high level for calculating the reference speed of the platoon and a low one to track it and implement it realistically. All these works use the presence of CAVs in traffic to improve traffic systems, but a proper simulation tool would help trying and improving these strategies. A solution for that is in [125] where a framework for microscopic simulations in SUMO that uses agents to represent CAVs in traffic is proposed and tested, as shown in Figure 2.9. However on the macroscopic levels, models that are able to incorporate control schemes based on using CAVs as actuators are needed. That's why a work presented in this thesis in Section 2.4 proposes a control-oriented CTM that represents CAVs as clusters, allowing for vehicle-based control strategies to be performed.

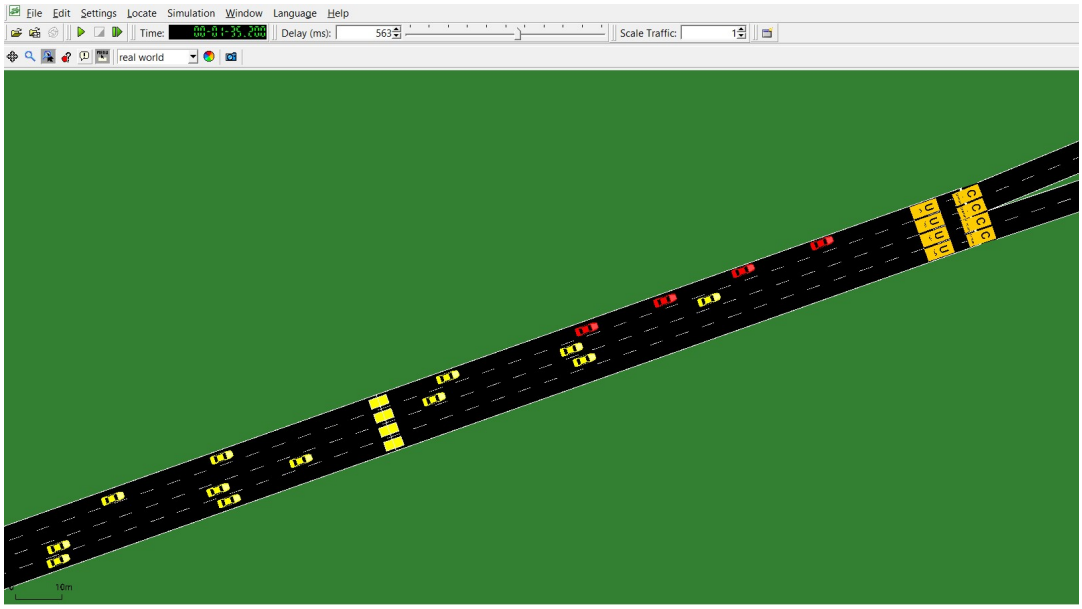

FIGURE 2.9: A SUMO simulation showing CAVs grouped in a cluster (in red) in mixed traffic with HVs (in yellow), using the AGAMAS framework presented in [125]

2.6 A control-oriented highway traffic CTM with clusters of CAVs

The model presented in this section is a CTM version update to represent the presence of CAVs used as control actuators in a traffic stream composed of HVs and is based on the work presented in the ITSC 2023 [31]. The main peculiarity of this control-oriented model concerns the introduction of CAVs into the traffic flow, traveling in a close formation within groups of vehicles, named clusters, that act as moving bottlenecks whose purpose, if properly controlled, is to regularize traffic in the presence of congestion created by downstream capacity reductions (due, for example, to traffic accidents, road works and so on). This allows for less traveling times and shorter congestion duration or even prevention of congestion formation. Two forms of this model are presented. The first one is a single-lane form, that considers a stretch of the highway without distinguishing between lanes. It allows to control the speed of the clusters of CAVs, reducing the speed of the traffic behind them, to form a smoother vehicles flow and to reduce congestion ahead. The number of CAVs forming the cluster can be changed, as well as the inter-vehicular distance, the number of clusters entering the mainstream during a time period and their entrance times. The only thing missing from this model is the capability of the clusters to block a number of particular lanes that is

less or equal to the total number of lanes. To address this, a multi-lane form, inspired by [123] is presented. It considers an additional aspect of traffic dynamics which is lane changing and allows for clusters to enter the mainstream from one particular lane (or more), instead of all lanes, and they can also change lanes during their trip. This gives a new ability to control HVs traffic by forcing a lane change ahead of a congestion.

The single-lane model with no on-ramps or off-ramps is presented in Section 2.6.1, while Section 2.6.2 presents the multi-lane model. A case study for each model and its results are shown and studied in Section 2.7.

2.6.1 The single-lane model

As mentioned previously, the version of the model adopted here is simply representing a one-way freeway road without ramps. Like the conventional CTM, the road is composed of N cells and the time horizon is divided into K time intervals with sample time T [h]. In the model, $i = 1, ..., N$ denotes cell i of the freeway and $k = 1, ..., K$ indicates the time step.

Contrarily to the conventional CTM, CAVs are introduced to traffic in clusters. let us denote with C the multiple clusters of CAVs present in the network, where c represents a single cluster. The parameters of each cluster are:

- n^c is the number of CAVs in the cluster c;
- h^c is the time headway for the CAVs traveling in cluster c, in [h];
- L^c is the length of the cluster c, in [km];
- ρ^c is the density in the cluster c, in [veh/km];
- V^c is the desired speed of a cluster c, in [km/h], that is the control variable in the presence of control.

In this model, we assume that CAVs within a cluster travel always maintaining the fixed time headway, hence the length of a cluster and the density within a cluster strictly depend on the chosen h^c.

The variables describing the dynamics of each cluster are:

- $\tilde{v}_c(k)$ is the speed which is actually implemented by the cluster c at time instant kT, in accordance with the encountered traffic conditions in [km/h];

- $p_F^c(k)$ is the position of the front of the cluster c at time instant kT, in [km], i.e., the position of the front bumper of the CAV leading the cluster;
- $p_B^c(k)$ is the position of the back of the cluster c at time instant kT, in [km], i.e., the position of the rear bumper of the CAV that is at the tail of the cluster.

The position of the front and the back of the cluster are respectively updated according to:

$$p_F^c(k+1) = p_F^c(k) + \tilde{v}^c(k) \cdot T \qquad k = 0, \dots, K-1, \quad (2.33)$$

$$p_B^c(k+1) = p_F^c(k) + \tilde{v}^c(k) \cdot T - L^c = p_B^c(k) + \tilde{v}^c(k) \cdot T \qquad k = 0, \dots, K-1. \quad (2.34)$$

As traffic behaves differently around the clusters, the cells of the highway are divided into two types: cells with a cluster in them and those without a cluster. The front and back positions of the cluster, mentioned previously, are used to detect which cells contain CAVs and which do not. Naturally, each type of cell is modeled differently and the dynamics equations to both types are presented in the following sections.

Dynamics of cells without the presence of CAVs

The equations describing the traffic density in these cells are the ones of the conventional CTM without considering any ramps:

$$\rho_i(k+1) = \rho_i(k) + \frac{T}{\Delta_i}\left[\Phi_i(k) - \Phi_{i+1}(k)\right] \qquad i = 1, \dots, N \quad k = 0, \dots, K-1, \quad (2.35)$$

where, as a reminder, Δ_i is the length of cell i in [km], $\Phi_i(k)$ is the flow entering cell i and $\Phi_{i+1}(k)$ is the flow exiting cell i and entering cell $i+1$. The flow entering cell i is the minimum between the demand of the previous cell

$i-1$ and the supply of cell i:

$$\Phi_i(k) = \min\{D_{i-1}(k), S_i(k)\} \qquad i = 1,\dots,N \quad k = 0,\dots,K-1, \tag{2.36}$$

where the demand and supply of cell i are, respectively, given by:

$$D_i(k) = \min\left\{v_i^{\mathrm{f}} \cdot \rho_i(k), q_i^{\max}\right\} \qquad i = 1,\dots,N \quad k = 0,\dots,K-1, \tag{2.37}$$

$$S_i(k) = \min\left\{w_i \cdot (\rho_i^{\max} - \rho_i(k)), q_i^{\max}\right\} \qquad i = 1,\dots,N \quad k = 0,\dots,K-1, \tag{2.38}$$

with $q_i^{\max}$ representing the maximum flow in cell i [veh/h], $\rho_i^{\max}$ representing the maximum density in section i [veh/km], and w_i being the congestion wave speed of cell i [km/h].

Two conditions of the flow, as shown in (2.124), are distinguished as follows: the free-flow case, where there is enough space for the flow that wants to enter cell i, i.e.:

$$D_{i-1}(k) \leq S_i(k) \tag{2.39}$$

then:

$$\Phi_i(k) = D_{i-1}(k) \tag{2.40}$$

and the congested case, which is the opposite of the previous case, in which not all the flow that wants to enter cell i can actually be received by it, i.e.:

$$D_{i-1}(k) > S_i(k) \tag{2.41}$$

then:

$$\Phi_i(k) = S_i(k) \tag{2.42}$$

Dynamics of cells with the presence of CAVs

Let us now introduce the dynamics of cells in which CAVs are present. Specifically in this model, we assume that each cell can contain at most one cluster of CAVs. Then, some binary parameters are included in the model to identify the presence of a cluster in a cell, and more in detail to identify whether the

cluster is present completely in a cell or is traveling between two cells. The following variables are introduced:

- $\delta^c_{F,i}(k)$, which is equal to 1 if the front of the cluster is in cell i, and equal to 0 otherwise, i.e.:

$$\delta^c_{F,i}(k) = \begin{cases} 1 & \text{if } 0 < \frac{p^c_F(k)}{\sum_{j=1}^{i-1}\Delta j} \leq \frac{\sum_{j=1}^{i}\Delta j}{\sum_{j=1}^{i-1}\Delta j} \\ 0 & \text{otherwise} \end{cases} \tag{2.43}$$

- $\delta^c_{B,i}(k)$, which is equal to 1 if the back of the cluster is in cell i, and equal to 0 otherwise, i.e.:

$$\delta^c_{B,i}(k) = \begin{cases} 1 & \text{if } 0 < \frac{p^c_B(k)}{\sum_{j=1}^{i-1}\Delta_j} \leq \frac{\sum_{j=1}^{i}\Delta_j}{\sum_{j=1}^{i-1}\Delta_j} \\ 0 & \text{otherwise} \end{cases} \tag{2.44}$$

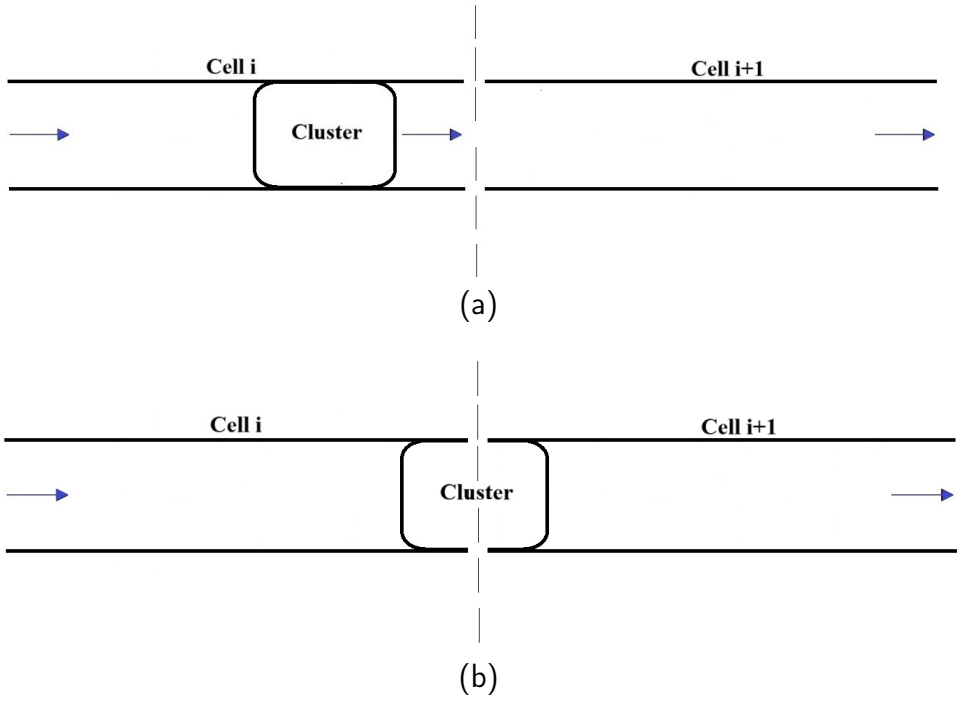

FIGURE 2.10: The two examples of a cell with a cluster in it: full cluster present in cell i (2.10a) and cluster divided between cells i and $i+1$ (2.10b)

From the definitions of these two binary parameters, the position of the cluster can be identified as follows:

- if $\delta^c_{F,i}(k)$=$\delta^c_{B,i}(k)$=1, then the cluster is entirely contained in cell i (as shown in Figure 2.10a);

- if $\delta^c_{F,i}(k)$=1 and $\delta^c_{B,i}(k)$=0, then the front of the cluster is in cell i while the back is still in cell $i-1$;
- if $\delta^c_{F,i}(k)$=0 and $\delta^c_{B,i}(k)$=1, then the back of the cluster is in cell i while the front is in cell $i+1$ (as shown in Figure 2.10b).

The whole purpose of the clusters is to block traffic, i.e. HVs behind the CAVs cannot pass them. As their presence changes traffic behavior, when a cluster is entirely contained in a cell (Figure 2.10a.a), we suppose that the part of this cell not occupied by the cluster is virtually divided as follows:

- the portion of the cell downstream the cluster, with dynamic length $\Delta^D_i(k)$, in [km];
- the portion of the cell upstream the cluster (not null only if the cluster is fully contained in the cell), with dynamic length $\Delta^U_i(k)$, in [km];

which are respectively computed as:

$$\Delta^D_i(k) = \sum_{j=1}^{i} \Delta_j - p^c_F(k)$$

$$i = 1, \dots, N \quad k = 0, \dots, K-1, \quad (2.45)$$

$$\Delta^U_i(k) = p^c_B(k) - \sum_{j=1}^{i-1} \Delta_j$$

$$i = 1, \dots, N \quad k = 0, \dots, K-1. \quad (2.46)$$

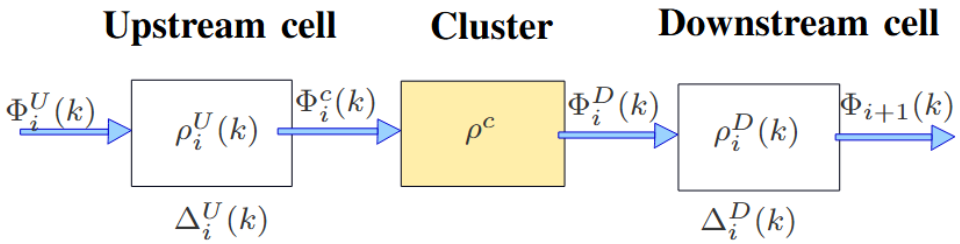

FIGURE 2.11: Macroscopic variables and parameters of a cell with a cluster

When the cluster is divided between two cells (Figure 2.10b), the cell where the front of the cluster is has only a downstream cell, and the one where the back of the cluster is, has only an upstream cell.

The quantities described in the model showing the dynamic traffic evolution over time and space in cells where a cluster of CAVs is present (Figure 2.11) are:

- $\rho_i^U(k)$ is the traffic density of the upstream part to the cluster of cell i at time instant kT, in [veh/km];
- $\rho_i^D(k)$ is the traffic density of the downstream part to the cluster of cell i at time instant kT, in [veh/km];
- $\Phi_i^U(k)$ is the traffic flow entering the upstream part to the cluster of cell i during time interval $[kT, (k+1)T)$, in [veh/h];
- $\Phi_i^D(k)$ is the traffic flow entering the downstream part to the cluster of cell i during time interval $[kT, (k+1)T)$, in [veh/h];
- $D_i^U(k)$ and $D_i^D(k)$ are the demands of the upstream and downstream parts of the cell i respectively during time interval $[kT, (k+1)T)$, in [veh/h];
- $S_i^U(k)$ and $S_i^D(k)$ are the supplies of the upstream and downstream parts of cell i during time interval $[kT, (k+1)T)$, in [veh/h];
- Φ_i^c is the traffic flow entering the cluster c during time interval $[kT, (k+1)T)$, in [veh/h];
- $D_i^c(k)$ and $S_i^c(k)$ are the demand and supply respectively of the cluster c during time interval $[kT, (k+1)T)$, in [veh/h].

Then the density dynamics in the parts of the cell upstream and downstream the cluster are given respectively as follows. For the first time step in which the cluster enters the cell, it yields:

$$\rho_i^U(k+1) = \frac{\Delta_i^U(k)}{\Delta_i} \cdot \rho_i(k) + \frac{T}{\Delta_i^U(k)} \cdot \left[\Phi_i^U(k) - \Phi_i^c(k)\right] \qquad i = 1, \dots, N \quad k = 0, \dots, K-1, \quad (2.47)$$

$$\rho_i^D(k+1) = \left(1 - \frac{\Delta_i^U(k)}{\Delta_i}\right) \cdot \rho_i(k) + \frac{T}{\Delta_i^D(k)} \cdot \left[\Phi_i^D(k) - \Phi_{i+1}(k)\right] \qquad i = 1, \dots, N \quad k = 0, \dots, K-1. \quad (2.48)$$

For the remaining time steps until the back of the cluster leaves the cell (as long as the condition $\delta^c_{B,i}(k) = 1$ holds) we have:

$$\rho_i^U(k+1) = \rho_i^U(k) + \frac{T}{\Delta_i^U(k)} \cdot \left[\Phi_i^U(k) - \Phi_i^c(k)\right] \qquad i = 1,\dots,N \quad k = 0,\dots,K-1, \tag{2.49}$$

$$\rho_i^D(k+1) = \rho_i^D(k) + \frac{T}{\Delta_i^D(k)} \cdot \left[\Phi_i^D(k) - \Phi_{i+1}(k)\right] \qquad i = 1,\dots,N \quad k = 0,\dots,K-1. \tag{2.50}$$

The overall density in a cell (excluding the presence of the cluster) is always calculated as follows:

$$\rho_i(k) = \rho_i^U(k) + \rho_i^D(k) \qquad i = 1,\dots,N \quad k = 0,\dots,K-1. \tag{2.51}$$

It is important to note that there is no direct interaction between CAVs and HVs, so the cluster neither receives nor sends vehicles in adjacent cells, therefore:

$$\Phi_i^c(k) = 0 \tag{2.52}$$

$$S_i^c(k) = 0 \tag{2.53}$$

The demand $D_i^c(k)$, computed as follows, is defined only to assess whether the cluster can be hosted in subsequent cells:

$$D_i^c(k) = \tilde{v}_c(k) \cdot \rho^c \tag{2.54}$$

Consequently, in the upstream cell, there is no outflow but an inflow can be received from the preceding cell $i-1$, given by:

$$\Phi_i^U(k) = \min\left\{D_{i-1}(k), S_i^U(k)\right\} \tag{2.55}$$

$$D_i^U(k) = 0 \tag{2.56}$$

$$S_i^U(k) = \min\left\{ w_i \cdot \left(\frac{\Delta_i^U(k)}{\Delta_i} \cdot \rho_i^{\max} - \rho_i^U(k) \right), q_i^{\max} \right\} \tag{2.57}$$

In the downstream cell, on the contrary, there is no flow from upstream:

$$\Phi_i^D(k) = 0 \tag{2.58}$$

$$D_i^D(k) = \min\left\{ v_i^{\mathrm{f}} \cdot \rho_i^D(k), q_i^{\max} \right\} \tag{2.59}$$

$$S_i^D(k) = \min\left\{ w_i \cdot \left(\frac{\Delta_i^D(k)}{\Delta i} \cdot \rho_i^{\max} - \rho_i^D(k) \right), q_i^{\max} \right\} \tag{2.60}$$

and the outflow depends on the availability in the next cell $i+1$:

$$\Phi_{i+1}(k) = \min\left\{ D_i^D(k), S_{i+1}(k) \right\} \tag{2.61}$$

Speed dynamics of the clusters

The previous equations model very well the behavior of traffic in the presence of these CAV clusters. But as mentioned earlier, this is a control-oriented model, specifically to control the speed of the clusters. In this thesis, a simple control case is presented where the cluster takes either a predefined speed or the speed of traffic in the cell where it is present. Actually, for the first time step when the cluster enters the cell, the speed of the cluster is set to the traffic speed of this cell:

$$\tilde{v}^c(k) = \min\left\{ \frac{\Phi_{i+1}(k)}{\rho_i^D(k)}, V^c \right\} \tag{2.62}$$

Then, for the following time steps until the front of the cluster leaves the cell, the speed of the cluster depends on the availability in the cell where the front of the cluster would be if it proceeds with the previous speed:

$$\tilde{p}_F^c(k+1) = p_F^c(k) + \tilde{v}^c(k) \cdot T \tag{2.63}$$

where

$$\tilde{v}^c(k) = \tilde{v}^c(k-1) \tag{2.64}$$

Using Equation (2.43) and the predicted position of the front, $\tilde{p}_F^c(k+1)$, $\delta_{F,i}^c(k+1)$ and $\delta_{F,i+1}^c(k+1)$ are calculated.

If the predicted position of the front of the cluster is in cell i (Figure 2.12),

i.e. $\delta^c_{F,i}(k+1) = 1$ and $\delta^c_{F,i+1}(k+1) = 0$, then a comparison must be done between the demand of the cluster and the supply in the downstream cell in order to determine the speed of the cluster. If the supply is greater than the cluster's demand, the CAVs move on at their maximum speed. Otherwise, if the supply is less than the demand, a final check must be done to verify if the density of the receiving downstream cell is null or not: in the first case, the cluster can have its maximum speed, while in the second case, it should have the traffic speed of the cell. The previously mentioned cases are further explained in the following:

- if $D^c_i(k) \leq S^D_i(k)$, then $\tilde{v}^c(k) = V^c$;
- if $D^c_i(k) > S^D_i(k)$:
  - if $\rho^D_i(k) = 0$, then $\tilde{v}^c(k) = V^c$;
  - if $\rho^D_i(k) \neq 0$, then:

$$\tilde{v}^c(k) = \frac{\Phi_{i+1}(k)}{\rho^D_i(k)}. \tag{2.65}$$

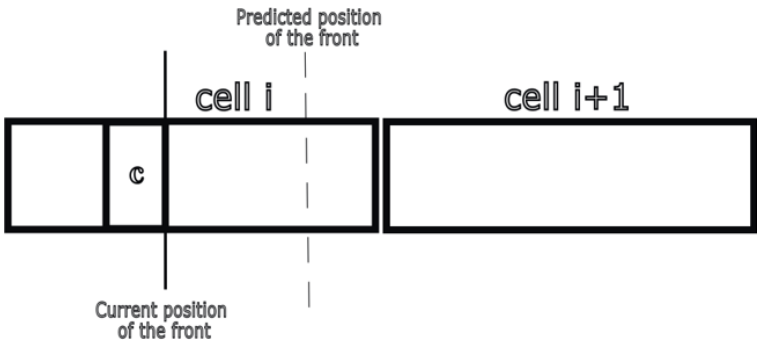

FIGURE 2.12: The case where using the current speed of the cluster, its predicted position in the next time step will stay in cell i

If the predicted position of the front of the cluster is in cell $i+1$ (Figure 2.13), i.e. $\delta^c_{F,i}(k+1) = 0$ and $\delta^c_{F,i+1}(k+1) = 1$, then a comparison must be done between the demand of the cluster and the sum of the supplies of the downstream cell and the next cell $i+1$:

- if the demand of the cluster is less than the sum of supplies, i.e. $D^c_i(k) \leq S^D_i(k) + S_{i+1}(k)$, the cluster proceeds at the minimum speed between its maximum speed and the traffic speeds of cells i and $i+1$:

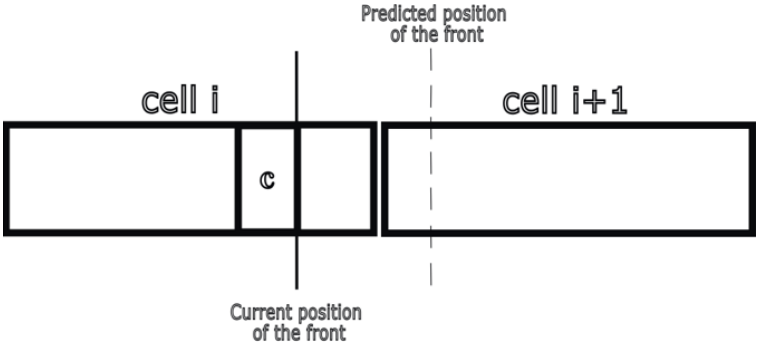

FIGURE 2.13: The case where using the current speed of the cluster, its predicted position in the next time step will be in cell $i+1$

$$\tilde{v}^c(k) = \min\left\{\frac{\Phi_{i+1}(k)}{\rho_i^D(k)}, \frac{\Phi_{i+2}(k)}{\rho_{i+1}(k)}, V^c\right\}; \tag{2.66}$$

- in the opposite case, i.e. $D_i^c(k) > S_i^D(k) + S_{i+1}(k)$, a check is done to the densities of the downstream cell and the cell $i+1$:
  - if both densities are null, i.e. $\rho_i^D(k) = 0$ and $\rho_{i+1}(k) = 0$, then the cluster takes its maximum speed: $\tilde{v}^c(k) = V^c$;
  - if the downstream cell density is not null, i.e. $\rho_i^D(k) \neq 0$, then the cluster takes the minimum between the traffic speeds of cell i and cell $i+1$:
$$\tilde{v}^c(k) = \min\left\{\frac{\Phi_{i+1}(k)}{\rho_i^D(k)}, \frac{\Phi_{i+2}(k)}{\rho_{i+1}(k)}\right\}; \tag{2.67}$$
  - and finally if the downstream cell has zero density and the density of cell $i+1$ is not null, i.e. $\rho_i^D(k) = 0$ and $\rho_{i+1}(k) \neq 0$, then the cluster proceeds at the traffic speed of cell $i+1$:
$$\tilde{v}^c(k) = \frac{\Phi_{i+2}(k)}{\rho_{i+1}(k)}. \tag{2.68}$$

2.6.2 The multi-lane model

This version model considers the lanes of the one-way freeway stretch separately, allowing for lane changes for both the CAV clusters and the HVs. Moreover, it models the on-ramps and off-ramps of the stretch. As in the single-lane model, the road is divided into N cells and the time horizon into

K time steps of sample time T [h]. Again, $k = 1, ..., K$ indicates the time step and $i = 1, ..., N$ denotes cell i of the highway, but in this model every cell i has a number of lanes equal to J_i so $j = 1, ..., J_i$ represents a lane of cell i. As this model takes into consideration the on-ramps and off-ramps of the network, $\hat{i}$ represents a cell where there is an off-ramp and $\hat{j}$ represents the shoulder lane that leads to the off-ramp of cell $\hat{i}$. For the rest of this model, the on-ramp is considered to be at the beginning of a cell and the off-ramp to be at the end of it.

Clusters in this model behave similarly to ones in the single-lane model, except that they can enter the mainstream through a number of lanes that is less or equal to the total number of lanes, which means they do not necessarily need to block the traffic in the entire cell. For this purpose, one more cluster variable is added to the ones mentioned in Section 2.6.1, which is $j^c(k)$, the current lane where cluster c is present at time step k, that can be constant through the whole time horizon or vary to simulate a lane change of the cluster. For the sake of simplicity in the equations stated in this section, we consider that the cluster does not change lanes through the whole simulation, so $j^c(k)$ becomes independent from the time step k and is denoted as j^c. The front and back positions of a cluster are updated exactly like described in Section 2.6.1 and they are again used here to determine which cells contain a cluster and which ones do not.

The parameters that represent characteristics of the highway and of individual cells are:

- $v^f_{i,j}$ is the free-flow speed in lane j of cell i [km/h];
- $w_{i,j}$ is the congestion wave speed in lane j of cell i [km/h],
- $q^{max}_{i,j}$ is the capacity of lane j of cell i [veh/h],
- $\rho^{max}_{i,j}$ is the jam density of lane j of cell i [veh/km],
- Δ_i is the length of cell i in [km],

Dynamics of cells without the presence of CAVs

As lanes are distinguished from each other in this model, flows are categorized into lateral and longitudinal and calculated by determining the longitudinal and lateral demands and supplies. HVs can perform lane changes based on the natural aggregate lane-changing behavior of traffic among adjacent lanes of the same cell and rules are defined in order to properly assign

and bound lateral flows. The quantities described in the model showing the dynamic traffic evolution over time and space for each cell $i = 1, ..., N$, and for each time step $k = 0, ..., K$ are:

- the density $\rho_{i,j}(k)$, i.e. the number of vehicles in cell i, lane j, with no cluster at time step k, divided by the segment length Δ_i;
- $\Phi_{i,j}(k)$ is the longitudinal traffic flow entering cell i through lane j during time interval $[kT, (k+1)T)$, in [veh/h];
- $D_{i,j}^{Long}(k)$ is the longitudinal demand of lane j in cell i during time interval $[kT, (k+1)T)$, in [veh/h];
- $S_{i,j}^{Long}(k)$ is the longitudinal supply of lane j in cell i during time interval $[kT, (k+1)T)$, in [veh/h];
- $\Phi_{i,j}^{on}(k)$ is the flow entering from the on-ramp located in lane j of cell i during time interval $[kT, (k+1)T)$, in [veh/h];
- $\Phi_{i,j}^{off}(k)$ is the flow exiting from the off-ramp located in lane j of cell i during time interval $[kT, (k+1)T)$, in [veh/h];
- $\gamma_{i,j}(k)$ is the turning rate of traffic at the off-ramp of segment (i, j).
- $f_{i,j,\bar{j}}(k)$, with $\bar{j} \neq j$ being an adjacent lane to j, is the lateral traffic flow moving from lane j to lane $\bar{j}$ in cell i during time interval $[kT, (k+1)T)$, in [veh/h];
- $D_{i,j,\bar{j}}^{Lat}(k)$ is the lateral demand to move from lane j to lane $\bar{j}$ in cell i during time interval $[kT, (k+1)T)$, in [veh/h];
- $S_{i,j}^{Lat}(k)$ is the lateral supply of lane j in cell i during time interval $[kT, (k+1)T)$, in [veh/h];
- $F_{i,j}(k)$ is the maximum available flow for lateral movements in the segment (i, j) at time step k;
- $A_{i,j,\bar{j}}(k)$ is the attractiveness rate that shows how much an adjacent lane $\bar{j}$ is attractive for the driver to change its current lane j to, i.e. if it offers a lower density.

The traffic flow variables in a multi-lane cell that does not contain a cluster are shown in Figure 2.14.

Flow dynamics in cells without the presence of a cluster of CAVs

To calculate the lateral flow, we need to know the maximum available flow for lateral movement in cell i lane j, which is based on the current number of vehicles available in the segment (i, j) :

$$F_{i,j}(k) = \frac{\Delta_i}{T} \cdot \rho_{i,j}(k). \tag{2.69}$$

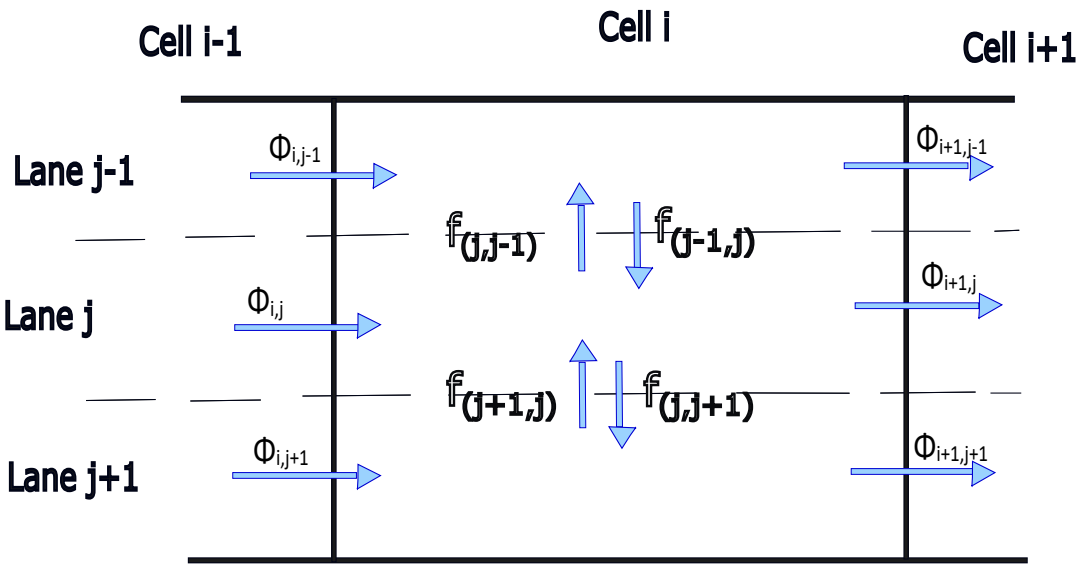

FIGURE 2.14: Macroscopic flow variables in a cell not containing a cluster

The lateral flow from segment (i, j) to $(i,\bar{j})$, where $\bar{j}$ can be $j-1$ or $j+1$, is calculated based on the attractiveness rate $A_{i,j,\bar{j}} \in [0, 1]$ of the value $F_{i,j}(k)$. It takes into consideration that the driver might consider a lane change when one of the adjacent lanes offers a lower density:

$$A_{i,j,\bar{j}}(k) = \mu \cdot \max\left\{0, \frac{P_{i,j,\bar{j}}(k) \cdot \rho_{i,j}(k) - \rho_{i,\bar{j}}(k)}{P_{i,j,\bar{j}}(k) \cdot \rho_{i,j}(k) + \rho_{i,\bar{j}}(k)}\right\}, \tag{2.70}$$

where:

- μ is a unique parameter that reflects the aggressiveness in lane-changing of the drivers and is in the range of $[0, 1]$;
- $P_{i,j,\bar{j}}$ is a factor that is mostly equal to 1 but it should be tuned to reflect particular effects on lane-changing behavior that are dependent on time or location, if existent depending on the network and the types of vehicles. This factor takes into account the same difference in density between the adjacent lanes, irrespectively of the considered lane-changing

direction, thus it respects the relation:

$$P_{i,j,\bar{j}}(k) = \frac{1}{P_{i,\bar{j},j}(k)} \tag{2.71}$$

Having the maximum possible flow and the attractiveness rate, the lateral demand is determined as:

$$D^{Lat}_{i,j,\bar{j}}(k) = A_{i,j,\bar{j}}(k) \cdot F_{i,j}(k). \tag{2.72}$$

In a cell $\hat{i}$ where there is an off-ramp, specifically for the flow towards the shoulder lane $\hat{j}$, a different approach is considered for the lateral demand: the number of vehicles in the shoulder lane $\hat{j}$ should be sufficient to feed the flow of the off-ramp, $\Phi^{off}_{\hat{i},\hat{j}}(k)$, which is a portion of the total flow passing through the all the lanes of the cell i:

$$\Phi^{off}_{\hat{i},\hat{j}}(k) = \gamma_{\hat{i},\hat{j}}(k) \sum_{j=1}^{J} \Phi_{\hat{i}+1,j}(k). \tag{2.73}$$

So in case where the flow entering segment $(\hat{i},\hat{j})$ is lower than $\Phi^{off}_{\hat{i},\hat{j}}(k)$, the minimum lateral flow towards lane $\hat{j}$ to satisfy the off-ramp flow should be calculated as follows:

$$f^{off}_{\hat{i},\hat{j}-1,\hat{j}}(k) = \gamma_{\hat{i}}(k) \sum_{j=1}^{J} \Phi_{\hat{i}+1,j}(k) - \Phi_{\hat{i},\hat{j}}(k), \tag{2.74}$$

and the lateral flow out of the shoulder lane $f_{\hat{i},\hat{j},\hat{j}-1}(k)$ is considered 0. The lateral demand of the flow towards lane $\hat{j}$ is then calculated as follows:

$$D^{Lat}_{\hat{i},\hat{j}-1,\hat{j}}(k) = \max\left\{A_{\hat{i},\hat{j}-1,\hat{j}}(k) \cdot F_{\hat{i},\hat{j}-1}(k), f^{off}_{\hat{i},\hat{j}-1,\hat{j}}(k)\right\}. \tag{2.75}$$

Equation 2.75 calculates the flow that will actually happen if there is enough space in the target segment $(\hat{i},\hat{j})$ and also allows for the rejection of negative values of $f^{off}_{\hat{i},\hat{j}-1,\hat{j}}(k)$.

Calculating the lateral supply of a road segment (i,j) is done similarly to the single-lane model where the space available is the difference between the maximum density of the segment and the current one, as shown in the following:

$$S^{Lat}_{i,j}(k) = [\rho^{\max}_{i,j}(k) - \rho_{i,j}(k)] \cdot \frac{\Delta_i}{T} \tag{2.76}$$

Having the lateral demands and supplies, the lateral flows to lane j from lanes $j-1$ and $j+1$ in cell i are proportionally distributed to take into consideration that the available space in the receiving lane might not be sufficient to accept the lateral flow entering from both sides:

$$f_{i,j-1,j}(k) = \min\left\{1, \frac{S^{Lat}_{i,j}(k)}{D^{Lat}_{i,j+1,j}(k) + D^{Lat}_{i,j-1,j}(k)}\right\} \cdot D^{Lat}_{i,j-1,j}(k) \tag{2.77}$$

$$f_{i,j+1,j}(k) = \min\left\{1, \frac{S^{Lat}_{i,j}(k)}{D^{Lat}_{i,j+1,j}(k) + D^{Lat}_{i,j-1,j}(k)}\right\} .D^{Lat}_{i,j+1,j}(k) \tag{2.78}$$

Now to determine the longitudinal flows between cells, we need to calculate their longitudinal demands and supplies. These quantities depend, additionally in this model, on the availability of space or lack of it that is created by lateral flows. That being said, the longitudinal demand and supply of segment (i, j) are calculated respectively as follows:

$$D^{Long}_{i,j}(k) = \min\{v^{\mathrm{f}}_i \cdot \rho_{i,j}(k), q^{\max}_{i,j}, \frac{L_i}{T} \cdot \rho_{i,j}(k) + f_{i,j-1,j}(k) + f_{i,j+1,j}(k) - f_{i,j,j+1}(k) - f_{i,j,j-1}(k)\}, \tag{2.79}$$

$$S^{Long}_{i,j}(k) = \min\{w_{i,j} \cdot \left(\rho^{\max}_{i,j} - \rho_{i,j}(k)\right), q^{\max}_{i,j}, \frac{L_i}{T} \cdot \rho_{i,j}(k) - f_{i,j-1,j}(k) - f_{i,j+1,j}(k) + f_{i,j,j+1}(k) + f_{i,j,j-1}(k)\}, \tag{2.80}$$

Then the longitudinal flow entering cell i through lane j is determined as follows:

$$\Phi_{i,j}(K) = \min\{D^{Long}_{i-1,j}(k), S^{Long}_{i,j}(k)\}. \tag{2.81}$$

As in the previous model, we can see that the value of longitudinal flow is defined by the state of the traffic: if the traffic is in a free flow state, i.e.:

$$D_{i-1,j}^{Long}(k) < S_{i,j}^{Long}(k), \tag{2.82}$$

then:

$$\Phi_{i,j}(K) = D_{i-1,j}^{Long}(k), \tag{2.83}$$

otherwise, in a congested case, i.e.:

$$D_{i-1,j}^{Long}(k) > S_{i,j}^{Long}(k), \tag{2.84}$$

then:

$$\Phi_{i,j}(K) = S_{i,j}^{Long}(k). \tag{2.85}$$

Density dynamics in cells without the presence of a cluster of CAVs

After determining the flows that will enter and leave segment (i, j), either laterally or longitudinally, its density is calculated as follows:

$$\begin{aligned}\rho_{i,j}(k+1) = \rho_{i,j}(k) + \frac{T}{L_i} \cdot \Big[& \Phi_{i,j}(k) - \Phi_{i+1,j}(k) \\ & + \Phi_{i,j}^{on}(k) - \Phi_{i,j}^{off}(k) + f_{i,j-1,j}(k) \\ & + f_{i,j+1,j}(k) - f_{i,j,j+1}(k) - f_{i,j,j-1}(k) \Big]\end{aligned} \tag{2.86}$$

Dynamics of cells with the presence of CAVs

We again assume, specifically in this model, that each lane of a certain cell can contain at most one cluster of CAVs. The binary parameters $\delta_{F,i}^{c}(k)$ and $\delta_{B,i}^{c}(k)$ introduced in Section 2.6.1, along with the lane $j^c(k)$ of a cluster c, help determine the exact position of the cluster longitudinally and laterally. The cell that fully contains the cluster is, divided into a downstream cell and an upstream cell of dynamic lengths Δ_i^D and Δ_i^U respectively, computed like in the previous model. In adjacent lanes to $j^c(k)$, the middle portion of the lane labeled with 'M' and parallel to the cluster (as shown in Figure 2.15) moves with it while keeping a constant length Δ^M equal to L^c. The model detailed below describes that two clusters contained in one cell are treated separately

but obviously it can be modified to represent these two clusters as one with an additional parameter of the cluster that shows how many and which lanes it is occupying.

Let us denote by N^c the set of cells i that contain a cluster in them. That being said, the quantities described in the model showing the dynamic traffic evolution over time and space for each cell $i \in N^c$ that has a cluster $c = 1, ..., C$, either fully or partially, for each time step $k = 0, ..., K$ are:

- the density $\rho_{i,j}^{U}(k)$, i.e. the number of vehicles in the upstream segment of cell i, lane j, with a cluster at time step k, divided by the segment length $\Delta_i^U(k)$;
- the density $\rho_{i,j}^{D}(k)$, i.e. the number of vehicles in the downstream segment of cell i, lane j, with a cluster at time step k, divided by the segment length $\Delta_i^D(k)$;
- the density $\rho_{i,j}^{M}(k)$, i.e. the number of vehicles in the middle segment of cell i and lane j adjacent to the lane of the cluster at time step k, divided by the segment length Δ^M, which is equal to the length of the cluster;
- $\Phi_{i,j}^{U}(k)$ is the longitudinal traffic flow entering the upstream part to the cluster of cell i through lane j during time interval $[kT, (k+1)T)$, in [veh/h];
- $\Phi_{i,j}^{M}(k)$ is the longitudinal traffic flow entering the middle segment of cell i adjacent to the lane of the cluster through lane j during time interval $[kT, (k+1)T)$, in [veh/h];
- $\Phi_{i,j}^{D}(k)$ is the longitudinal traffic flow entering the downstream part to the cluster of cell i through lane j during time interval $[kT, (k+1)T)$, in [veh/h];
- $D_{i,j}^{U,Long}(k)$ is the longitudinal demand of the upstream part of lane j to the cluster in cell i during time interval $[kT, (k+1)T)$, in [veh/h];
- $D_{i,j}^{M,Long}(k)$ is the longitudinal demand of the middle segment of lane j in cell i parallel to the cluster during time interval $[kT, (k+1)T)$, in [veh/h];
- $D_{i,j}^{D,Long}(k)$ is the longitudinal demand of the downstream part of lane j to the cluster in cell i during time interval $[kT, (k+1)T)$, in [veh/h];
- $S_{i,j}^{U,Long}(k)$ is the longitudinal supply of the upstream part of lane j to the cluster in cell i during time interval $[kT, (k+1)T)$, in [veh/h];

- $S_{i,j}^{M,Long}(k)$ is the longitudinal supply of the middle segment of lane j in cell i parallel to the cluster during time interval $[kT,(k+1)T)$, in [veh/h];
- $S_{i,j}^{D,Long}(k)$ is the longitudinal supply of the downstream part of lane j to the cluster in cell i during time interval $[kT,(k+1)T)$, in [veh/h];
- $f_{i,j,\bar{j}}^{U}(k)$, with $\bar{j} \neq j$ being an adjacent lane to j, is the lateral traffic flow moving from lane j to lane $\bar{j}$ in the upstream part to the cluster of cell i during time interval $[kT,(k+1)T)$, in [veh/h];
- $f_{i,j,\bar{j}}^{D}(k)$, with $\bar{j} \neq j$ being an adjacent lane to j, is the lateral traffic flow moving from lane j to lane $\bar{j}$ in the downstream part to the cluster of cell i during time interval $[kT,(k+1)T)$, in [veh/h];
- $D_{i,j,\bar{j}}^{U,Lat}(k)$ is the lateral demand to move from lane j to lane $\bar{j}$ in the upstream part to the cluster of cell i during time interval $[kT,(k+1)T)$, in [veh/h];
- $D_{i,j,\bar{j}}^{D,Lat}(k)$ is the lateral demand to move from lane j to lane $\bar{j}$ in the downstream part to the cluster of cell i during time interval $[kT,(k+1)T)$, in [veh/h];
- $S_{i,\bar{j}}^{U,Lat}(k)$ is the lateral supply of the upstream part to the cluster of lane j in cell i during time interval $[kT,(k+1)T)$, in [veh/h];
- $S_{i,j}^{M,Lat}(k)$ is the lateral supply of the middle segment of lane j in cell i parallel to the cluster during time interval $[kT,(k+1)T)$, in [veh/h];
- $S_{i,\bar{j}}^{D,Lat}(k)$ is the lateral supply of the downstream part to the cluster of lane j in cell i during time interval $[kT,(k+1)T)$, in [veh/h];
- $F_{i,j}^{U}(k)$ is the number of vehicles available in the upstream part to the cluster of segment (i,j) at time step k;
- $F_{i,j}^{D}(k)$ is the number of vehicles available in the downstream part to the cluster of segment (i,j) at time step k;
- $A_{i,j,\bar{j}}^{U}(k)$ is the attractiveness rate for a lane change from lane j to lane $\bar{j}$ in the upstream part to the cluster of cell i.
- $A_{i,j,\bar{j}}^{D}(k)$ is the attractiveness rate for a lane change from lane j to lane $\bar{j}$ in the downstream part to the cluster of cell i.
- $\Phi_i^{c,Long}$ and $\Phi_i^{c,Lat}$ are the longitudinal and lateral traffic flows respectively entering the cluster c during time interval $[kT,(k+1)T)$, in [veh/h];

- $D_i^{c,Long}(k)$ and $S_i^{c,Long}(k)$ are the longitudinal demand and supply respectively of the cluster c during time interval $[kT, (k+1)T)$, in [veh/h].
- $D_i^{c,Lat}(k)$ and $S_i^{c,Lat}(k)$ are the lateral demand and supply respectively of the cluster c during time interval $[kT, (k+1)T)$, in [veh/h].

Flow dynamics in cells with the presence of a cluster of CAVs

To calculate the lateral flows in a cell with a cluster, first the maximum available flows for lateral movement in the upstream and downstream cells are calculated respectively as:

$$F_{i,j}^{U}(k) = \frac{\Delta_i^U(k)}{T} \cdot \rho_{i,j}^{U}(k) \tag{2.87}$$

$$F_{i,j}^{D}(k) = \frac{\Delta_i^D(k)}{T} \cdot \rho_{i,j}^{D}(k) \tag{2.88}$$

In addition to that, the attractiveness rates in the upstream and downstream cells respectively are:

$$A_{i,j,\bar{j}}^{U}(k) = \mu \cdot \max\left\{0, \frac{P_{i,j,\bar{j}}^{U}(k) \cdot \rho_{i,j}^{U}(k) - \rho_{i,\bar{j}}^{U}(k)}{P_{i,j,\bar{j}}^{U}(k) \cdot \rho_{i,j}^{U}(k) + \rho_{i,\bar{j}}^{U}(k)}\right\} \tag{2.89}$$

$$A_{i,j,\bar{j}}^{D}(k) = \mu^D \cdot \max\left\{0, \frac{P_{i,j,\bar{j}}^{D}(k) \cdot \rho_{i,j}^{D}(k) - \rho_{i,\bar{j}}^{D}(k)}{P_{i,j,\bar{j}}^{D}(k) \cdot \rho_{i,j}^{D}(k) + \rho_{i,\bar{j}}^{D}(k)}\right\} \tag{2.90}$$

The presence of the cluster decreases the density in front of it and increases the density behind it. This will cause lane changing behavior of the HVs into the cluster's lane in the downstream cell and out of the cluster's lane in the upstream cell of cell i. This is shown in the attractiveness rates written before where they are positive in the direction from the high density parts of the lanes into the lower density parts and zero in the other directions. Human drivers may choose to trust the CAVs and not move into its lane in the downstream part of the cell, and to model this we can consider an aggressiveness rate for downstream cells lower than the normal rate, shown as μ^D in Equation 2.90. To model the perfect blocking of the cluster to the traffic flow, the absence of direct interaction between CAVs and HVs is represented as:

$$\Phi_i^{c,Long}(k) = 0, \tag{2.91}$$

$$\Phi_i^{c,Lat}(k) = 0, \tag{2.92}$$

$$S_i^{c,Long}(k) = 0, \tag{2.93}$$

and

$$S_i^{c,Lat}(k) = 0, \tag{2.94}$$

meaning that the cluster does not receive nor send vehicles longitudinally or laterally in adjacent cells, as it only moves as a whole. The longitudinal demand $D_i^{c,Long}(k)$, computed respectively as follows, is defined only to assess whether the cluster can be hosted in subsequent cells:

$$D_i^{c,Long}(k) = \tilde{v}_c(k) \cdot \rho^c. \tag{2.95}$$

On the other hand, the lateral demand $D_i^{c,Lat}(k)$ is used only in the case where the cluster is ordered to perform a lane change and is calculated as the maximum lateral flow the cluster can make based on the number of CAVs forming it:

$$D_i^{c,Lat}(k) = \frac{L^c}{T}\rho^c. \tag{2.96}$$

When a lane change is requested, the cluster performs it only if there is space macroscopically in the cell 'M' in the target lane, i.e. its lateral demand is smaller than the supply of cell 'M' of the target lane:

$$D_i^{c,Lat}(k) \leq S_{i,j}^{M,Lat}(k), \tag{2.97}$$

with the mentioned supply being calculated as:

$$S_{i,j}^{M,Lat}(k) = [\rho_{i,j}^{M,\max}(k) - \rho_{i,j}^{M}(k)] \cdot \frac{\Delta_i^M(k)}{T}, \tag{2.98}$$

where

$$\rho_{i,j}^{M,\max}(k) = \frac{\Delta_i^M(k)}{\Delta_i} \cdot \rho_{i,j}^{\max} \tag{2.99}$$

is the maximum density of the middle part of lane j adjacent to j_c of cell i. The lateral demands of the HVs in the upstream and downstream cells are calculated respectively as:

$$D_{i,j,\bar{j}}^{U,Lat}(k) = A_{i,j,\bar{j}}^{U}(k) \cdot F_{i,j}^{U}(k) \tag{2.100}$$

$$D_{i,j,\bar{j}}^{D,Lat}(k) = A_{i,j,\bar{j}}^{D}(k) \cdot F_{i,j}^{D}(k). \tag{2.101}$$

and the lateral supplies in the upstream and downstream cells are respectively determined as follows:

$$S_{i,j}^{U,Lat}(k) = [\rho_{i,j}^{U,\max}(k) - \rho_{i,j}^{U}(k)] \cdot \frac{\Delta_i^U(k)}{T} \tag{2.102}$$

$$S_{i,j}^{D,Lat}(k) = [\rho_{i,j}^{D,\max}(k) - \rho_{i,j}^{D}(k)] \cdot \frac{\Delta_i^D(k)}{T}, \tag{2.103}$$

where:

$$\rho_{i,j}^{U,\max}(k) = \frac{\Delta_i^U(k)}{\Delta_i} \cdot \rho_{i,j}^{\max} \tag{2.104}$$

and

$$\rho_{i,j}^{D,\max}(k) = \frac{\Delta_i^D(k)}{\Delta_i} \cdot \rho_{i,j}^{\max} \tag{2.105}$$

are the maximum densities of the upstream and downstream respectively of segment (i, j). Now it is possible to calculate the lateral flows in the upstream and downstream cells respectively in both directions:

$$f_{i,j-1,j}^{U}(k) = \min\left\{1, \frac{S_{i,j}^{U,Lat}(k)}{D_{i,j+1,j}^{U,Lat}(k) + D_{i,j-1,j}^{U,Lat}(k)}\right\} \cdot D_{i,j-1,j}^{U,Lat}(k) \tag{2.106}$$

$$f_{i,j+1,j}^{U}(k) = \min\left\{1, \frac{S_{i,j}^{U,Lat}(k)}{D_{i,j+1,j}^{U,Lat}(k) + D_{i,j-1,j}^{U,Lat}(k)}\right\} .D_{i,j+1,j}^{U,Lat}(k) \tag{2.107}$$

$$f_{i,j-1,j}^{D}(k) = \min\left\{1, \frac{S_{i,j}^{D,Lat}(k)}{D_{i,j+1,j}^{D,Lat}(k) + D_{i,j-1,j}^{D,Lat}(k)}\right\} \cdot D_{i,j-1,j}^{D,Lat}(k) \tag{2.108}$$

$$f^{D}_{i,j+1,j}(k) = \min\left\{1, \frac{S^{D,Lat}_{i,j}(k)}{D^{D,Lat}_{i,j+1,j}(k) + D^{D,Lat}_{i,j-1,j}(k)}\right\}.D^{D,Lat}_{i,j+1,j}(k). \tag{2.109}$$

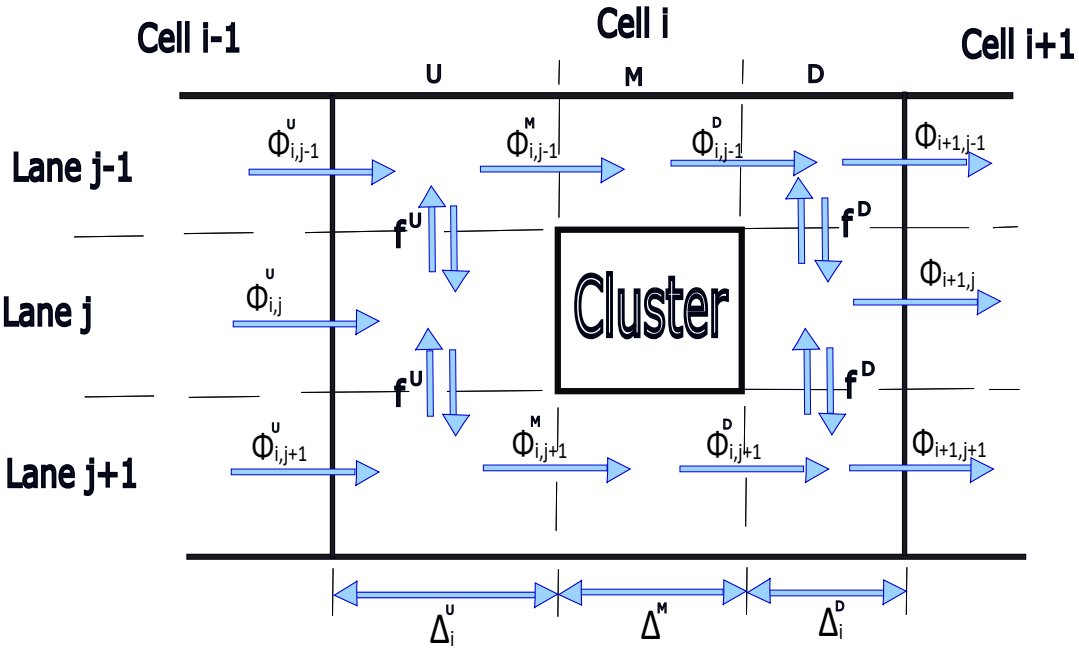

FIGURE 2.15: Macroscopic flow variables in a cell fully containing a cluster

The lateral flows between two lanes that do not contain a cluster, even if one of them is adjacent to a lane that contains one, are calculated based on the equations describing the dynamics of the cells without a cluster. That being said, the two lanes in question are treated as full lanes not divided into upstream, middle and downstream parts.

In order to determine the longitudinal flows, we need to differentiate between the lane of the cluster and the other lanes because traffic is blocked from moving forward behind the cluster only in the lane where it is present:

- the longitudinal demands in the upstream and downstream cells in the lanes of the cluster $j = j_c$ are respectively:

$$D^{U,Long}_{i,j_c}(k) = 0, \tag{2.110}$$

$$D_{i,j_c}^{D,Long}(k) = \min\{v_i^{\mathrm{f}} \cdot \rho_{i,j_c}^{D}(k), q_{i,j_c}^{\max}, \frac{\Delta_i^D}{T} \cdot \rho_{i,j}(k) + f_{i,j_c-1,j_c}^{D}(k) + f_{i,j_c+1,j_c}^{D}(k) - f_{i,j_c,j_c+1}^{D}(k) - f_{i,j_c,j_c-1}^{D}(k)\}; \quad (2.111)$$

- the longitudinal demands in the upstream, middle and downstream cells of the other lanes $j \neq j_c$ are respectively:

$$D_{i,j}^{U,Long}(k) = \min\{v_i^{\mathrm{f}} \cdot \rho_{i,j}^{U}(k), q_{i,j}^{\max}, \frac{\Delta_i^U}{T} \cdot \rho_{i,j}(k) + f_{i,j-1,j}^{U}(k) + f_{i,j+1,j}^{U}(k) - f_{i,j,j+1}^{U}(k) - f_{i,j,j-1}^{U}(k)\}, \quad (2.112)$$

$$D_{i,j}^{M,Long}(k) = \min\left\{v_i^{\mathrm{f}} \cdot \rho_{i,j}^{M}(k), q_{i,j}^{\max}\right\}, \quad (2.113)$$

$$D_{i,j}^{D,Long}(k) = \min\{v_i^{\mathrm{f}} \cdot \rho_{i,j}^{D}(k), q_{i,j}^{\max}, \frac{\Delta_i^D}{T} \cdot \rho_{i,j}(k) + f_{i,j-1,j}^{D}(k) + f_{i,j+1,j}^{D}(k) - f_{i,j,j+1}^{D}(k) - f_{i,j,j-1}^{D}(k)\}; \quad (2.114)$$

- the longitudinal supplies in the upstream and downstream cells for all lanes j are respectively:

$$S_{i,j}^{U,Long}(k) = \min\left\{w_{i,j} \cdot \left(\frac{\Delta_i^U(k)}{L_i} \cdot \rho_{i,j}^{\max} - \rho_{i,j_c}^{U}(k)\right), q_{i,j}^{\max}\right\} - f_{i,j-1,j}^{U}(k) - f_{i,j+1,j}^{U}(k) + f_{i,j,j+1}^{U}(k) + f_{i,j,j-1}^{U}(k), \quad (2.115)$$

$$S_{i,j}^{D,Long}(k) = \min\left\{w_{i,j} \cdot \left(\frac{\Delta_i^D(k)}{L_i} \cdot \rho_{i,j}^{\max} - \rho_{i,j}^{D}(k)\right), q_{i,j}^{\max}\right\} - f_{i,j-1,j}^{D}(k) - f_{i,j+1,j}^{D}(k) + f_{i,j,j+1}^{D}(k) + f_{i,j,j-1}^{D}(k); \quad (2.116)$$

- the longitudinal supply in the middle parts of the adjacent lanes without a cluster:

$$S_{i,j}^{M,Long}(k) = \min\left\{ w_{i,j} \cdot \left(\frac{\Delta_i^M}{L_i} \cdot \rho_{i,j}^{\max} - \rho_{i,j}^M(k) \right), q_{i,j}^{\max} \right\}; \tag{2.117}$$

- the longitudinal flows in the lanes with a cluster $j = j_c$:

$$\Phi_{i,j_c}(k) = \Phi_{i,j_c}^U(k) = \min\left\{ D_{i-1,j_c}^{Long}(k), S_{i,j_c}^{U,Long}(k) \right\}, \tag{2.118}$$

$$\Phi_{i,j_c}^D(k) = 0, \tag{2.119}$$

$$\Phi_{i+1,j_c}(k) = \min\left\{ D_{i,j_c}^{D,Long}(k), S_{i+1,j_c}^{Long}(k) \right\}; \tag{2.120}$$

- the longitudinal flows in the lanes without a cluster $j \neq j_c$:

$$\Phi_{i,j}^c(k) = \min\left\{ D_{i,j}^{U,Long}(k), S_{i,j}^{M,Long}(k) \right\}, \tag{2.121}$$

$$\Phi_{i,j}(k) = \Phi_{i,j}^U(k) = \min\left\{ D_{i-1,j}^{Long}(k), S_{i,j}^{U,Long}(k) \right\}, \tag{2.122}$$

$$\Phi_{i,j}^D(k) = \min\left\{ D_{i,j}^{M,Long}(k), S_{i,j}^{D,Long}(k) \right\}, \tag{2.123}$$

$$\Phi_{i+1,j}(k) = \min\left\{ D_{i,j}^{D,Long}(k), S_{i+1,j}^{Long}(k) \right\}. \tag{2.124}$$

Flow dynamics in shoulder lanes leading to an off-ramp in cells with the presence of a cluster of CAVs

Similarly to cells with off-ramp and no clusters, the off-ramp flow should be satisfied. This calls for the lateral flows $f_{\hat{i},\hat{j}-1,\hat{j}}^{D,off}(k)$ and $f_{\hat{i},\hat{j}-1,\hat{j}}^{U,off}(k)$ towards the shoulder lane $\hat{j}$ in the downstream and upstream cells respectively of cell $\hat{i}$ to be calculated. As equation (4) shows, the flow exiting the off-ramp is determined based on a percentage of the flows passing through all the lanes of the cell, so the minimum lateral flow towards the shoulder lane $\hat{j}$

that satisfies the off-ramp flow should take into consideration the sum of the lateral flows in the downstream and upstream cells, mentioned previously:

$$f^{D,off}_{\hat{i},\hat{j}-1,\hat{j}}(k) + f^{U,off}_{\hat{i},\hat{j}-1,\hat{j}}(k) = \gamma_{\hat{i},\hat{j}}(k) \sum_{j=1}^{J} \Phi_{\hat{i}+1,j}(k) - \Phi_{\hat{i},\hat{j}}(k). \tag{2.125}$$

In this case we have $f^{U}_{\hat{i},\hat{j},\hat{j}-1}(k) = f^{D}_{\hat{i},\hat{j},\hat{j}-1}(k) = 0$ and we can calculate the lateral demand and supply that will determine the lateral flow towards the shoulder lane $\hat{j}$:

$$\begin{aligned} D^{Lat}_{\hat{i},\hat{j}-1,\hat{j}}(k) = \max\{ & A^{D}_{\hat{i},\hat{j}-1,\hat{j}}(k) \cdot F^{D}_{\hat{i},\hat{j}-1}(k) + A^{U}_{\hat{i},\hat{j}-1,\hat{j}}(k) \cdot F^{U}_{\hat{i},\hat{j}-1}(k), \\ & f^{D,off}_{\hat{i},\hat{j}-1,\hat{j}}(k) + f^{U,off}_{\hat{i},\hat{j}-1,\hat{j}}(k)\}, \end{aligned} \tag{2.126}$$

$$S^{Lat}_{\hat{i},\hat{j}}(k) = [\rho^{\max}_{\hat{i},\hat{j}}(k) - \rho_{\hat{i},\hat{j}}(k)] \cdot \frac{\Delta_{\hat{i}}}{T}, \tag{2.127}$$

$$f_{\hat{i},\hat{j}-1,\hat{j}}(k) = \min\left\{ D^{Lat}_{\hat{i},\hat{j}-1,\hat{j}}(k), S^{Lat}_{\hat{i},\hat{j}}(k) \right\}. \tag{2.128}$$

Density dynamics of cells with the presence of a cluster of CAVs

For each part of the segment (i, j), the density is calculated based on the lateral and longitudinal flows entering and exiting. For the lane of the cluster $j = j_c$, the densities of the upstream part, the downstream part and the whole lane are calculated respectively as follows:

$$\begin{aligned} \rho^{U}_{i,j_c}(k+1) = \rho^{U}_{i,j_c}(k) + \frac{T}{\Delta^{U}_{i}(k)} \cdot \Big[& \Phi^{U}_{i,j_c}(k) + f^{U}_{i,j_c-1,j_c}(k) \\ & + f^{U}_{i,j_c+1,j_c}(k) - f^{U}_{i,j_c,j_c+1}(k) - f^{U}_{i,j_c,j_c-1}(k) \Big] \end{aligned} \tag{2.129}$$

$$\begin{aligned} \rho^{D}_{i,j_c}(k+1) = \rho^{D}_{i,j_c}(k) + \frac{T}{\Delta^{D}_{i}(k)} \cdot \Big[& -\Phi_{i+1,j_c}(k) + f^{D}_{i,j_c-1,j}(k) \\ & + f^{D}_{i,j_c+1,j_c}(k) - f^{D}_{i,j_c,j_c+1}(k) - f^{D}_{i,j_c,j_c-1}(k) \Big] \end{aligned} \tag{2.130}$$

$$\rho_{i,j_c}(k+1) = \rho^D_{i,j_c}(k+1) + \rho^U_{i,j_c}(k+1); \tag{2.131}$$

For a lane without cluster $j \neq j_c$, the densities of the upstream, middle and downstream parts and the whole lane are calculated respectively as follows:

$$\rho^U_{i,j}(k+1) = \rho^U_{i,j}(k) + \frac{T}{\Delta^U_i(k)} \cdot \Big[\Phi^U_{i,j}(k) - \Phi^M_{i,j}(k) + \Phi^{on}_{i,j}(k) + f^U_{i,j-1,j}(k) + f^U_{i,j+1,j}(k) - f^U_{i,j,j+1}(k) - f^U_{i,j,j-1}(k)\Big] \tag{2.132}$$

$$\rho^M_{i,j}(k+1) = \rho^M_{i,j}(k) + \frac{T}{\Delta^M_i(k)} \cdot \Big[\Phi^M_{i,j}(k) - \Phi^D_{i,j}(k)\Big] \tag{2.133}$$

$$\rho^D_{i,j}(k+1) = \rho^D_{i,j}(k) + \frac{T}{\Delta^D_i(k)} \cdot \Big[\Phi^D_{i,j}(k) - \Phi_{i+1,j}(k) - \Phi^{off}_{i,j}(k) + f^D_{i,j-1,j}(k) + f^D_{i,j+1,j}(k) - f^D_{i,j,j+1}(k) - f^D_{i,j,j-1}(k)\Big] \tag{2.134}$$

$$\rho_{i,j}(k+1) = \rho^D_{i,j}(k+1) + \rho^M_{i,j}(k+1) + \rho^U_{i,j}(k+1); \tag{2.135}$$

Speed dynamics of the clusters

In case of no control scheme, the cluster is bounded to the minimum between a maximum designated speed and the speed of traffic in the segment it is in. Its predicted position is calculated like in Equation 2.63 and then its speed is decided based on several traffic conditions in front of it, like for the single-lane model in Section 2.6.1.

2.7 Case studies and results

2.7.1 For the single-lane model

The model proposed in the Section 2.6.1 is tested using a stretch of the A20 highway in the Netherlands, which is located in the Dutch province of South Holland and connects the N213 road from the Westland municipality with the cities of Rotterdam and Gouda. The stretch has two lanes and a length of 2.1 km with no on-ramps or off-ramps, shown with a red line in Figure 2.16.

FIGURE 2.16: The highway considered and the stretch (in red) used in the simulation

Considering a cell length of Δ_i=0.3 km $\forall i$, the stretch is divided into N=7 cells. The free-flow speed of traffic in the network is v_i^{f}=100 km/h, the sample time used in this case study is assumed to be T=10 seconds and the total time of the simulation is equal to 2 hours and 20 minutes, which sets the total number of time steps to K=840 time steps. Other parameters concerning the network are: the maximum flow $q_i^{\max}$ equals to 2200 veh/h/lane and the maximum density $\rho_i^{\max}$ equals to 150 veh/km/lane. As the model considers the stretch as having only one lane, the maximum speed and density are multiplied by the number of lanes, which is equal to 2 in this case.

Regarding the clusters, the maximum speed a cluster can take is limited in this study to be V^c=60 km/h and 4 CAVs are considered to form each cluster, with 5 meters as the average length of a CAV and a time headway between the CAVs of 1 second, which sets the length of the cluster to 70 meters on a speed of 60 km/h. The data used to model the demand of HVs are taken from real detectors on the highway on February 1st of the year 2023 from 15:20 till 17:40, and is shown in Figure 2.17.

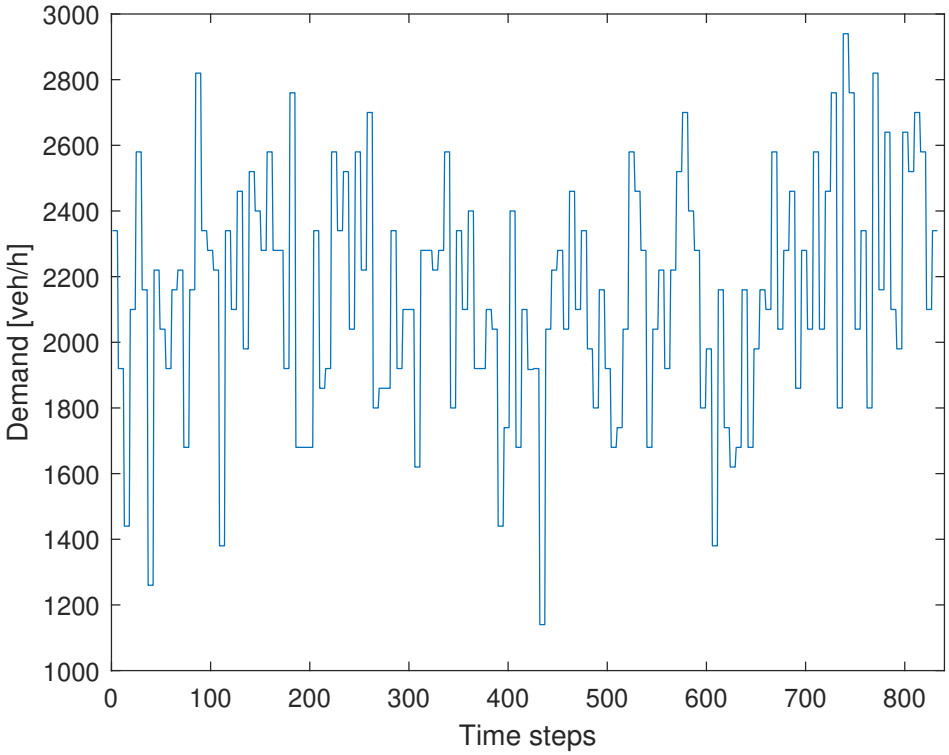

FIGURE 2.17: The real demand at the entrance of the considered stretch of the highway

For the sake of testing the new model and the effect of the clusters on traffic and congestion, we created a virtual bottleneck in the last section between time steps k=100 and k=450 by reducing the capacity of the road, as shown in Figure 2.18a and Figure 2.18b, representing respectively the densities and average traffic speeds in the network.

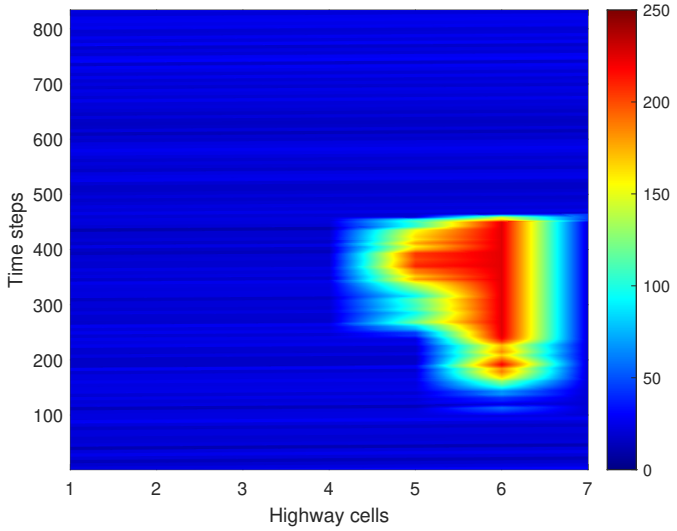

(a)

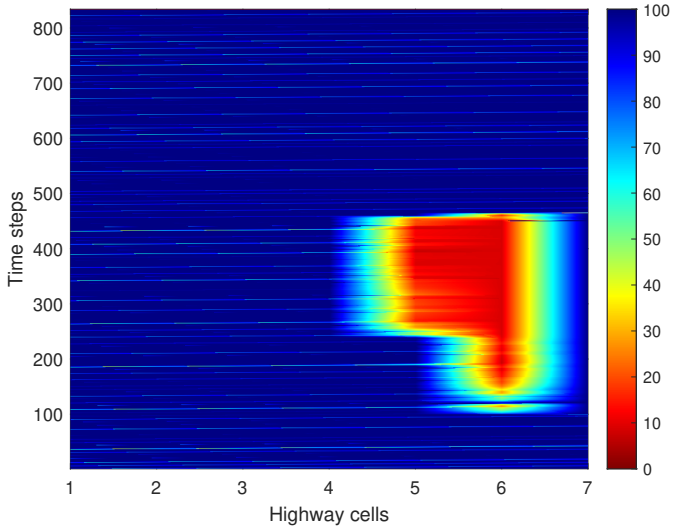

(b)

FIGURE 2.18: The density (2.18a) and speed (2.18b) in the network with a congestion created in the last cell, in the case without clusters

Then the clusters are introduced at different time steps from the beginning of the first cell of the stretch where the first and last clusters enter respectively around the beginning and the end of the congestion. Different entering time steps are chosen for all the clusters in order to evaluate their effect on the congestion, and the results are shown in Figure 2.19 to Figure 2.25. All the scenarios include 8 clusters except for the one shown in Figure 2.25 where 9 clusters enter the network.

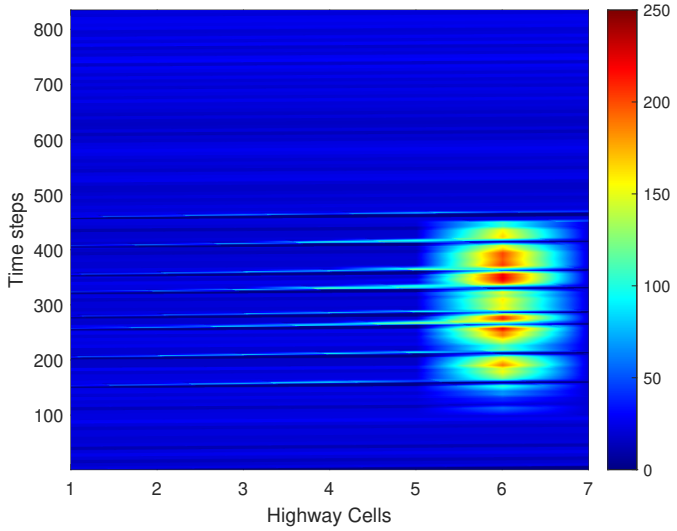

FIGURE 2.19: The density in the network with clusters entering at time steps 150, 202, 254, 276, 320, 352, 404 and 456

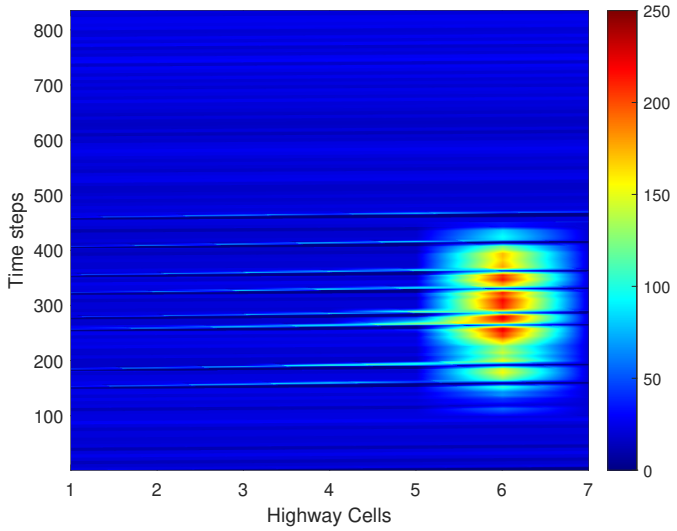

FIGURE 2.20: The density in the network with clusters entering at time steps 150, 182, 254, 276, 320, 352, 404 and 456

The moving bottlenecks are behaving as expected, where they slow down the HVs behind them, creating an increase in density which is obvious in the density plots. Doing so, they create a void in front of them, shown by the drop in the density upstream. Depending on the times of the entrance of the clusters into the network, their effect on the congestion varies because it also depends on the mainstream demand, as it is not constant. Some examples show that inserting more clusters during a fixed period of time improves the congestion, but obviously it is not realistic anymore and the penetration rate of CAVs in traffic must be very high.

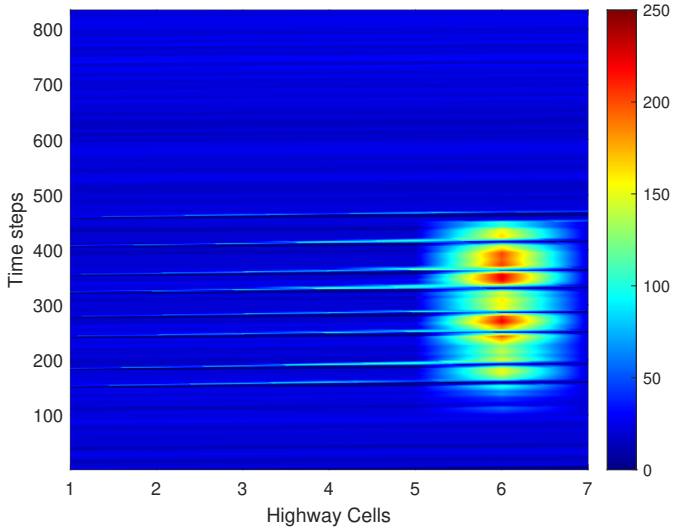

FIGURE 2.21: The density in the network with clusters entering at time steps 150, 182, 240, 276, 320, 352, 404 and 456

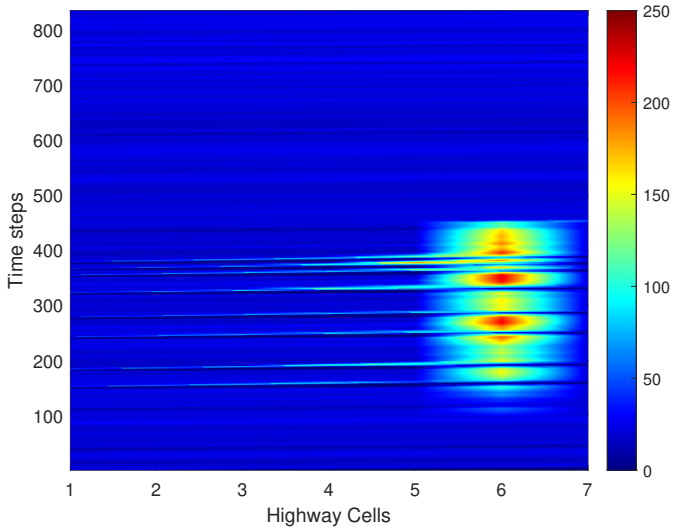

FIGURE 2.22: The density in the network with clusters entering at time steps 150, 182, 240, 276, 320, 352, 364 and 376

The results show that the clusters are able to greatly reduce congestion: in the case reported in Figure 2.21, the total time spent (TTS) of the vehicles in the network is reduced to 132 [veh.h] from 177 [veh.h] for the congested case (Figure 2.18a) and the time steps when cells were congested are reduced to 40 time steps from 300 time steps for the congested case. They are quite promising and better performance is expected when the clusters are actually controlled, especially in real time.

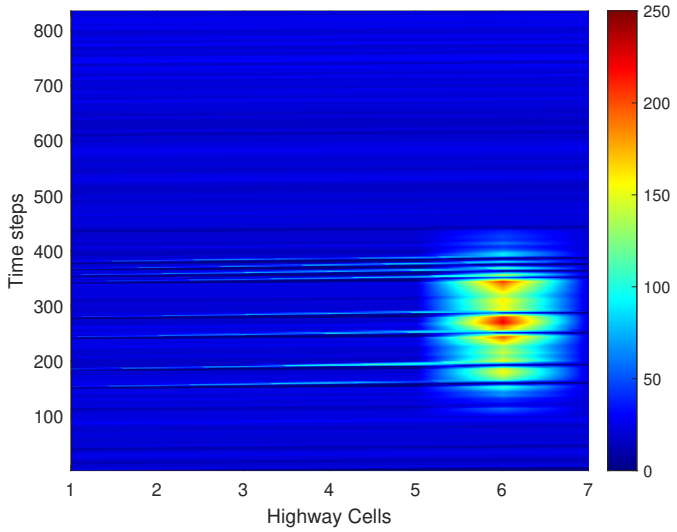

FIGURE 2.23: The density in the network with clusters entering at time steps 150, 182, 240, 276, 340, 352, 364 and 376

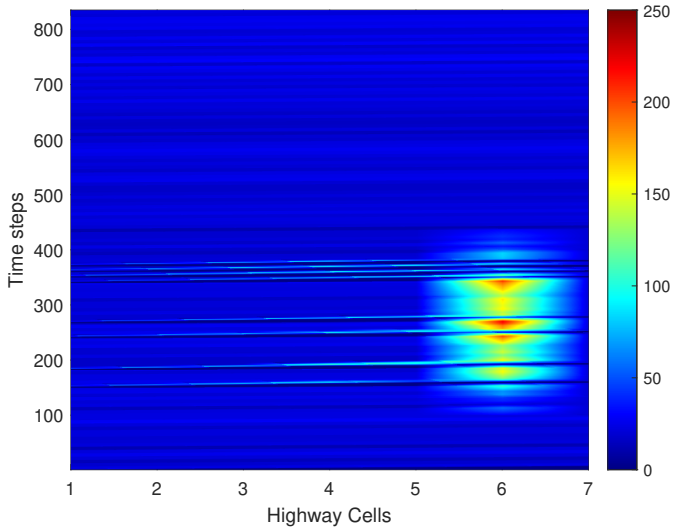

FIGURE 2.24: The density in the network with clusters entering at time steps 150, 182, 240, 267, 340, 350, 360 and 370

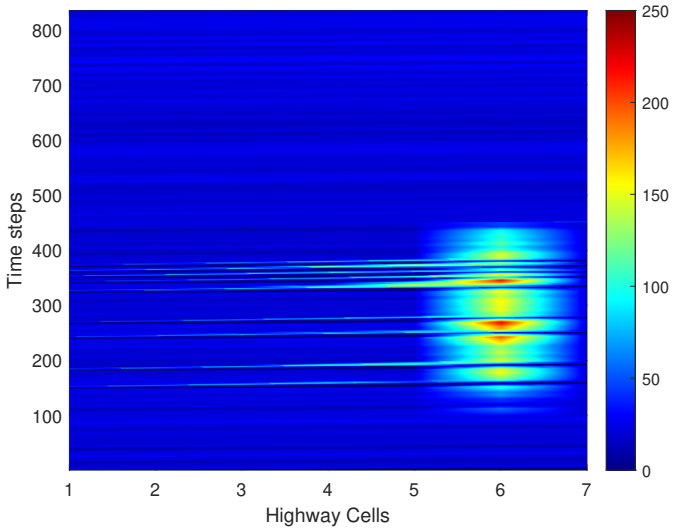

FIGURE 2.25: The density in the network with clusters entering at time steps 150, 182, 240, 267, 323, 340, 350, 360 and 370 (one more cluster, total of 9 clusters)

2.7.2 For the multi-lane model

The same A20 highway is used to test the proposed multi-lane model, but this time a longer stretch is used; it has a length of 5.2 [km] with two on-ramps and two off-ramps, shown with a red line in Figure 2.26. The number of lanes varies between 2 and 5 from one section of the stretch to another, depending on the position of the off-ramps and on-ramps; the stretch starts with 4 lanes and ends with 3 lanes and there are two lanes that remain from the beginning of the stretch until its end.

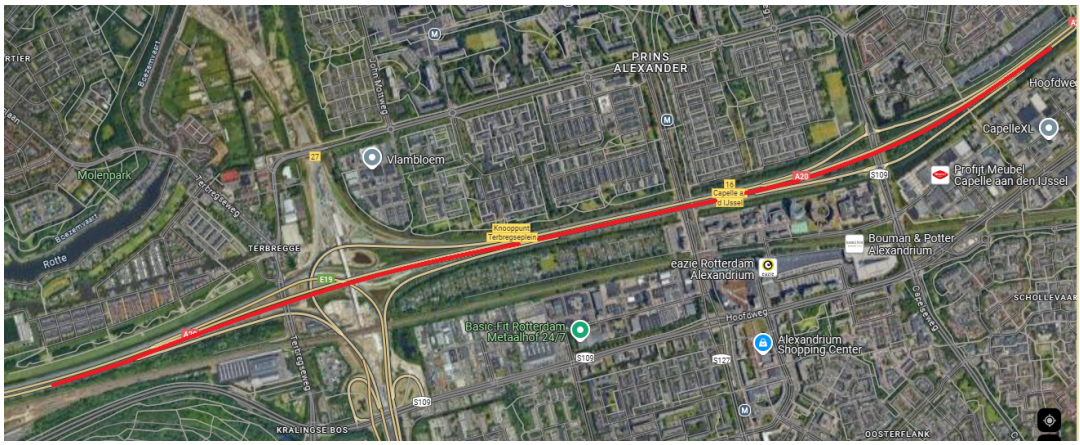

FIGURE 2.26: The highway considered and the stretch (in red) used in the simulation for the multi-lane model

Considering a cell length of Δ_i=0.4 [km] $\forall i$, the stretch is divided into N=13 cells. The free-flow speed of traffic in the network is v_i^{f}=144 [km/h], the sample time used in this case study is assumed to be T=10 seconds and the total time of the simulation is equal to 10 hours and 19 minutes, which sets the total number of time steps to K=3714 time steps. Other parameters concerning the network are: the maximum flow $q_{i,j}^{\max}$ equals to 2400 [veh/h/lane] and the maximum density $\rho_{i,j}^{\max}$ equals to 150 [veh/km/lane].

Regarding the clusters, the maximum speed a cluster can take is limited in this study to be V^c=80 [km/h] and 4 CAVs are considered to form each cluster, with 5 meters as the average length of a CAV and a time headway between the CAVs of 1 second, which sets the length of the cluster to about 87 meters on a speed of 80 [km/h]. The data used to model the demand of HVs are taken from real detectors on the highway on February 1st of the year 2023 starting from 15:20, and is shown in Figure 2.27.

For the sake of testing the new model and the effect of the clusters on traffic and congestion, we created a virtual bottleneck in the last section between

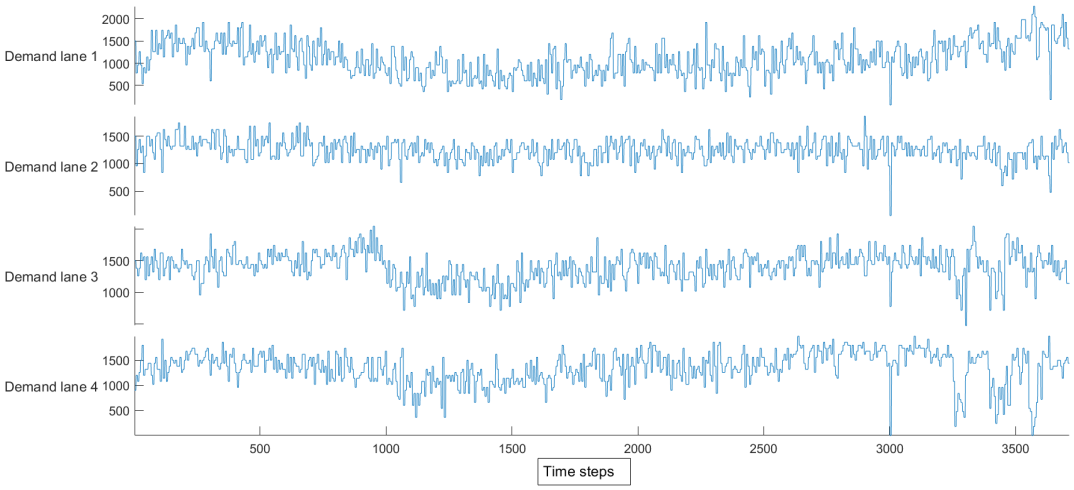

FIGURE 2.27: The real demand at the entrance of the considered stretch of the highway, for all four lanes

time steps k=100 and k=600 by reducing the capacity of the road, as shown in Figure 2.28, representing the total density in a cell, not per lane.

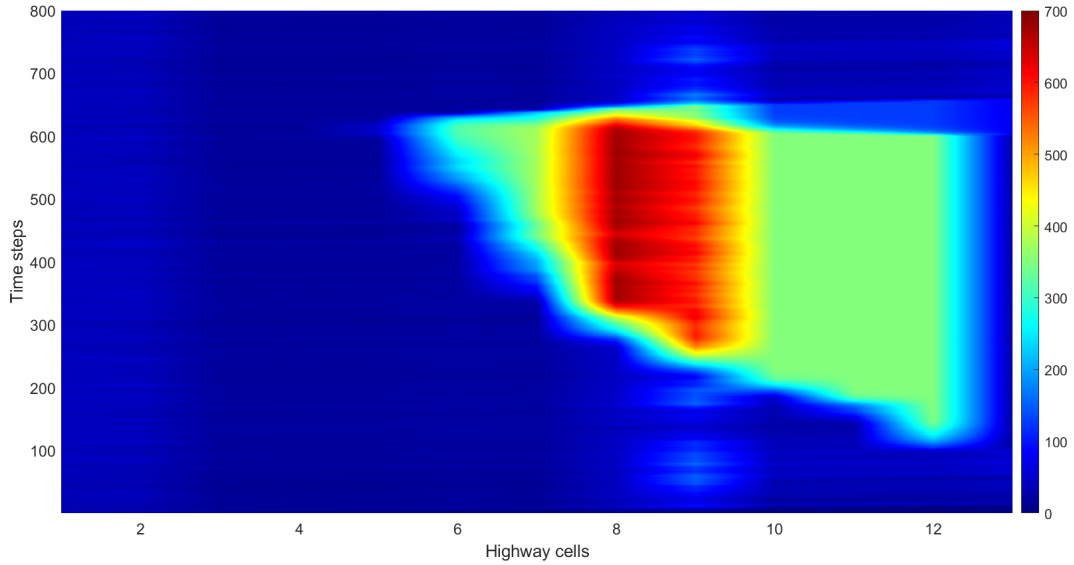

FIGURE 2.28: The density in the network with a congestion created in the last cell, in the case without clusters

Then the clusters are introduced at different time steps from the beginning of the first cell of the stretch where the first and last clusters enter respectively around the beginning and the end of the congestion. In order for the clusters to travel all the stretch without changing lanes, they are inserted in the first two lanes that remain from the beginning of the stretch until its end. Twenty clusters are introduced in total, alternated between the two lanes. The results are shown in Figure 2.29.

Like in the single-lane model, the moving bottlenecks are behaving as expected, where they slow down the HVs behind them, creating an increase in density which is obvious in the density plot when a certain cluster progresses forward in the network. While creating a void in front of them, they limit the effect of the capacity drop as now less cars are entering the congested area per time step. The results prove that, shown by less congestion compared to the no-cluster case: the TTS of the vehicles in the network was reduced from 1994 [veh.h] for the congested case (Figure 2.28) to 1642 [veh.h] (Figure 2.29) and the time steps when cells were congested were reduced from 5844 time steps for the congested case to 2975 time steps.

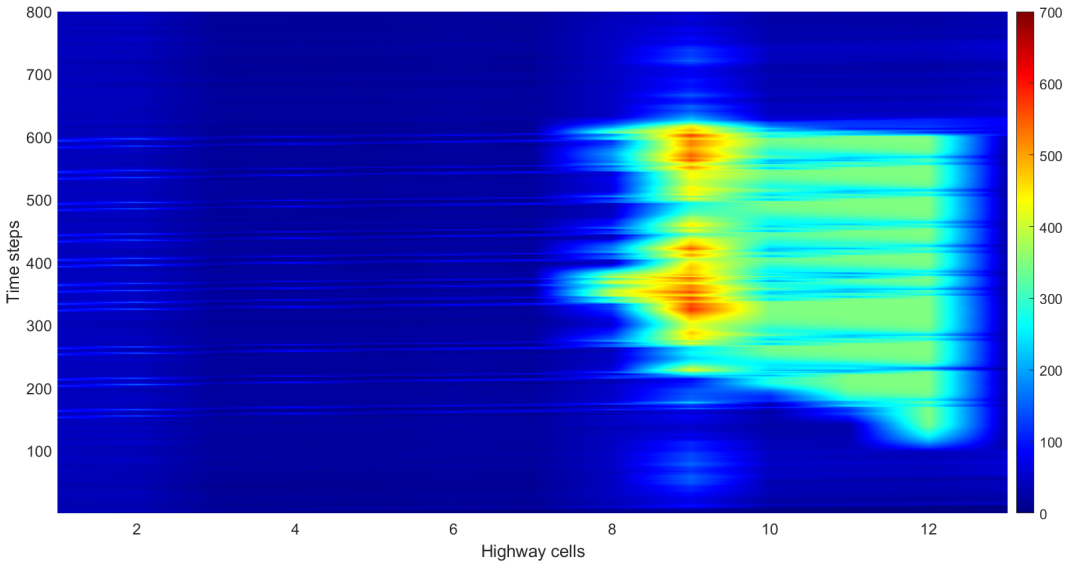

FIGURE 2.29: The density in the network with a congestion created in the last cell, with clusters entering the highway

This model opens the door for control strategies to be implemented, allowing to find the best control inputs to the system, either variables as the speed and the lane of a cluster or parameters as the number of clusters, the length of a cluster, and the schedule of entrance in the network.

2.8 Conclusions

In this chapter a review of the literature present on existing traffic flow models has been treated. In particular the best-known traffic models have been distinguished for level of detail, namely in: microscopic, mesoscopic and macroscopic models. Moreover, the state of the art concerning models of mixed traffic (HVs and CAVs) have been investigated.

In accordance with the objectives of this thesis, the METANET model has been introduced and deeply discussed, as it will be used in the work of Chapter 3.

Then, the CTM was presented in details as it is the basis to the work presented in this chapter, which is a control-oriented version of the CTM for mixed traffic. This model represents CAVs in traffic as groups, or clusters, and opens the way for vehicle-based control approaches, allowing the control of these clusters to improve the traffic flow and reduce congestion. The highway is divided to cells, thanks to the characteristics of the CTM; knowing the positions of the back and front of the clusters, these cells are divided into two categories: cells with and without CAVs. The flow and density dynamics are the modeled in a cell, depending on which category it falls into; if it is a cell without CAVs, it is modeled based on the equations of the original CTM. On the other hand, if it contains CAVs, it is divided into three parts: the cluster and two parts downstream and upstream the cluster. The whole idea of the cluster is to reduce the traffic speed behind it, so to block the flow; this allows reducing the congestion ahead or even preventing it from ever happening. Then, in this work, based on the demand of the cluster and the supplies of the downstream cell and the next cell, the speed of the cluster is simply decided based on the minimum between a fixed maximum speed (lower than the free flow speed) and the speed of traffic, but it can be the control variable in complex control schemes. A multi-lane version of this model is also presented in details, representing the lateral flows of HVs traffic. This allows the clusters to block one or more lanes instead of all of them, forcing a lane change upon traffic in addition to speed reduction. Finally, a case study for each version of the model was presented, and the results show their effectiveness in modeling mixed traffic and reducing congestion, even in the case of no control.

Chapter 3

Truck platooning

3.1 Introduction

Today's world is shaped by the technological advancements we reached since the dawn of time. Moreover, the lifestyle and the way of life of humans are maintained by the possibility of transporting people and goods all around the world, in a relatively short time like mentioned in previous chapters.

Unfortunately, also mentioned previously, the economic growth over the last decades had a toll on the environment and the natural resources of our planet. Terms like "efficiency" and "sustainability" started to appear more frequently in research and agenda for the future, as the global transportation demand is expected to keep increasing, drastically. One popular mode is the road freight transportation thanks to the flexibility and agility in scheduling, maximum traceability, and door to door services. At the same time, road haulage has several drawbacks that can be summarized into pollution (air pollution in particular), traffic congestion and road safety issues.

A possible way to mitigate the negative effects of road freight transport is to incentivize cooperation among haulers that may take place in several ways. A possible form of cooperation among carriers is known as horizontal cooperation [106] where a coalition is formed among carriers who are willing to share their transportation demand or a portion of it. In this form of cooperation, monetary compensation policies are defined for carriers who give up a trip in favor of a coalition partner. Hence, the final goal is to optimally plan the trips of the carriers so that unprofitable trips are minimized, and monetary profits are maximized so that all carriers benefit from the cooperation [26].

Another effective way to implement cooperation among carriers is the formation of truck platoons [6] which is an emerging technology in the transportation industry that involves a group of trucks traveling closely together in a convoy, usually with the assistance of advanced driver assistance systems (ADAS) and V2V communication. This technology offers potential benefits, including improved fuel efficiency, reduced traffic congestion, and enhanced road safety [129]. Several studies showed these benefits, for example [92] explores the penetration of truck platooning into the road transport in Italy, compares it to other freight transport modes cost wise and concludes that it has a very good potential in competing in the transport market. Another study is the report by the American Transportation Research Institute (ATRI) [9] that delves into the feasibility and implications of truck platooning in the U.S. and presents the challenges, impacts and benefits, including the significant potential savings in fuel costs and increasing in operational efficiency. Cooperation among carriers requires haulers to share a part of their route to form a convoy of trucks with the main objective of minimizing fuel consumption by taking advantage of the lower aerodynamic drag of trucks traveling within the platoon [81, 7].

This chapter discusses some aspects of platoon formation, like strategies, challenges, scheduling and control. Truck platooning specifically continues to garner attention nowadays as it is a highly relevant and active research area because it aligns with connected autonomous driving, sustainable logistics and smart transportation, in addition to having economic significance. Governments and organizations, especially in Europe and the US, are investing in pilot programs and standardizing platoon operations like for example the European Truck Platooning Challenge (ETPC) [44] which demonstrated large-scale viability, connecting countries like the Netherlands, Germany, and Sweden. Although the traffic conditions actually encountered during the route strongly influence the possibilities of effectively implementing platooning plans, only a few works in the literature include traffic predictions in defining the planning and control schemes for truck platoons. For this reason, the work presented in this chapter fits into this line of research by proposing a centralized control scheme executed off-board in which the optimal speeds of platoons, that might share a portion of the trip, are defined online based on the expected traffic conditions along their route. Section 3.2 gives an overview of truck platoon management, from scheduling to control and Section 3.3 presents the challenges facing platooning as well as solutions and policies to address them. Section 3.4 is based on the work published

in the 2024 European Control Conference (ECC), held in Stockholm, Sweden [32]. It presents a centralized control scheme for real-time re-planning of platoons plans defined at a strategic level, based on traffic conditions encountered along their route predicted by the METANET model that was explained in Section 2.3. This work deals with the optimal speed control of platoons traveling in freeways and, in particular, addresses the merging phase of two platoons for which it has been decided, at the strategic level, that they will meet at a specific hub located on the shared part of their routes. The two platoons have different priorities. The former has higher priority and must reach its final destination within a predefined time window, while the latter has more flexibility. The proposed control scheme has a centralized nature and is applied periodically by the platoons coordinator which receives in real time the state of the platoons and the traffic measurements on the network, based on which a traffic prediction is made. Considering the predicted traffic state, the coordinator applies an optimal control algorithm in order to decide if the merging is convenient or not and to compute the optimal speed profiles of the two platoons before the merging, during the shared journey and after the diverging phase. The proposed control scheme is tested on a case study of a freeway network in two cases, respectively in a case in which the merging of the platoons is considered convenient and one in which it is not.

3.2 The complete cycle of a platoon

3.2.1 Platoon formation and management on the low level

The first idea that needs to be explained about truck platooning is actually how a platoon is formed and managed and the technology that made it possible. This is considered under the tactical and operational levels of platooning [73] and it is the process of grouping trucks into clusters that can travel together under coordinated control to achieve operational benefits like energy efficiency, reduced travel time and enhanced safety, along with benefits for the traffic in the network like increased road capacity. The formation is handled by the vehicles themselves and once the platoon is formed, its operation must be managed to maintain safety, efficiency and robustness against disturbances using a low-level decentralized/distributed control. At first, a V2V communication is established between the trucks for real-time coordination of speed, acceleration and braking commands, using DSRC (Dedicated

Short-Range Communications), 5G, or C-V2X (Cellular V2X) [105] . Another variable needed to be controlled is the spacing between the trucks or the inter-vehicle distance in other terms. This one needs to be optimized to balance safety and aerodynamic benefits otherwise the usefulness of forming a platoon is lost. All this is possible thanks to onboard sensors that enable the trucks to perceive their surroundings and ensure safety during dynamic maneuvers:

- Lidar and Radar: detect distances to nearby vehicles and obstacles;
- Cameras: identify lane markings, road signs and surrounding traffic;
- GPS and IMU: provide precise location and orientation for accurate positioning.

The control systems that use all these data to provide optimal solutions are algorithms that maintain stability, safety and performance within a platoon, like the ACC that adjusts the speed based on the distance to the vehicle ahead, and the CACC that extends ACC by leveraging V2V communication (sharing acceleration and braking data for example) to achieve lower inter-vehicle distance and better response to disturbances. Others, like Linear Quadratic Regulation (LQR) and Model Predictive Control (MPC) are often used to provide string stability and ensure that disturbances (sudden breaking for example) do not amplify as they propagate through the platoon. In addition to that, V2I provides the trucks with data like traffic signals, road conditions and weather updates that help them optimize their routing, speed, acceleration/deceleration and inter-vehicular distance. Some studies explore adaptive control approaches, like in [162], where the authors propose an event-triggered control algorithm and even include dynamic scheduling to improve communication efficiency and system reliability during platoon formation and maintenance. Other works in the literature deal with the definition of path planning of vehicles traveling within a truck convoy. These studies involve the development of automatic control strategies to actuate longitudinal and lateral control of vehicles [49, 15] and to follow the trajectory defined by the leader truck and maintain a predetermined intra-vehicle space [17]. Moreover, AI was recently added to the list helping vehicles take some decisions and reconfigure the platoon based on real-time conditions [159]. It also can detect issues like sensor failures, communication disruptions or erratic driver behavior. All these technologies also allow trucks or smaller platoons to join and form a bigger one, or split, dynamically on the road without stopping, which is useful when trucks have different origins

and/or destinations, but this decided by a higher level of control and coordination. The study in [41] investigates efficient platoon formation at unsignalized intersections, leveraging advanced coordination protocols to reduce delays and improve traffic flow. Key technologies include V2V and V2I communication. [41] also emphasizes the importance of predictive merging strategies for dynamic environments.

3.2.2 Platoon formation and scheduling on the high level

The ultimate goal of transportation companies is to deliver the merchandise from an origin to a destination before a deadline. Scheduling ensures that this goal is achieved and delays are minimized by planning the right departure times of the trucks/platoons and the places where they can meet to form a bigger platoon, or split. Schedules can be pre-planned, based on historical data and traffic patterns, or they can be dynamic and get adjusted in real-time based on live traffic data, weather conditions, vehicle delays, etc.

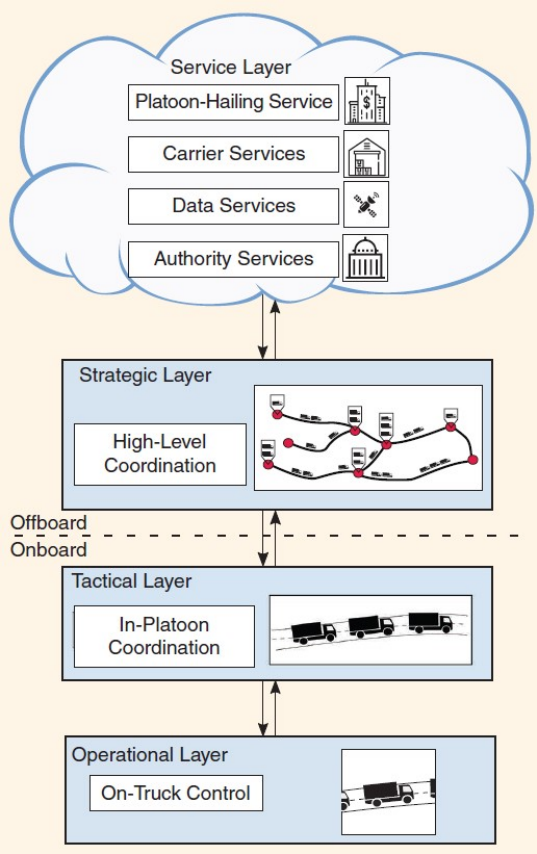

FIGURE 3.1: The different levels of the platooning system. *Source: A. Johansson et al. 2022 [73]*

The levels of platooning here are higher than those of the previous sections and are called the service and strategic levels [73], where high-level decisions are made that are executed off-board to define the platoon plans and in particular to coordinate trucks that have compatible schedules and missions, defining times, rendezvous points, and speed profiles required to join a platoon. On these levels, the cooperation among carriers is studied as well. The definition of planning and control schemes for truck platooning has been extensively studied in the scientific literature and put into practice through various research projects (see for instance [25, 51, 120]). In particular, the most recent projects on this topic, Sweden4Platooning [12] and ENSEMBLE [116], have addressed multi-brand platooning by also considering competing carriers. As part of the latter projects, a scheme of the hierarchical decision-making structure for the formation and control of platoons has been developed. Many research works are devoted to the optimal definition of platoon plans, i.e. the definition of compatible truck trips, platoon routing, platoon formation and management, meeting points, and so on (see for instance the works in [73, 1, 64, 45]). In fact, coming from different origins, trucks can join together to form a platoon in several ways: during the route [63, 86] or at a certain point in the network (a parking area, gas station, etc.) where one truck, or platoon, can wait for other trucks to join it [74, 82]. The more platoons are formed in a day, where trucks join each other on the common part of their trip, the more the rewards and profits are higher [83]. The idea is to maximize the profit from platooning (fuel savings, cost reduction, less congestion, etc.) while respecting the schedule of the deliveries and not increasing the overtime payments of the drivers (see [18] for a complete overview of truck platooning planning).

3.3 Key difficulties and challenges

Truck platooning from beginning to end is not an easy task. Like discussed before, it is a complex problem that presents several challenges arising in the domains of scheduling, control, communication, formation, and overall operational efficiency. Trucks can originate from different locations and/or carriers and this complicates forming and maintaining the efficiency of platoons. The coordinator has to synchronize the whole operation with the complications of variable times, routes, and destinations and ensure that no significant or even minor delays occur. Possible solutions could be platoon formation in

hubs, like studied in [74, 82] and predictive scheduling to dynamically coordinate platoons like in [65].

In addition to the complexity of managing thousands of trucks in urban and interurban scenarios, fuel efficiency has to be balanced with operational costs and delivery time constraints, otherwise platooning has no direct benefit to the carriers. Some studies focus on this challenge, like the one in [17] where the authors propose a delay-based spacing policies to optimize fuel efficiency. The goal is to address environmental regulations and carbon footprint goals while ensuring that fuel savings outweigh the costs as the economic viability of truck platooning depends on effective coordination among stakeholders. It is worth noting that fuel consumption is strongly correlated with traffic conditions encountered during the route. Despite that, only a few works in the literature include traffic prediction in defining the planning or control scheme of platoons (see, for example, the works in [87, 112, 124, 23]). The thesis work described in this chapter falls in this line of work, considering that traffic accidents or unexpected congestion can disrupt schedules, leading to delays or missed opportunities for platooning.

Another high level challenge is the multi-carrier cooperation and achieving it can be faced with competitive interest and lack of trust among carriers, especially when it comes to sharing operational data and resources. Data privacy is crucial and the collection and sharing of data among platooning trucks and infrastructure elements must comply with data privacy regulations. Protecting sensitive information, such as vehicle locations and operational data is very important for fleet owners to have trust in forming platoons with others [47]. Truck platooning relies heavily on interconnected systems and requires constant communication between vehicles, that's why ensuring the cybersecurity of these systems and the integrity and security of V2V communication channels is essential to prevent unauthorized access, data breaches, and potential cyberattacks [138] [46] that could cause interference and tampering with communication or even leak sensitive data [56]. Various security and policy considerations must be addressed for the successful implementation of multi-carrier cooperation, including establishing global standards for V2V communication that ensures compatibility not only across manufacturers but also across regions especially for cross-border operations. Governments should offer subsidies or tax breaks for fleets adopting platooning technology along with dedicated infrastructure such as road lanes for platoons, reducing conflicts with other traffic especially human driven vehicles.

During the Dutch presidency of the EU, The Netherlands initiated the European Truck Platooning Challenge (ETPC) [44] that explores the potential of truck platooning in Europe and the steps required to integrate it into the transportation system. The initiatives of this project aim to maximize the environmental and economic benefits while addressing challenges related to safety, liability, and technology adoption, and one of them is evaluating platooning performance on dedicated lanes to optimize traffic flow and improve fuel efficiency.

3.4 Real-time planning of platoons coordination decisions based on traffic prediction

Many projects implemented planning and control strategies for truck platooning (like Sweden4Platooning and ENSEMBLE, mentioned earlier) and they consider a scheme of hierarchical decision-making structure for the formation and control of platoons that has been developed. Like described in Section 3.2, this scheme is given in [73] and consists of four levels: service, strategic, tactical, and operational. The service and strategic levels are the two decision-making levels that produce high-level decisions, which are executed off-board to define the platoon plans and in particular to coordinate trucks that have compatible schedules and missions, defining times, rendezvous points, and speed profiles required to join in a platoon. The tactical and operational levels are performed on-board and consist of maintaining vehicle cohesion within each platoon and safely executing the maneuvers of trucks entering and exiting from the platoons (tactical level) and longitudinal control of each vehicle so as to meet the acceleration and speed profiles defined at the tactical level (operational level).

The work reported in this section was presented in the ECC 2024 [32] and falls between the strategic and tactical levels by proposing a centralized control scheme executed off-board that aims to re-plan the coordination decisions taken at the strategic level, considering the influence of traffic conditions predicted in real time. This is a crucial aspect, since traffic conditions can significantly influence the choices defined at a higher planning level, making the decision to merge platoons no longer convenient or even not feasible. Unlike existing studies in the literature, in this work the speed profiles of the platoons are defined online by a *platoons coordinator* that, with a predictive control scheme, periodically makes a prediction of traffic conditions

on the routes in which the platoons are traveling and determines whether it is convenient or not to meet and the optimal speed they should maintain to respect their schedule. In more detail, this preliminary work focuses on the coordination of two platoons for which it has been decided, at the strategic level, that they will meet at a specific hub (rendezvous point) located on the shared part of their routes. It is worth noting that considering the influence of traffic conditions in the coordination of platoons is even more important if the platoons that have to meet have different time requirements; thus, we consider the case in which one of the two platoons is constrained to arrive at its final destination within a predefined time window (e.g., the case of a platoon that needs to reach in time a seaport gate equipped with truck appointment systems), while the second platoon has more flexibility in reaching its final destination. Therefore, from now on we will call *priority platoon* the platoon that has the main objective of reaching the final destination at a given time, while we will call *non-priority platoon* the one that has more flexibility, but for which the choice of merging depends on the time when the priority platoon is expected to arrive at the rendezvous point.

3.4.1 The control scheme of the platoons coordinator

The proposed control scheme has a centralized nature since the online platoons coordinator knows the schedules and missions of both platoons and receives in real time the state of the platoons and the traffic measurements on the network used to initialize the traffic prediction. Based on this information, the coordinator solves some cascading problems. The first optimal control problem solved by the coordinator determines the optimal speed that allows the priority platoon to arrive at its final destination at the scheduled time. Based on the solution of this optimization problem, the expected arrival time of the priority platoon at the hub is determined and used to solve a second optimal control problem. This second optimal control problem aims to determine whether it is convenient to meet at the hub and, if so, to define the optimal speed the non-priority platoon must maintain to arrive at the hub at the expected arrival time of the priority platoon. If, conversely, the solution of this optimization problem shows that the meeting is not convenient or even impossible, the two platoons proceed disjointly. This means that the platoons coordinator periodically solves, for both the platoons, two optimization problems (as the one solved for the priority platoon) allowing them to reach the final destination at the scheduled time, as shown in Fig. 3.2.

Both optimization problems use the traffic speed along the routes of the platoons calculated by the traffic prediction model METANET (Section 2.3) to determine the speed profile that the platoons should follow.

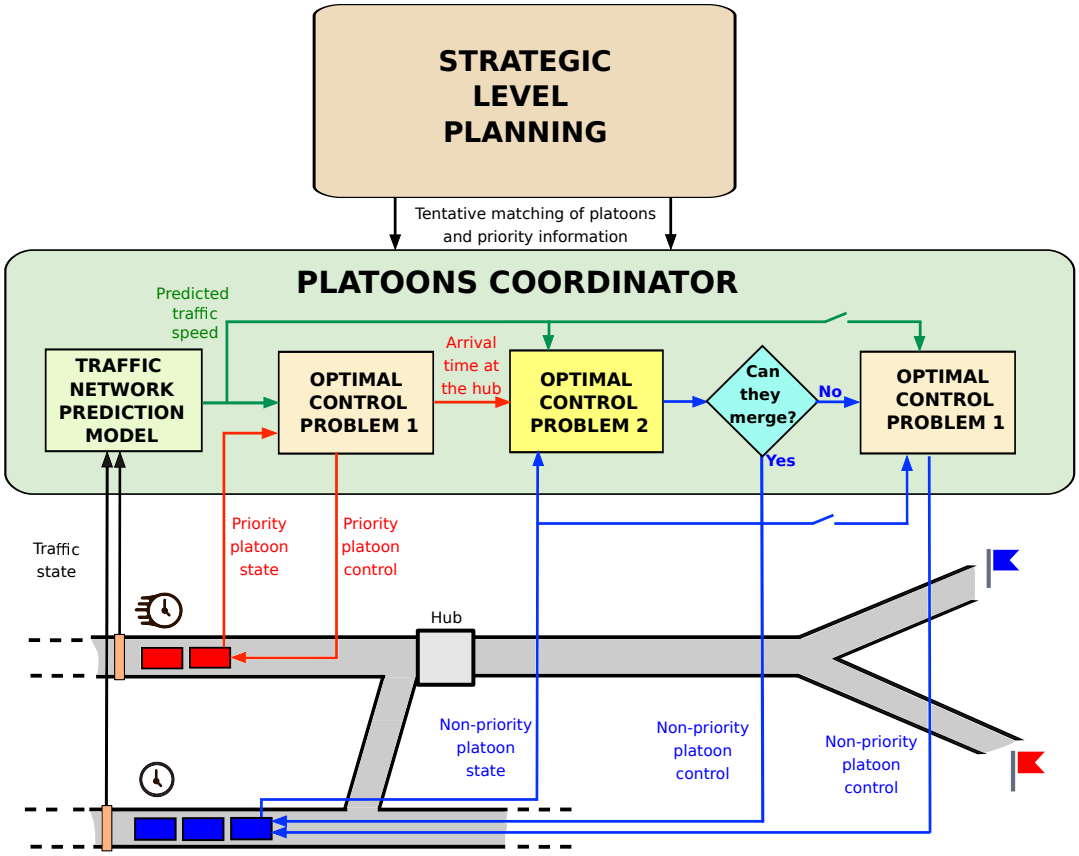

FIGURE 3.2: The proposed control scheme for determining the convenience of the merging between platoons.

In case the meeting at the hub is convenient, the first optimal control problem is solved periodically (with the goal of minimizing the delay of the priority platoon) from the time in which the two platoons merge until when they diverge to reach their respective final destinations. Then, starting from the time in which the platoons diverge, the first optimal control problem is again solved periodically but disjointly for the two platoons with the objective of meeting their respective schedules.

In the following sections, the optimization problems and the control algorithms solved by the online platoons coordinator are presented.

3.4.2 Traffic-based optimal control problems

This section introduces the optimal control problems solved in cascade by the platoons coordinator to define the optimal speed profiles of the priority and

non-priority platoons. In the following we will refer to the priority platoon using the superscript P, to the non-priority platoon using the superscript N, while we will use the superscript X to denote a generic platoon that can be either a priority platoon or a non-priority platoon. Furthermore, we denote with $\mathcal{K}^{\mathrm{X}}$ the set of k time steps composing the time horizon associated with platoon X. The optimal control problems presented below are based on the traffic prediction obtained by applying the METANET model described in Section 2.3 on the portion of the network consisting of the set of freeway links $\mathcal{M}^{\mathrm{X}}$, the set of sections $\mathcal{I}^{m,\mathrm{X}}$, the set of origin links $\mathcal{O}^{\mathrm{X}}$, and the set of nodes $\mathcal{N}^{\mathrm{X}}$ that belong to the route of platoon X.

Optimal control problem to reach the final destination

This optimal control problem allows to define the optimal speed of a platoon that aims to reach the final destination of its journey while limiting delays from its scheduled arrival time. Let us consider a generic platoon X whose final destination has a distance Π^{X} from its initial position, expressed in [km], and must be reached at time step $K^{\mathrm{fin,X}}$. The optimal platoon speed is found by considering the predicted traffic speed $v_{m,i}(k)$ for all $i \in \mathcal{I}^{m,\mathrm{X}}$, $m \in \mathcal{M}^{\mathrm{X}}$ and for all $k \in \mathcal{K}^{\mathrm{X}}$ and considering that the platoon X has a truck minimum speed $v^{\mathrm{min,X}}$, defined to comply with the traffic laws and for reasons of cost-effectiveness of the trip (fuel consumption, driving hours, etc.). Moreover, $v^{\mathrm{max,X}}$ denotes the maximum speed of the platoon.

For platoon X the state variable is the position $p^{\mathrm{X}}(k)$, in [km], defined as the distance from the initial position of the platoon, while the control variable is the speed that is denoted with $v^{\mathrm{X}}(k)$ in [km/h]. Some auxiliary variables are needed in order to compute the position of the platoon in the network used for the traffic prediction (see the traffic model described in Section 2.3) and to have linear constraints. To this end we denote with $p_{m,i}$ the position in [km] of the beginning of section $i \in \mathcal{I}^{m,\mathrm{X}}$ of link $m \in \mathcal{M}^{\mathrm{X}}$, then the auxiliary variables are defined as follows:

- $y^{\mathrm{X}}_{m,i}(k) \in \{0,1\}$ is equal to 1 if $p^{\mathrm{X}}(k) \geq p_{m,i}$, i.e. if platoon X is after the beginning of section i of link m at time step k, 0 otherwise;
- $w^{\mathrm{X}}_{m,i}(k) \in \{0,1\}$ is equal to 1 if $p^{\mathrm{X}}(k) \leq p_{m,i+1}$, i.e. if platoon X is before the beginning of section $i+1$ of link m at time step k, 0 otherwise;
- $\lambda^{\mathrm{X}}_{m,i}(k) \in \{0,1\}$ is introduced to represent the product $y^{\mathrm{X}}_{m,i}(k) \cdot w^{\mathrm{X}}_{m,i}(k)$, therefore $\lambda^{\mathrm{X}}_{m,i}(k)$ is equal to 1 if platoon X is in section i of link m at time

step k (i.e. if $y^{\mathrm{X}}_{m,i}(k) = w^{\mathrm{X}}_{m,i}(k) = 1$), 0 otherwise.

The optimal control problem to reach the final destination of a platoon X, which can be a priority platoon, with $\mathrm{X} = \mathrm{P}$, or a non-priority platoon, with $\mathrm{X} = \mathrm{N}$, can be stated with the following mixed-integer linear quadratic formulation.

Problem 1

$$\begin{aligned} \min \quad & \alpha_1 \left(\Pi^{\mathrm{X}} - p^{\mathrm{X}}(K^{\mathrm{fin,X}}) \right)^2 \\ & + \alpha_2 \sum_{k \in \mathcal{K}^{\mathrm{X}}} \left(v^{\mathrm{X}}(k+1) - v^{\mathrm{X}}(k) \right)^2 \end{aligned} \tag{3.1}$$

subject to:

$$p^{\mathrm{X}}(k+1) = p^{\mathrm{X}}(k) + v^{\mathrm{X}}(k)T \qquad k \in \mathcal{K}^{\mathrm{X}} \tag{3.2}$$

$$p^{\mathrm{X}}(k) - p_{m,i} + M\big(1 - y^{\mathrm{X}}_{m,i}(k)\big) \geq \epsilon \qquad i \in \mathcal{I}^{m,\mathrm{X}},\ m \in \mathcal{M}^{\mathrm{X}},\ k \in \mathcal{K}^{\mathrm{X}} \tag{3.3}$$

$$p_{m,i} - p^{\mathrm{X}}(k) + M y^{\mathrm{X}}_{m,i}(k) \geq 0 \qquad i \in \mathcal{I}^{m,\mathrm{X}},\ m \in \mathcal{M}^{\mathrm{X}},\ k \in \mathcal{K}^{\mathrm{X}} \tag{3.4}$$

$$p_{m,i+1} - p^{\mathrm{X}}(k) + M\big(1 - w^{\mathrm{X}}_{m,i}(k)\big) \geq 0 \qquad i \in \mathcal{I}^{m,\mathrm{X}},\ m \in \mathcal{M}^{\mathrm{X}},\ k \in \mathcal{K}^{\mathrm{X}} \tag{3.5}$$

$$p^{\mathrm{X}}(k) - p_{m,i+1} + M w^{\mathrm{X}}_{m,i}(k) \geq \epsilon \qquad i \in \mathcal{I}^{m,\mathrm{X}},\ m \in \mathcal{M}^{\mathrm{X}},\ k \in \mathcal{K}^{\mathrm{X}} \tag{3.6}$$

$$\lambda^{\mathrm{X}}_{m,i}(k) \leq y^{\mathrm{X}}_{m,i}(k) \qquad i \in \mathcal{I}^{m,\mathrm{X}},\ m \in \mathcal{M}^{\mathrm{X}},\ k \in \mathcal{K}^{\mathrm{X}} \tag{3.7}$$

$$\lambda^{\mathrm{X}}_{m,i}(k) \leq w^{\mathrm{X}}_{m,i}(k) \qquad i \in \mathcal{I}^{m,\mathrm{X}},\ m \in \mathcal{M}^{\mathrm{X}},\ k \in \mathcal{K}^{\mathrm{X}} \tag{3.8}$$

$$\lambda^{\mathrm{X}}_{m,i}(k) \geq y^{\mathrm{X}}_{m,i}(k) + w^{\mathrm{X}}_{m,i}(k) - 1 \qquad i \in \mathcal{I}^{m,\mathrm{X}},\ m \in \mathcal{M}^{\mathrm{X}},\ k \in \mathcal{K}^{\mathrm{X}} \tag{3.9}$$

$$v^X(k) \geq \sum_{m \in \mathcal{M}^X} \sum_{i \in \mathcal{I}^{m,X}} \lambda^X_{m,i}(k) v^{\min,X}_{m,i}(k) \qquad k \in \mathcal{K}^X \tag{3.10}$$

$$v^X(k) \leq \sum_{m \in \mathcal{M}^X} \sum_{i \in \mathcal{I}^{m,X}} \lambda^X_{m,i}(k) v^{\max,X}_{m,i}(k) \qquad k \in \mathcal{K}^X \tag{3.11}$$

where ϵ is a small quantity arbitrarily chosen and M is a large quantity arbitrarily chosen.

In the objective function of Problem 1, the first term, weighted with α_1, penalizes the quadratic difference between the actual position of the platoon $p^X(K^{\text{fin},X})$ at the final time step and its expected final position Π^X. The second cost term, weighted with α_2, allows to limit the oscillations of the speed between two consecutive time steps.

Constraints (3.2) are the state equations for the platoon and compute the covered distance on the basis of its speed. Constraints (3.3)-(3.9) are introduced to correctly define the position of the platoon along the freeway network. Specifically, according with the state variable $p^X(k)$, constraints (3.3)-(3.4) allow to define the binary variables $y^X_{m,i}(k)$, (3.5)-(3.6) allow to define the binary variables $w^X_{m,i}(k)$, while constraints (3.7)-(3.9) define $\lambda^X_{m,i}(k)$ on the basis of $y^X_{m,i}(k)$ and $w^X_{m,i}(k)$.

Constraints (3.10)-(3.11) impose lower and upper bounds for the speeds. More in detail, (3.10) impose that the speed of the platoon has to be greater than the speed $v^{\min,X}_{m,i}(k)$ defined as $v^{\min,X}_{m,i}(k) = \min\{v^{\min,X}, v_{m,i}(k)\}$. Constraints (3.11) impose that the speed of the platoon cannot exceed $v^{\max,X}_{m,i}(k)$ defined as $v^{\max,X}_{m,i}(k) = \min\{v^{\max,X}, v_{m,i}(k)\}$.

Optimal control problem to reach the hub

This optimal control problem allows to define the speed of a non-priority platoon that wants to join the priority platoon in a predefined hub position π^{hub} at the time step $\tilde{k}^{\text{P}}$ defined by taking into account the position of the priority platoon in the optimal solution of Problem 1. The hub position is defined with respect to the original position of the non-priority platoon N and is expressed in [km]. The decision of the non-priority platoon to join or not the priority platoon depends whether it can arrive at the meeting point on time or not. In particular, the decision of not merging can occur under two circumstances: first, the non-priority platoon arrives too late (e.g., the non-priority platoon finds congestion along its route); second, the non-priority platoon arrives too early and the waiting time at the meeting point is not compensated

by the benefit obtainable from platooning (e.g., the priority platoon finds congestion on its route and the resulting expected arrival time at meeting point is not convenient for the non-priority platoon).

Analogously to Problem 1, the state variable is represented by the position of the non-priority platoon $p^{\mathrm{N}}(k)$ and the control variable is the speed of the platoon $v^{\mathrm{N}}(k)$. In order to formalize the optimal control problem, an auxiliary binary variable must be added expressing whether or not the non-priority platoon joins the priority platoon:

- $z^{\mathrm{N}} \in \{0,1\}$ is equal to 1 if the merging occurs and equal to 0 if it does not occur.

Furthermore, let us denote with B the profit [€] that the non-priority platoon can obtain by joining the priority platoon, and with W the unit waiting cost for the non-priority platoon if it arrives early at the meeting point [€/km]. Thus, the objective of this optimal control problem is to define the speed of the non-priority platoon so as to maximize the profit achievable by traveling with the priority platoon, taking into account the cost due to waiting at the meeting point, i.e.

$$\max \quad Bz^{\mathrm{N}} - W\left(p^{\mathrm{N}}(\tilde{k}^{\mathrm{P}}) - \pi^{\mathrm{hub}}\right) \cdot z^{\mathrm{N}} \tag{3.12}$$

The objective function (3.12) has a nonlinear form, then the auxiliary variable Γ^{N} is introduced in order to formulate a mixed-integer linear problem. Specifically, this variable is included to express the product $p^{\mathrm{N}}(\tilde{k}^{\mathrm{P}}) \cdot z^{\mathrm{N}}$ and is defined as follows

$$\Gamma^{\mathrm{N}} = \begin{cases} p^{\mathrm{N}}(\tilde{k}^{\mathrm{P}}) & \text{if } z^{\mathrm{N}} = 1 \\ 0 & \text{if } z^{\mathrm{N}} = 0 \end{cases} \tag{3.13}$$

Hence, using the auxiliary variable Γ^{N}, the optimal control problem can be stated with the following mixed-integer linear formulation.

Problem 2

$$\max \quad Bz^{\mathrm{N}} - W\left(\Gamma^{\mathrm{N}} - z^{\mathrm{N}}\pi^{\mathrm{hub}}\right) \tag{3.14}$$

subject to constraints (3.2)-(3.11), *with* $\mathrm{X} = \mathrm{N}$, *and to:*

$$p^{\mathrm{N}}(\tilde{k}^{\mathrm{P}}) - \pi^{\mathrm{hub}} + \sigma \geq -L^{\max} + (L^{\max} + \delta)z^{\mathrm{N}} \quad (3.15)$$

$$-\overline{\Delta V} \leq v^{\mathrm{N}}(k+1) - v^{\mathrm{N}}(k) \leq \overline{\Delta V} \quad k \in \mathcal{K}^{\mathrm{N}} \setminus \{K^{\mathrm{N}} - 1\} \quad (3.16)$$

$$\Gamma^{\mathrm{N}} \leq L^{\max} z^{\mathrm{N}} \quad (3.17)$$

$$\Gamma^{\mathrm{N}} \geq 0 \quad (3.18)$$

$$\Gamma^{\mathrm{N}} \leq p^{\mathrm{N}}(\tilde{k}^{\mathrm{P}}) \quad (3.19)$$

$$\Gamma^{\mathrm{N}} \geq p^{\mathrm{N}}(\tilde{k}^{\mathrm{P}}) - L^{\max}(1 - z^{\mathrm{N}}) \quad (3.20)$$

where σ and δ are small quantities.

The first term of the objective function of Problem 2 refers to the profit obtainable by traveling in platoon, while the second term determines the waiting cost at the hub.

Constraints (3.15) allow the decision variable z^{N} to be appropriately defined. Specifically, the constraint is defined so that if $p^{\mathrm{N}}(\tilde{k}^{\mathrm{P}}) - \pi^{\mathrm{hub}} \geq 0$ (the non-priority platoon is early or on time), the decision variable z^{N} can take either value 0 or value 1 in accordance with the goal of maximizing (3.14). If $p^{\mathrm{N}}(\tilde{k}^{\mathrm{P}}) - \pi^{\mathrm{hub}} < 0$ (the non-priority platoon is late), then the decision variable can only be $z^{\mathrm{N}} = 0$. In (3.15) σ is a tolerance on position and is defined such that $\sigma > \delta$, while $L^{\max}$, in [km], is the maximum path length that the non-priority platoon can travel.

Constraints (3.16) allow to avoid undesired fluctuations of speed imposing that the speed variation between one time step and the next one cannot exceed $\overline{\Delta V}$ [km/h]. Note that K^{N} is fixed as $K^{\mathrm{N}} = \tilde{k}^{\mathrm{P}} + \varpi$, with ϖ being a given tolerance.

Finally, constraints (3.17)-(3.20) are included to impose the relation defined in (3.13).

3.4.3 The control algorithm of the platoons coordinator

As introduced above, the traffic prediction model reported in Section 2.3 and the optimal control problems described in Section 3.4.2 are periodically run by the platoons coordinator. In particular, let us assume that they are run at

each time step $\bar{k} = nS$, where $n = 0, 1, 2, \ldots$ and S is an integer representing the number of time steps between one run and the next one.

The considered time horizon for Problem 1 starts from the actual time $\bar{k}$ and goes until the expected arrival time at destination, which is in general different for the two platoons since it depends on the time required to cover their routes, and is given by $K^{\text{fin,P}}$ and $K^{\text{fin,N}}$ respectively. Let $K = \max\{K^{\text{fin,P}}, K^{\text{fin,N}}\}$. As for Problem 2, instead, the time horizon starts in $\bar{k}$ and goes to $\tilde{k}^{\text{P}} + \varpi$.

In particular, three different control schemes are applied according to the decision of merging or not. More precisely, Control Algorithm 1 is applied by the platoons coordinator at a generic time step $\bar{k}$ if the merging decision is still valid and up to $\tilde{k}^{\text{P}}$. If the merge is executed, i.e., $z^{\text{N}} = 1$, the Control Algorithm 2 is applied to find the optimal speed of the platoon created at the hub, which for simplicity of notation is still called priority platoon, that has the goal of reaching the final destination at $K^{\text{fin,P}}$. Control Algorithm 2 is applied periodically until the platoons diverge to reach their respective final destinations or until the end of the considered horizon if the two platoons have the same destination. Control Algorithm 3 is instead applied periodically, until the end of the time horizon, after the platoons diverge or if, by applying Control Algorithm 1, it results that the merging phase is not convenient or impossible, i.e., $z^{\text{N}} = 0$.

Control Algorithm 1 Control algorithm applied by the platoons coordinator before the platoon merging

1: Measure the traffic state $\rho_{m,i}(\bar{k})$,$v_{m,i}(\bar{k})$ $m = 1,\dots,M$, $i = 1,\dots,N_m$, $l_o(\bar{k})$, $o = 1,\dots,O$ - Go to Step 2
2: Run the traffic prediction model with $\mathcal{K} = \{\bar{k},\dots,K\}$ - Go to Step 3
3: Measure the priority platoon state $p^{\mathrm{P}}(\bar{k})$ - Go to Step 4
4: Solve Problem 1 with X = P and $\mathcal{K}^{\mathrm{P}} = \{\bar{k},\dots,K^{\mathrm{fin,P}}\}$, and compute $\tilde{k}^{\mathrm{P}}$ - Go to Step 5
5: Actuate the optimal speed profile of the priority platoon $v^{\mathrm{P}}(k)$, $\bar{k} \leq k \leq \bar{k}+S-1$ - Go to Step 6
6: Measure the non-priority platoon state $p^{\mathrm{N}}(\bar{k})$ - Go to Step 7
7: Solve Problem 2 with X = N and $\mathcal{K}^{\mathrm{N}} = \{\bar{k},\dots,\tilde{k}^{\mathrm{P}}+\varpi\}$, with $\tilde{k}^{\mathrm{P}}$ obtained in Step 4 - Go to Step 8
8: Check the value of z^{N}. If $z^{\mathrm{N}} = 1$, go to Step 9, otherwise go to Step 10
9: Actuate the optimal speed profile of the non-priority platoon $v^{\mathrm{N}}(k)$, $\bar{k} \leq k \leq \bar{k}+S-1$
10: Communicate to the platoons the decision of not merging - Go to Step 11
11: Solve Problem 1 with X = N and $\mathcal{K}^{\mathrm{N}} = \{\bar{k},\dots,K^{\mathrm{fin,N}}\}$ - Go to step 12
12: Actuate the optimal speed profile of the non-priority platoon $v^{\mathrm{N}}(k)$, $\bar{k} \leq k \leq \bar{k}+S-1$ - Go to step 13
13: Apply Control Algorithm 1 from now on

Control Algorithm 2 Control algorithm applied by the platoons coordinator after the merging and until the platoons diverge

1: Measure the traffic state $\rho_{m,i}(\bar{k})$,$v_{m,i}(\bar{k})$ $m = 1,\dots,M$, $i = 1,\dots,N_m$, $l_o(\bar{k})$, $o = 1,\dots,O$ - Go to Step 2
2: Run the traffic prediction model with $\mathcal{K} = \{\bar{k},\dots,K\}$ - Go to Step 3
3: Measure the priority platoon state $p^{\mathrm{P}}(\bar{k})$ - Go to Step 4
4: Solve Problem 1 with X = P and $\mathcal{K}^{\mathrm{P}} = \{\bar{k},\dots,K^{\mathrm{fin,P}}\}$ - Go to Step 5
5: Actuate the optimal speed profile of the priority platoon $v^{\mathrm{P}}(k)$, $\bar{k} \leq k \leq \bar{k}+S-1$

Control Algorithm 3 Control algorithm applied by the platoons coordinator if the merging decision is not valid or after the platoons diverge

1: Measure the traffic state $\rho_{m,i}(\bar{k})$,$v_{m,i}(\bar{k})$ $m = 1,\dots,M$, $i = 1,\dots,N_m$, $l_o(\bar{k})$, $o = 1,\dots,O$ - Go to Step 2
2: Run the traffic prediction model with $\mathcal{K} = \{\bar{k},\dots,K\}$ - Go to Step 3
3: Measure the priority platoon state $p^{\mathrm{P}}(\bar{k})$ - Go to Step 4
4: Solve Problem 1 with X = P and $\mathcal{K}^{\mathrm{P}} = \{\bar{k},\dots,K^{\mathrm{fin,P}}\}$ - Go to Step 5
5: Actuate the optimal speed profile of the priority platoon $v^{\mathrm{P}}(k)$, $\bar{k} \leq k \leq \bar{k}+S-1$ - Go to Step 6
6: Measure the non-priority platoon state $p^{\mathrm{N}}(\bar{k})$ - Go to Step 7 Solve Problem 1 with X = N and $\mathcal{K}^{\mathrm{N}} = \{\bar{k},\dots,K^{\mathrm{fin,N}}\}$ - Go to step 8
7: Actuate the optimal speed profile of the non-priority platoon $v^{\mathrm{N}}(k)$, $\bar{k} \leq k \leq \bar{k}+S-1$

3.5 Case study and results

In order to test the proposed control scheme, two cases considering the possible pairing of two platoons have been taken into account. Specifically, we have applied the control algorithms introduced in Section 3.4.3 to two couples of platoons traveling on a freeway network of ten links (m1 to m10), two origin links (o1 and o2), five on-ramp links (o3 to o7), and in which the hub where the meeting may occur is located at the beginning of the first section of link m7, as shown in Fig. 3.3. In this case study we have assumed that the sample time interval T is equal to 10 seconds, while the number of time steps between two executions of the optimal control problems S has been set to 6, implying a recalculation of the control actions every minute. Furthermore, for each platoon, we have assumed that the maximum speed is $v^{\max,X}$=75 km/h, while the minimum speed is $v^{\min,X}$ = 50 km/h.

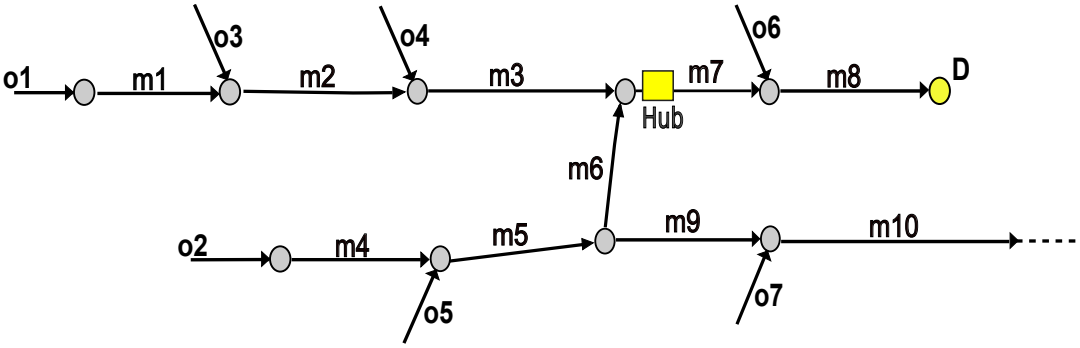

FIGURE 3.3: The freeway network in which the platoons are traveling.

Concerning the first pair of platoons, the priority platoon starts its journey at $k = 0$ from link o1 and must arrive at destination D at $K^{\text{fin,P}}$ = 95, passing through sections m1, m2, m3, m7 and m8. The total trajectory length of the priority platoon to its destination is Π^{P} = 15.4 km, while the non-priority platoon starts its journey again at $k = 0$, but entering from link o2 and passing through links m4, m5 and m6 to reach the hub located in link m7, which makes the length of the path of the non-priority platoon to that point π^{hub} = 8.4 km. If the non-priority platoon does not join the priority platoon, it continues its path alone, through links m7 and m8 after the meeting point, to reach the destination D at $K^{\text{fin,N}}$ = 100, which makes its route length Π^{N} = 14 km.

For this case, the platoons coordinator, based on the traffic prediction on the road network, determines with Control Algorithm 1 that the platoons

merging is convenient (see the traffic speed predicted overall by the platoon coordinator in Fig. 3.4). The meeting takes place at time step $\tilde{k}^{\mathrm{P}} = 52$, and the speed profiles to be implemented by the priority platoon and the non-priority platoon to perform the rendezvous at the hub are shown in Figs. 3.5a and 3.5b, respectively, while Fig. 3.5c depicts the speed profile of the platoon created at the hub to reach the final destination.

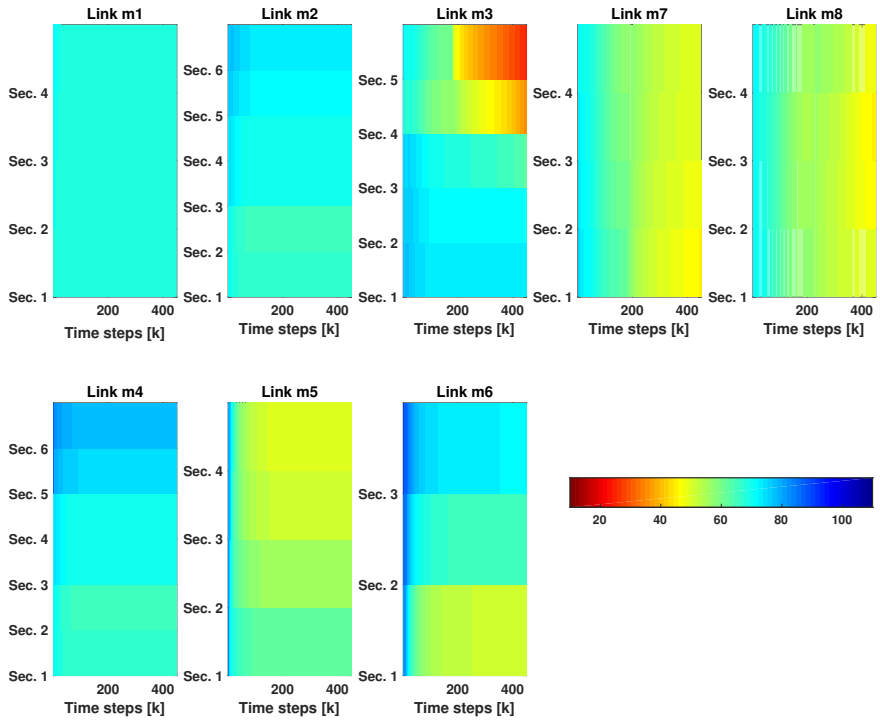

FIGURE 3.4: Traffic speed predicted by the platoons coordinator on the platoon routes.

Let us now consider the second pair of platoons examined in this case study, which cover the same routes of the first couple of platoons but in different time frames. Specifically, the priority platoon begins its journey at $k = 300$ and must reach its final destination at $K^{\mathrm{fin,P}} = 395$, while the non-priority platoon starts its journey at $k = 320$ and should reach its destination at $K^{\mathrm{fin,N}} = 420$. The platoons coordinator predicts congestion on the path of the priority platoon, which makes the meeting with the non-priority platoon at the hub impossible. Therefore, the platoons coordinator optimizes the speed of each platoon disjointly according to Control Algorithm 3, and the resulting speed profiles for each platoon are displayed in Fig. 3.6.

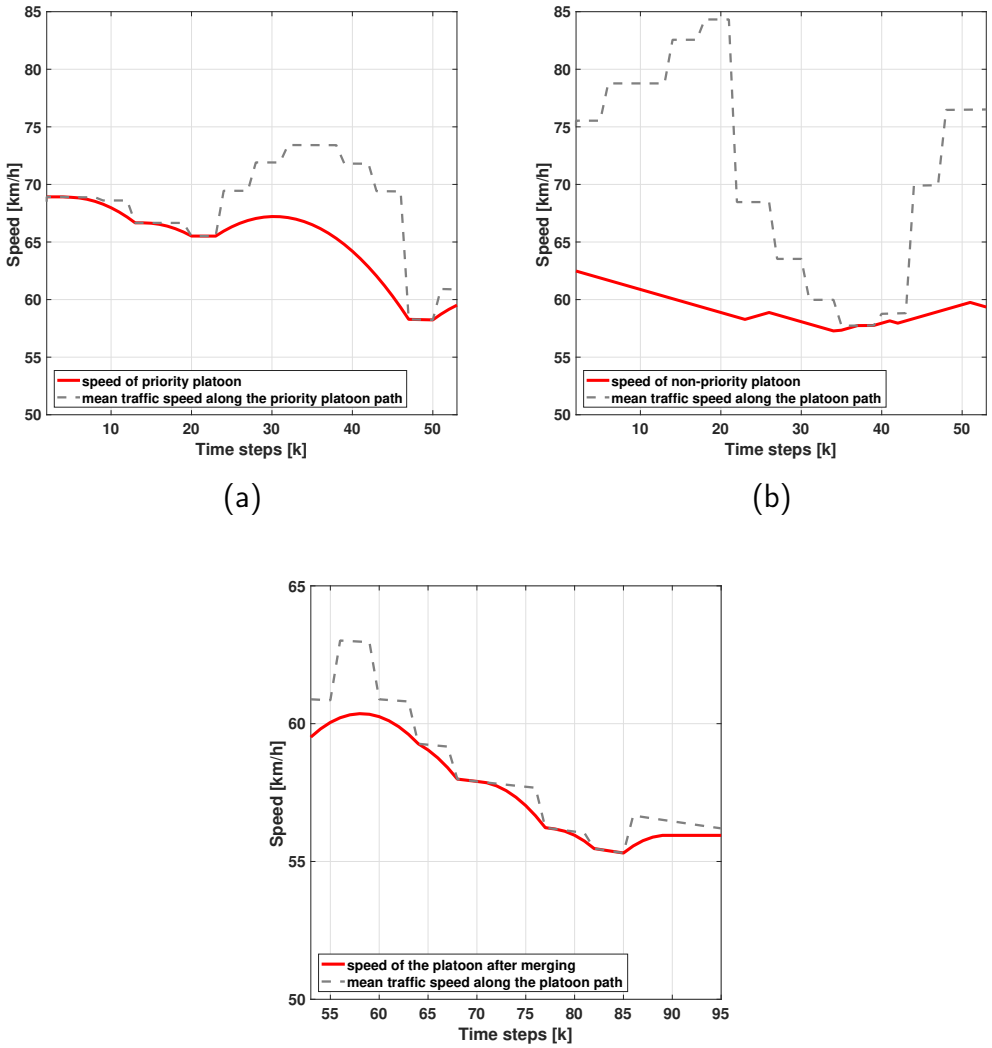

FIGURE 3.5: Speeds implemented by the first pair of platoons (red lines) compared with the mean traffic speed in the stretch where the platoons are traveling (dashed gray lines): speed of the priority platoon (3.5a) and the non-priority platoon (3.5b) before the merging at the hub, speed of the platoon created after the merging at the hub up to the final destination (3.5c).

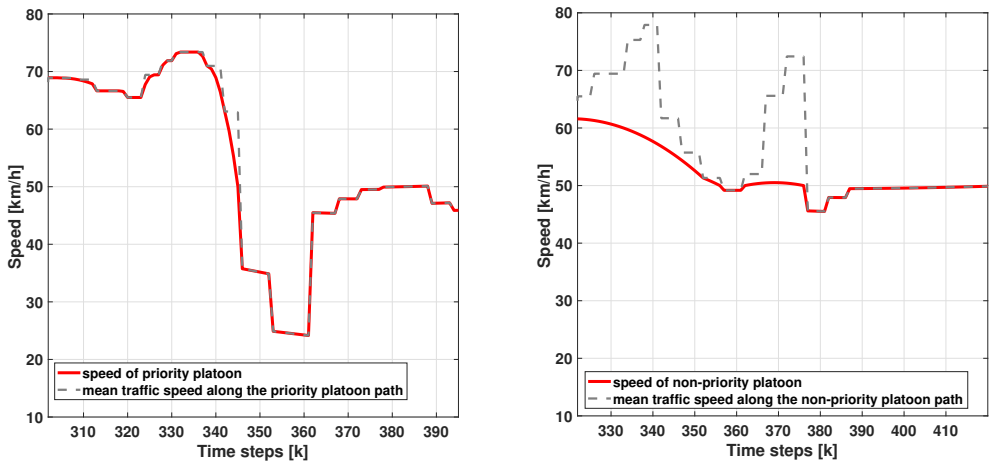

FIGURE 3.6: Speeds implemented by the second pair of platoons (red lines) compared with the mean traffic speed in the stretch where the platoons are traveling (dashed gray lines): speed of the priority platoon (3.6a) and the non-priority platoon (3.6b) to reach their final destinations.

3.6 Conclusions

This chapter focuses on truck platooning and its steps and process, from the technology that made it possible all the way to the planning and scheduling to allow the trucks to arrive at their destinations on time. The chapter starts with the importance nowadays of platooning, especially for trucks, in the terms of sustainability and improving traffic flow conditions. The complete cycle of a platoon is presented through a literature review: on the low level, the many innovations that allow for the grouping of trucks into platoons, and on the high level, the strategies and schemes that improve the scheduling and open the door for cooperation among different carriers.

In addition to that, this chapter also shows the difficulties and challenges that were and still are standing in the way. One of these problems is the effect of unpredicted traffic conditions on the arrival on time of the trucks. Unfortunately, this aspect was not studied very well in the literature, and the work in this chapter of the thesis comes as a contribution to that part of the state of the art. A centralized control scheme has been proposed for real-time re-planning of platoons plans defined at a strategic level. The proposed control scheme consists of optimizing the speeds of the platoons before the merging, during the shared journey and after the diverging phase, based on predictions of traffic conditions on the routes traveled by the platoons. In addition, the proposed control problems also allow the determination of whether or not it is convenient for the platoons to merge into a single platoon and share part of their route. The proposed control algorithms are based on the periodic resolution of mixed-integer linear problems, either with a quadratic cost or with a linear cost, while the prediction of traffic conditions is performed by the METANET model.

Chapter 4

Eco-driving

4.1 Introduction

As a part of the global plan to achieve environmental sustainability, eco-driving defines a set of driving behaviors that benefit both the drivers, by reducing fuel or energy consumption, and the environment, by mitigating emissions. Researchers have been working on various strategies to enhance eco-driving, such as developing advanced control algorithms for autonomous and connected vehicles, optimizing vehicle trajectories to minimize energy usage, and integrating real-time traffic and road condition data for improved efficiency. Additionally, efforts have been made to incorporate regenerative braking systems, especially in electric vehicles, to further reduce energy losses. These advancements are crucial in creating more sustainable transportation systems, particularly as the demand for mobility continues to rise globally.

Eco-driving falls under the sustainability theme of this thesis; in this chapter, overviews of the techniques and energy/fuel consumption models used are outlined in Section 4.2 and Section 4.3 respectively, while Section 4.4 presents in details the energy consumption model used as cost criterion for the work proposed in Section 4.5 that refers to eco-driving concepts for electric vehicles with regenerative braking. It was submitted to a scientific journal, is currently under review and is available as a pre-print [33]. Specifically, this work aims to find the optimal kinematic trajectory of an EV, driving from any current initial state (position and speed) to a fixed final state, within a fixed or free time horizon, with the primary objective of mitigating the energy consumption of the vehicle. In more details, such trajectories are determined as solutions of an optimal control problem having the acceleration of the electric vehicle as control input, and the position and speed as state variables.

A power-based energy model, detailed in Section 4.4, is used to calculate the consumption of energy and its regeneration while braking, resulting in a non-smooth model with some discontinuities. In order to solve the problem, different approaches are considered, based on different approximations of the power-based model. Subsequently, an intermediary stop point problem is created where a traffic signal is placed on the way of the vehicle, and the previous approaches are modified accordingly by adding new constraints. Comparison among results obtained from all the approaches are reported and discussed for diverse initial state and signal timing scenarios. In particular, it is demonstrated that the simple square-of-acceleration approximation delivers excellent eco-driving control trajectories, something that may be leveraged to simplify problems arising in other eco-driving situations.

4.2 Overview of eco-driving techniques

Along with economic growth, human society is witnessing environmental problems and resource scarcity. Environmental consciousness has led lately the industries to target a more sustainable future, including the automotive industry, which is a significant contributor to greenhouse emissions, from the manufacturing of the vehicles to their operation and end-of-life disposal. The incessant rise in global fuel consumption, coupled with environmental concerns and the escalating price of energy, demands a thorough reassessment of current practices. On the individual level, the behavior of the driver impacts substantially the energy efficiency of their vehicle [96]. From this principle, an eco-friendly driving approach emerges and fosters sustainability: eco-driving [14] requires drivers to adopt a set of fuel-efficient behaviors, like gradual acceleration/deceleration and keeping an optimal steady speed when possible. The drivers are also asked to minimize idling, reduce excess weight, optimally use the gears, and other prudent driving approaches. Nowadays with autonomous driving, eco-driving takes a step beyond individual actions and incorporates advancements in technology to further enhance fuel economy. Previous studies used predictive algorithms to optimize cruise control settings based on upcoming road conditions, traffic, and topography for fuel efficiency. For example, in [69], the optimal values of starting-up acceleration and cruising speed over hilly terrains or flat roads were determined for fuel-efficient driving; in [151], an eco-cooperative adaptive cruise control (Eco-CACC) system was developed that computes the fuel-optimum vehicle trajectory through a signalized intersection. The method used was

initially the formulation of an optimal control problem and its solution using mainly dynamic programming (DP) [14, 94, 75]; but because of its impracticality, DP was replaced with other faster methods, like linear programming [43] and non-linear programming methods (NLP) [149]. On the other hand, the Pontryagin's Maximum Principle (PMP) was also used, whose necessary optimality conditions transform the optimal control problem into a two-point boundary value problem [60]. This method gives an analytic solution that fits into a real-time calculation of speed since it requires low computational effort compared to nonlinear programming solutions [143].

Another significant facet in the face of global challenges posed by climate change and the finite nature of conventional energy sources, is the accelerating transition towards EVs as a pivotal element in the broader strategy to mitigate energy consumption. The convergence of advancements in battery technology, coupled with a growing societal awareness of environmental impacts, has propelled EVs into the spotlight as a transformative force in the transportation sector [5]. Eco-driving principles can be then extended to EVs, aligning with the broader goal of sustainable and energy-efficient transportation. While some traditional eco-driving practices still apply, the unique characteristics of EVs introduce specific considerations for maximizing efficiency and range. Similarly to conventional ICE vehicles, efficient use of an EV involves smooth acceleration and deceleration, and maintaining a consistent speed. An advantage that EVs have is regenerative braking, which contributes to energy efficiency by recovering and converting kinetic energy back into electrical energy. This process helps extend the vehicle range and improve overall efficiency by harnessing between 30% and 78% of energy that would be otherwise lost [22]. Many previous works studied eco-driving of EVs, either through data-driven techniques [84], or through the solution of an optimal control problem, [4][160], or using hybrid techniques [103][154], with the general goal to render transportation practices more sustainable and energy-efficient. For cases where a vehicle is approaching a traffic light, a family of systems called GLOSA (Green Light Optimal Speed Advisory) [134], were developed to provide real-time information to drivers about the optimal speed to approach a traffic signal in order to reduce stops, energy and emissions, and also improve traffic flow. Previous studies improved or modified GLOSA systems to be suitable for EVs. For example, [131] considers a multi-segment route in an urban environment where the EV must cross many consecutive traffic lights. On the other hand, [160] considers only one

intersection but takes into consideration the vehicle queue length at the traffic light and tracks the driver's speed tracking error. The work presented in Section 4.5 can pave the way for the usage of simpler methods in GLOSA to calculate the speed trajectories of the EVs [133] instead of the current algorithms.

4.3 Overview of fuel/energy consumption models

Energy consumption modeling has become an essential research area to optimize vehicle performance, enhance efficiency, and support sustainable transportation. In every work or study related to eco-driving, an energy (or fuel, for ICE vehicles) consumption model that estimates power requirement of the EV is essential and in [90], an overview of EV energy consumption models is presented, such as the Vehicle Specific Power (VSP) model [155] and the Virginia Tech Comprehensive Power-based EV Energy Consumption Model (VT-CPEM) [50]. These models take into consideration fundamental physical aspects of the vehicle and what is required to move it from one point to another. including speed conditions. The most important of these aspects are the traction force, the rolling resistance, the aerodynamic drag and the gravitational force, basically the vehicle dynamics, along with the powertrain efficiency. Some models take a step further by representing environmental conditions, driving cycles and behavior, and the vehicle load. For EVs, in addition to the battery and electric motor efficiencies, recent models incorporate the energy regeneration capability of the braking system [19] [158], with efficiency of recent ones ranging from 60% to 80%.
For ICE vehicles, using the squared acceleration as an approximation for the fuel consumption model [66][91] is a common approach in the field of eco-driving and vehicle energy management to avoid complex models. The reasoning behind using this approximation is that higher accelerations generally result in increased fuel consumption due to higher air resistance and power demands on the engine. Thus by penalizing rapid changes in velocity (acceleration), the optimization aims to find smoother and more fuel-efficient driving profiles. On the other hand, other researchers criticized this simplified model as it does not take into consideration the reduced fuel consumption during deceleration of the vehicle, but counts it as a normal phase. In [143], a comparison of optimal trajectories obtained from both this simple model and a complex fuel consumption model was carried out, and it was demonstrated that the simple model delivers excellent approximations

of the accurate control solutions. Concerning EVs, adding to the previous disadvantage, the squared acceleration does not reflect the regenerative braking during deceleration, which is a gained energy. A comparison between minimum-energy trajectories of specific scenarios obtained from this simple approach and more complex and realistic energy consumption models does not exist, to the best of our knowledge. The energy consumption model, detailed in the next section, incorporates energy recovery using regenerative braking and is used in Section 4.5.

4.4 Power-based model for estimating energy consumption and regeneration

Models that estimate power requirements of EVs share similarities and focus on the instantaneous resistive forces acting on the vehicle moving at the required acceleration and speed [53], which are:

- Inertia:
$$R_i(t) = m \cdot a(t) \tag{4.1}$$
where m is the mass of the vehicle $[kg]$ and $a(t)$ is the instantaneous acceleration of the EV $[m/s^2]$ at time t,

- Road friction:
$$R_f(t) = m \cdot g \cdot f \cdot \cos(\theta(t)) \tag{4.2}$$
where g is the gravitational acceleration $[m/s^2]$, f is the friction coefficient between the road and the wheels, and $\theta(t)$ is the inclination of the road at time t,

- Gravitational force:
$$R_g(t) = m \cdot g \cdot \sin(\theta(t)), \tag{4.3}$$

- Air drag:
$$R_d(t) = 1/2 \cdot \rho \cdot A \cdot C_d \cdot v(t)^2 \tag{4.4}$$
where ρ is the air density $[kg/m^3]$, A is the frontal surface area of the vehicle $[m^2]$, C_d is the drag coefficient and $v(t)$ is the instantaneous speed of the EV $[m/s]$ at time t.

Considering a horizontal road ($\theta(t) = 0$), the sum of the resistive forces F yields the following:

$$F(v(t), a(t)) = m \cdot a(t) + m \cdot g \cdot f + 1/2 \cdot \rho \cdot A \cdot C_d \cdot v(t)^2 \tag{4.5}$$

As mentioned previously, EVs currently are equipped with regenerative brakes that allow them to recover part of the energy that is otherwise totally lost as heat. While accelerating, an electric current flows from the batteries to the electric motors moving the wheels, and the total force acting on the car is positive. But during the braking phase, the total force is negative and the recovered energy serves as a current flowing back from the wheels to the battery, thus recharging it. That mentioned, the total force at the electric motors F_m is given by:

$$F_m(v(t), a(t)) = \begin{cases} F(v(t), a(t)) & if\ F(v(t), a(t)) > 0\ (accelerating), \\ \eta \cdot F(v(t), a(t)) & if\ F(v(t), a(t)) \leq 0\ (braking), \end{cases} \tag{4.6}$$

where η represents the efficiency of the regenerative braking of the EV. As $\eta < 1$, the force at the motors can be represented in a different way:

$$F_m(v(t), a(t)) = \max[F(v(t), a(t)), \eta F(v(t), a(t))]. \tag{4.7}$$

The power at the motors $P_m(v(t), a(t))$ can then be calculated using:

$$P_m(v(t), a(t)) = F_m(v(t), a(t)) \cdot v(t), \tag{4.8}$$

and the power produced or received by the batteries is calculated through [160]:

$$P_b(v(t), a(t)) = P_m(v(t), a(t)) \cdot \eta_b^{-\text{sign}(P_m(v(t), a(t)))} \cdot \eta_m^{-\text{sign}(P_m(v(t), a(t)))} + P_a \cdot \eta_b^{-1} \tag{4.9}$$

where η_b and η_m are the efficiencies of the battery and the electric motors respectively, and P_a represents the auxiliary power used for the radio, lights and air conditioning. This equation shows that, when braking, the battery is receiving power ($P_m(v(t), a(t))$ and $P_b(v(t), a(t))$ have negative values) less than the power produced at the wheels (reduced by the efficiencies η_b and η_m).

4.5 Optimal control methodologies for eco-driving of electric vehicles with regenerative braking

As mentioned in Section 4.1, this work is submitted to a scientific journal [33] and is still under review, and focuses on finding the optimal trajectory of an EV equipped with regenerative braking, driving from an initial state (position and speed) to a fixed final one, within a fixed or free time horizon, with the primary objective to reduce the energy consumption of the vehicle. To this end, an optimal control problem is defined that minimizes a cost function holding a dynamic power-based model that reflects energy consumption and restoration (through regenerative braking), with the acceleration of the vehicle serving as the control input. The energy consumption model presented in Section 4.4 is complex and includes some discontinuities and non-smooth parts that make it difficult to get an exact optimal solution. Therefore, a smoothened version of the original energy consumption model is considered to obtain a quasi exact numerical solution via an efficient feasible direction algorithm [109][110]. Furthermore, two simpler approximations are utilized to determine if they yield vehicle trajectories similar to the optimal ones. First, an analytical solution of the problem is obtained using PMP and a quadratic approximation of the power-based energy consumption model. Using the same methodology, the second approach consists of using an even simpler criterion that is based on the square-of-acceleration. Subsequently, the problem is extended with a stop point, reflecting a traffic signal on the way of the EV to its destination. This new problem is solved with similar approaches as the previous problem, but with new constraints added, taking into consideration that the traffic light switches from red to green after a fixed time. Comparison among results obtained from all the approaches for both problems are reported and discussed for diverse initial state and signal timing scenarios. In particular, it is demonstrated that the simple square-of-acceleration approximation delivers excellent eco-driving control trajectories. This is practically significant result that may be leveraged to simplify problems arising in other, more complex EV eco-driving situations.

4.5.1 Optimal control problems without stop points

Eco-driving aims at maximizing fuel/energy efficiency, in other words minimizing fuel/energy consumption, while driving from an origin to a destination safely and comfortably. In this work, an EV has to follow a trajectory from an initial state $\mathbf{x_0} = [p_0, v_0]^\top$, where p_0 and v_0 are the given initial position and speed of the vehicle respectively, to a final state $\mathbf{x_e} = [p_e, v_e]^\top$ within a time horizon T that can be fixed or free, where p_e and v_e are the fixed vehicle final position and speed, respectively. Note that the case of a free time horizon should be taken into consideration appropriately in the problem to ensure a logical and finite duration of the trip. As an eco-driving problem, the total energy consumption should be minimized while ensuring that the vehicle reaches its final state within T. That is achieved by finding the optimal control inputs (accelerations) over time in order to have the optimal speed trajectory.

The minimization problem mentioned above is formulated as the following optimal control problem, in which $p(t)$ and $v(t)$ represent the system state variables.

Problem 3 *Given the system initial conditions $p(0) = p_0$ and $v(0) = v_0$, find the optimal control $a(t)$, $t = 0, ..., T$, that minimizes*

$$J = \int_0^T P_b(v(t), a(t))dt. \tag{4.10}$$

subject to the state equations of vehicle motion:

$$\dot{p}(t) = v(t) \tag{4.11}$$

$$\dot{v}(t) = a(t), \tag{4.12}$$

and the final state conditions:

$$x(T) = x_e, \tag{4.13}$$

$$v(T) = v_e. \tag{4.14}$$

Acceleration may be bounded between a minimum and a maximum value, and the speed between zero and a maximum value, if necessary. More complex, e.g. speed-dependent, acceleration terms may be directly considered or

added to the above criterion as penalty terms. In the following subsections, some alternative approaches are reported to solve *Problem 1*.

Approach A-QA: Analytic solution using a quadratic approximation of the power-based energy consumption model

The first approach is to solve the problem analytically using a quadratic approximation of the power-based energy consumption model, i.e. the function $P_b(v(t), a(t))$ in (4.9). As P_b is a function of the instantaneous speed $v(t)$ and acceleration $a(t)$, its quadratic approximation, $\tilde{P}_b^{QA}(v(t), a(t))$, has the following form:

$$\tilde{P}_b^{QA}(v(t), a(t)) = b_1 + b_2 \cdot v(t) + b_3 \cdot a(t) + b_4 \cdot v(t) \cdot a(t) + b_5 \cdot v(t)^2 + b_6 \cdot a(t)^2. \tag{4.15}$$

One way to obtain the coefficients b_i, $i = 1, ..., 6$, and bypass the non differentiability of the max and sign functions, is by using the least square difference [42]. The method consists of finding the optimal values of the parameters by minimizing the sum of the squared difference between values of $P_b(v(t), a(t))$ and $\tilde{P}_b^{QA}(v(t), a(t))$ in (4.15):

$$\min \sum_{v=v_1}^{v_2} \sum_{a=a_1}^{a_2} (\tilde{P}_b^{QA}(v, a) - P_b(v, a))^2, \tag{4.16}$$

where v_1, v_2, a_1 and a_2 are the boundaries of the intervals of speed and acceleration respectively in which the fitting of $\tilde{P}_b^{QA}(v(t), a(t))$ to $P_b(v(t), a(t))$ is obtained. Those values also determine, along with the counting steps, the number of points used for the fitting. The function $\tilde{P}_b^{QA}(v(t), a(t))$ can be used as an approximation of the power-based model $P_b(v(t), a(t))$ within the optimal control problem.

The approximate fuel consumption optimal control problem considers then the minimization of the quadratic approximation for the energy consumption $\tilde{P}_b^{QA}(v(t), a(t))$, i.e. the optimal control problem to be solved is:

Problem 4 *Given the system initial conditions $p(0) = p_0$ and $v(0) = v_0$, find the optimal control $a(t)$, $t = 0, ..., T$, that minimizes*

$$J = \int_0^T \tilde{P}_b^{QA}(v(t), a(t)) dt, \tag{4.17}$$

with $\tilde{P}_b^{QA}$ given by (4.15), subject to the state equations (4.11) and (4.12), and the

final state conditions (4.13) and (4.14).

The use of a quadratic cost criterion results in smooth variations of both the state and control over time. The Hamiltonian function [117] for *Problem 2* reads

$$H(v(t), a(t), \lambda_1(t), \lambda_2(t)) = \tilde{P}_b^{QA}(v(t), a(t)) + \lambda_1(t)v(t) + \lambda_2(t)a(t) \quad (4.18)$$

where $\lambda_1(t)$ and $\lambda_2(t)$ are the co-state variables. The optimal control is calculated from $\frac{\partial H}{\partial a(t)} = 0$:

$$b_3 + b_4 v(t) + 2 \cdot b_6 a(t) + \lambda_2(t) = 0. \quad (4.19)$$

Solving (4.19) for $a(t)$, it yields:

$$a(t) = -\frac{b_3 + b_4 v(t) + \lambda_2(t)}{2 \cdot b_6}. \quad (4.20)$$

Substituting (4.20) into (4.18), the optimal Hamiltonian function $H_0 = H(v(t), \lambda_1(t), \lambda_2(t))$ is derived. The other conditions of optimality are:

$$\dot{p}(t) = \frac{\partial H_0}{\partial \lambda_1(t)} = v(t) \quad (4.21)$$

$$\dot{v}(t) = \frac{\partial H_0}{\partial \lambda_2(t)} = -\frac{b_3 + b_4 v(t) + \lambda_2(t)}{2b_6} \quad (4.22)$$

$$\dot{\lambda_1}(t) = -\frac{\partial H_0}{\partial p(t)} = 0 \quad (4.23)$$

$$\dot{\lambda_2}(t) = -\frac{\partial H_0}{\partial v(t)} = -b_2 + \frac{b_3 b_4 + b_4^2 v(t) + b_4 \lambda_2(t)}{2b_6} - 2b_5 v(t). \quad (4.24)$$

Using symbolic computation tools, the linear system of ordinary differential equations (4.21)-(4.24) can be solved analytically with ease. The solution is expressed through exponential functions of time, involving both state and co-state variables. The parameters determining the characteristics of the solution trajectories are contingent upon the initial and final conditions of the problem and the time horizon, as well as on the quadratic approximation used for the energy consumption model. *Approach A-QA* consists of substituting the analytic solution for $x(t), v(t), \lambda_1(t), \lambda_2(t)$ in (4.20) to get the analytic solution for the optimal acceleration $a(t)$.

Approach A-SA: Analytic solution using a simple approximated power-based energy consumption model

The square-of-acceleration is used sometimes in the literature instead of complex fuel consumption models for internal combustion engine vehicles for fuel minimization. It can be considered as a simple approximation of the already quadratic approximation model in (4.15), here denoted by $\tilde{P}_b^{SA}(a(t))$:

$$\tilde{P}_b^{SA}(a(t)) = \frac{1}{2}a(t)^2. \tag{4.25}$$

This simple model does not apply in case of vehicle deceleration (i.e. negative acceleration) and it does not take into consideration that the batteries are charging from regenerative braking, like shown in equation (4.7). In order to understand whether this simplification is able to give acceptable results, one of the objectives of this work is to compare results obtained by applying this method with the ones obtained from using the quadratic approximation of the original complex function, as in [143].

Following the same methodology of *Approach A-QA* and according to [104], the optimal control problem and the solution trajectory for the acceleration are formulated as follows.

Problem 5 *Given the system initial conditions $p(0) = p_0$ and $v(0) = v_0$, find the optimal control $a(t)$, $t = 0, ..., T$, that minimizes*

$$J = \int_0^T \tilde{P}_b^{SA}(a(t))dt, \tag{4.26}$$

with $\tilde{P}_b^{SA}(a(t))$ given by (4.25), subject to the state equations (4.11) and (4.12), and the final state conditions (4.13) and (4.14).

The Hamiltonian function for the approximate optimal control problem reads

$$H'(v(t), a(t), \lambda_1'(t), \lambda_2'(t)) = \tilde{P}_b^{SA}(v(t), a(t)) + \lambda_1' v(t) + \lambda_2' a(t) \tag{4.27}$$

where $\lambda_1'(t)$ and $\lambda_2'(t)$ are the co-state variables of this problem. The optimal control is calculated from $\frac{\partial H'}{\partial a(t)} = 0$:

$$a(t) + \lambda_2'(t) = 0. \tag{4.28}$$

Solving (4.28) for $a(t)$, yields:

$$a(t) = -\lambda_2'(t). \tag{4.29}$$

Substituting (4.29) into (4.27), the optimal Hamiltonian function $H_0' = H'(v(t), \lambda_1'(t), \lambda_2'(t))$ is derived:

$$H_0' = -\frac{1}{2}\lambda_2'(t)^2 + \lambda_1'(t)v(t). \tag{4.30}$$

The other conditions of optimality are:

$$\dot{x} = \frac{\partial H_0'}{\partial \lambda_1'(t)} = v(t) \tag{4.31}$$

$$\dot{v} = \frac{\partial H_0'}{\partial \lambda_2'(t)} = -\lambda_2'(t) \tag{4.32}$$

$$\dot{\lambda_1'}(t) = -\frac{\partial H_0'}{\partial p(t)} = 0 \tag{4.33}$$

$$\dot{\lambda_2'}(t) = -\frac{\partial H_0'}{\partial v(t)} = -\lambda_1'(t). \tag{4.34}$$

According to (4.33), $\lambda_1'(t)$ is a constant, i.e. $\lambda_1'(t) = c_1$, and using (4.34), we get $\lambda_2'(t) = -c_1 t + c_2$. Finally, taking into consideration equation (4.27), *Approach A-SA* consists of finding the solution trajectory for the acceleration, which is linear with respect to time t, as

$$a(t) = c_1 t - c_2, \tag{4.35}$$

where c_1 and c_2 are constants and may be calculated from the boundary conditions.

Both *Approaches A-QA* and *A-SA* produce a closed-form solution that depends on the initial and final conditions of the problem and can be computed virtually instantaneously (for more details, see [143]).

Approach N-SM: Numerical solution with the smoothed power-based energy consumption model

While the analytic solution of optimal control problems using the necessary conditions of optimality can be powerful, it comes with certain disadvantages as limited applicability to problems with complex dynamics, nonlinearity, and struggle with intricate and complex constraints. That is where

numerical solution algorithms come in handy. For the purposes of this work, a discrete-time version of the direction algorithm has been used, as in [110], which exploits the notion of reduced gradient to eliminate the state variables and solve the problem in the space of the control variables using well-known NLP methods. It is noted that the energy consumption function (4.9) features discontinuous first-order derivatives at the switching point when the value of $F(v(t), a(t))$ is zero, basically when $F_m(v(t), a(t))$ switches from $F(v(t), a(t))$ to $\eta F(v(t), a(t))$, or vice-versa. This may lead to difficulties when using gradient-based optimization methods. Hence, it is useful to have a smooth nonlinear cost function that is differentiable everywhere in its domain.

The derived power-based model in equation (4.9) can be written as follows:

$$\begin{aligned} P_b(v(t), a(t)) = v(t) \cdot \max[F(v(t), a(t)), \eta F(v(t), a(t))] \\ \cdot \eta_b^{-\text{sign}(v \cdot \max[F(v(t), a(t)), \eta F(v(t), a(t))])} \\ \cdot \eta_m^{-\text{sign}(v(t) \cdot \max[F(v(t), a(t)), \eta F(v(t), a(t))])} + P_a \cdot \eta_b^{-1}. \end{aligned} \tag{4.36}$$

The function $P_b(v(t), a(t))$ is non-smooth and discontinuous. The existence of both max and sign functions introduces discontinuous first-order derivatives when the value of F is zero. Consider a general non-smooth function $S_1 = \max[A_1, A_2]$. Such a function may be approximated via a smooth function called the smooth maximum unit (SMU) [21]:

$$S_1^{SM} = \frac{A_1 + A_2 + \sqrt{(A_1 - A_2)^2 + \epsilon_1}}{2} \tag{4.37}$$

where $\epsilon_1 \geq 0$ is a smoothing parameter and when $\epsilon_1 \to 0$, $S_1^{SM} \to S_1$.

By applying (4.37) to $F_m(v(t), a(t))$ in (4.8), we get:

$$\begin{aligned} & P_m^{SM}(v(t), a(t)) \\ & = v(t) \cdot \frac{F(v(t), a(t)) + \eta F(v(t), a(t)) + \sqrt{(F(v(t), a(t)) - \eta F(v(t), a(t)))^2 + \epsilon_1}}{2}. \end{aligned} \tag{4.38}$$

Consider a general discontinuous function $S_2 = \text{sign}[A]$. Such a function may be approximated by one of the Continuous Approximations of Sign

Function (CASF)[130]:

$$S_2^{SM} = \frac{A}{\sqrt{A^2 + \epsilon_2^2}} \tag{4.39}$$

where ϵ_2 is a smoothing parameter and when $\epsilon_2 \to 0$, $S_2^{SM} \to S_2$.

By applying (4.39), we get:

$$\text{sign}[P_m^{SM}(v(t), a(t))] \approx \frac{P_m^{SM}(v(t), a(t))}{\sqrt{(P_m^{SM}(v(t), a(t)))^2 + \epsilon_2}}. \tag{4.40}$$

The smooth, continuous and differentiable function $\tilde{P}_b^{SM}(v(t), a(t))$ in terms of $P_m^{SM}(v(t), a(t))$ is then obtained by replacing (4.40) in (4.9):

$$\tilde{P}_b^{SM}(v(t), a(t)) = P_m^{SM}(v(t), a(t)) \cdot \eta_b^{\frac{-P_m^{SM}(v(t),a(t))}{\sqrt{(P_m^{SM}(v(t),a(t)))^2+\epsilon_2^2}}} \cdot \eta_m^{\frac{-P_m^{SM}(v(t),a(t))}{\sqrt{(P_m^{SM}(v(t),a(t)))^2+\epsilon_2^2}}} + P_a \cdot \eta_b^{-1}. \tag{4.41}$$

The same function can be extended to be in terms of $F(v(t), a(t))$, by replacing $\tilde{P}_m^s(v(t), a(t))$ with (4.38) in (4.41), and in terms of $v(t)$ and $a(t)$ by replacing $F(v(t), a(t))$ with (4.5). Examples of the smoothed function $\tilde{P}_b^{SM}$ for different combinations of ϵ_1 and ϵ_2 can be found in Figure 4.1 where they are compared to the original function P_b in function of $a(t)$ for a constant $v(t) = 20m/s$. The best smoothed version that is the closest to the original and without a steep change of its derivative at the switching point is for $\epsilon_1 = 500000$ and $\epsilon_2 = 500$ (represented in blue in Figure 4.1).

The optimal control problem for minimizing energy consumption is transformed considering a discrete-time formulation as follows. The discrete-time version of the state equations (4.11), (4.12) is

$$p(k+1) = p(k) + v(k)\Delta t + \frac{1}{2}a(k)\Delta t^2 \tag{4.42}$$

$$v(k+1) = v(k) + a(k)\Delta t. \tag{4.43}$$

with Δt being the time step length and $k \cdot \Delta t = t$.
According to this discrete-time formulation, the optimal control problem is given by:

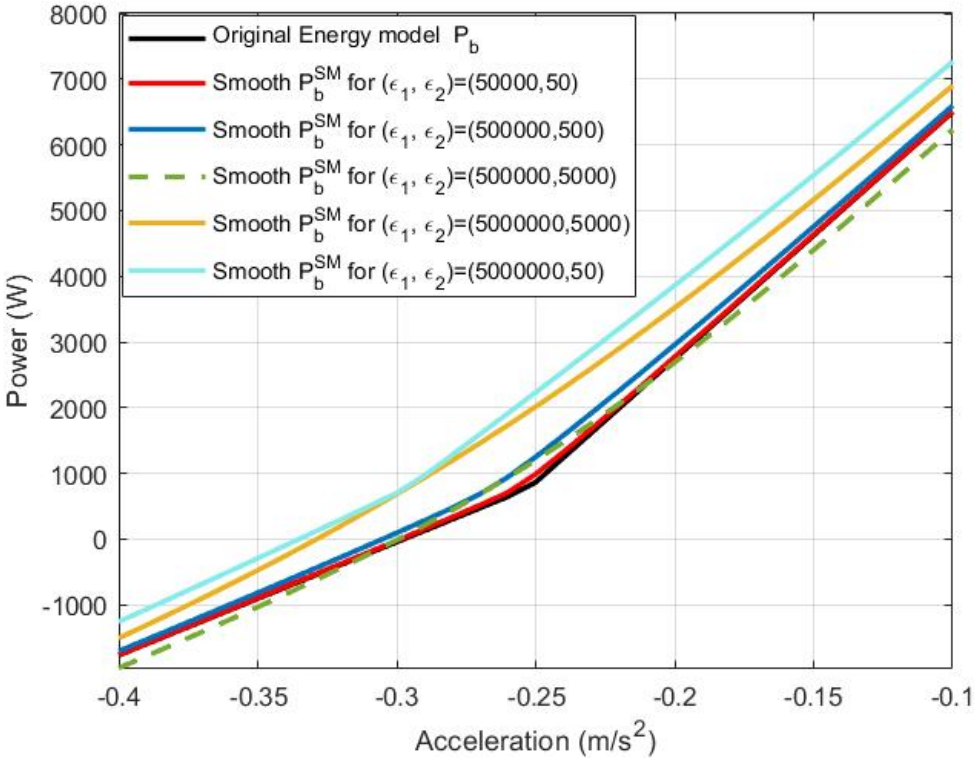

FIGURE 4.1: The original non smooth energy model P_b and versions of its smoothed variation $\tilde{P}_b^{SM}$ for different combinations of (ϵ_1, ϵ_2) in function of the acceleration for a constant speed of 20 m/s

Problem 6 *Given the system initial conditions $p(0) = p_0$ and $v(0) = v_0$, find the optimal control $a(k)$, $k = 0, ..., K-1$, that minimizes*

$$\begin{aligned} & J[v(k), a(k)] \\ & = \sum_{k=0}^{K-1} \left(p_1 \cdot \tilde{P}_b^{SM}(v(k), a(k)) \; + \; \frac{1}{2} p_2 \cdot \min[0, v(k) + \epsilon]^2 \right) \\ & + \frac{1}{2} p_3 \cdot [p_e - p(K)]^2 \; + \; \frac{1}{2} p_4 \cdot [v_e - v(K)]^2, \end{aligned} \tag{4.44}$$

subject to the state equations (4.42) and (4.43), and the final state conditions (4.13) and (4.14).

In $J[v(k), a(k)]$, $\tilde{P}_b^{SM}(v(k), a(k))$ is the smoothed nonlinear energy consumption function (4.41) and the last two quadratic penalty terms account for the final conditions of the vehicle position and speed, respectively, by penalizing deviations from the respective desired final states; the penalty weights p_3 and p_4 must be selected sufficiently large to ensure the virtual fulfillment

of the final state conditions. Moreover, a penalty term, with p_2 as the corresponding weight, ensures that no negative speed values will appear in the solution.

Approach N-SM consists in solving *Problem 4* numerically, by adopting the Feasible Direction Algorithm (FDA) [110][143]. This algorithm capitalizes on the structure of the state equations, transforming the optimal control problem into an NLP problem within the reduced space of control variables, specifically an mK-dimensional space, where m represents the number of control variables and is equal to 1 in this case. Therefore, the algorithm generates a control trajectory $a(k), k = 0, ..., K-1$, corresponding to a local minimum of the objective function, while simultaneously adhering to the state equations and constraints. In achieving this, the FDA leverages the reduced gradient $g(k) = [\partial f/\partial a(k)]^\top \lambda(k+1) + \partial \phi/\partial a(k)$ in the mK-dimensional space of control variables, provided that the states and co-states involved in the partial derivatives satisfy the corresponding state and co-state equations. The FDA operates iteratively, necessitating an initially feasible control trajectory that satisfies all state equations and constraints. In each iteration, the FDA computes a descent search direction using the reduced gradient information and determines the optimal step along this direction through a line-search procedure. Consequently, this process results in an enhanced feasible control trajectory with a diminished objective function value, serving as the initial trajectory for the subsequent iteration. It is important to note that the algorithm ensures improved objective values with each iteration and boasts global convergence, transitioning from any starting control trajectory to a local minimum.

4.5.2 Optimal control problems with a stop point: GLOSA

In order to take into consideration signalized intersections and traffic lights, *Problem 3* can be modified by adding a new condition. As the EV has to go from the initial state $x_0 = [p_0, v_0]^\top$ to a final state $x_e = [p_e, v_e]^\top$ within a time horizon T that can be fixed or free, it is not allowed to pass through a given position p_{SP} before a fixed time t_r, where p_{SP} is the position of the traffic light and t_r is the time from the moment the EV starts its trajectory until the traffic light switches from red to green. This new problem is labeled as the GLOSA problem where the vehicle should satisfy all the constraints including the traffic light one, while minimizing its energy consumption by adjusting its acceleration appropriately. The optimal objective value of the

Stop Point problem is $J_{SP}(t_{SP})$, a function of t_{SP} which is an intermediate time, at which the vehicle is required to cross the signal position, creating a new constraint. The optimal control problem to be solved in this case is the following;

Problem 7 *Given the system initial conditions $p(0) = p_0$ and $v(0) = v_0$, find the optimal control $a(t)$, $t = 0, ..., T$, that minimizes*

$$J_{SP}(t_{SP}) = \int_0^T P_b(v(t), a(t))dt \tag{4.45}$$

subject to the state equations (4.11) and (4.12), the final conditions (4.13) and (4.14), an intermediate equality constraint for the position of the EV:

$$p(t_{SP}) = p_{SP}, \tag{4.46}$$

and the constraint for the crossing time t_{SP}:

$$t_{SP} > t_r. \tag{4.47}$$

Problem 7 is solved with the same approaches described in Section 4.5.1 but with the addition of the new condition of the traffic signal: the continuous-time version analytically, using *Approaches A-QA-SP* and *A-SA-SP* (similar to *Approaches A-QA* and *A-SA* but with the stop point constraint), and the discrete-time version numerically, using *Approach N-SM-SP* (similar to *Approach N-SM* but with the stop point constraint).

Approach A-QA-SP

This approach consists of getting an analytical solution using an approximation of energy consumption model, thus replacing $P_b(v(t), a(t))$ in (4.45) with the quadratic approximation $\tilde{P_b}^{QA}(v(t), a(t))$ from (4.15).

Problem 8 *Given the system initial conditions $p(0) = p_0$ and $v(0) = v_0$, find the optimal control $a(t)$, $t = 0, ..., T$, that minimizes*

$$J_{SP}(t_{SP}) = \int_0^T \tilde{P_b}^{QA}(v(t), a(t))dt, \tag{4.48}$$

subject to the state equations (4.11) and (4.12), the final conditions (4.13) and (4.14), and constraints (4.46) and (4.47).

The optimal state and control trajectories have the following two-branch form over time:

$$a(t) = \begin{cases} a_1(t) & 0 \leq t \leq t_{SP}^- \\ a_2(t') & t_{SP}^+ \leq t \leq T \end{cases} \tag{4.49}$$

$$v(t) = \begin{cases} v_1(t) & 0 \leq t \leq t_{SP}^- \\ v_2(t') & t_{SP}^+ \leq t \leq T \end{cases} \tag{4.50}$$

$$p(t) = \begin{cases} p_1(t) & 0 \leq t \leq t_{SP}^- \\ p_2(t') & t_{SP}^+ \leq t \leq T \end{cases} \tag{4.51}$$

where $t' = t - t_{SP}$, and $a_1(t), a_2(t), v_1(t), v_2(t), p_1(t)$ and $p_2(t)$ represent the analytic solutions of the acceleration, speed and position respectively, obtained through the methodology of *Approach A-QA*. These solutions contain 8 constants that can be specified by solving a system of 8 equations consisting of: the initial and final states, the continuity conditions $a(t_{SP}^-) = a(t_{SP}^+)$, $v(t_{SP}^-) = v(t_{SP}^+)$, $p(t_{SP}^-) = p(t_{SP}^+)$ and the intermediate condition $p(t_{SP}) = p_{SP}$. Let us denote by t_{SP-1} the time when the EV reaches the traffic light position p_{SP} in *Problem 4*. As the GLOSA problem has an additional constraint compared to *Problem 4*, it yields that $J_{SP}(t_{SP}) \geq J \; \forall t_{SP}$. The value of $J_{SP}(t_{SP})$ is minimal when $t_{SP} = t_{SP-1}$, as expected, and increases monotonically as t_{SP} increases beyond t_{SP-1}. So to solve this constrained problem in presence of a traffic light at p_{SP} and switching time to green t_r, Algorithm 4 is applied and the following steps are taken:
1) Solve *Problem 4*; if $t_{SP-1} \geq t_r$, then the solution of *Problem 4* does not violate the green-light constraint and *Problem 8* is solved as well; else
2) Solve *Problem 8* with $t_{SP} = t_r$ to obtain the Stop Point problem solution.

Control Algorithm 4 Algorithm applied to solve the stop point problem

1: Solve *Problem 4* and compute t_{SP-1} - Go to Step 2
2: Compare t_{SP-1} to t_r. If $t_{SP-1} \geq t_r$, go to Step 3, otherwise go to Step 4
3: Apply the optimal solution from Step 1
4: Solve *Problem 8* - go to Step 5
5: Apply the optimal solution from Step 4

Approach A-SA-SP

Let us use now $\tilde{P}_b^{SA}(a(t))$ from (4.25), which gives us *Approach A-SA-SP*, and the optimal control problem to be solved in this case is the following:

Problem 9 *Given the system initial conditions $p(0) = p_0$ and $v(0) = v_0$, find the optimal control $a(t)$, $t = 0, ..., T$, that minimizes*

$$J_{SP}(t_{SP}) = \frac{1}{2}\int_0^T a(t)^2 dt, \tag{4.52}$$

subject to the state equations (4.11) and (4.12), the final conditions (4.13) and (4.14), and constraints (4.46) and (4.47).

The analytic solution of the acceleration is calculated similarly to *Approach A-SA* and in this case, the optimal state and control trajectories have the following two-branch form over time,

$$a(t) = \begin{cases} c_1 t + c_2 & 0 \le t \le t_{SP}^- \\ c_5 t' + c_6 & t_{SP}^+ \le t \le T \end{cases} \tag{4.53}$$

$$v(t) = \begin{cases} \frac{1}{2}c_1 t^2 + c_2 t + c_3 & 0 \le t \le t_{SP}^- \\ \frac{1}{2}c_5 t'^2 + c_6 t' + c_7 & t_{SP}^+ \le t \le T \end{cases} \tag{4.54}$$

$$p(t) = \begin{cases} \frac{1}{6}c_1 t^3 + \frac{1}{2}c_2 t^2 + c_3 t + c_4 & 0 \le t \le t_{SP}^- \\ \frac{1}{6}c_5 t'^5 + \frac{1}{2}c_6 t'^2 + c_7 t' + c_8 & t_{SP}^+ \le t \le T \end{cases} \tag{4.55}$$

where $t' = t - t_{SP}$. Assuming a fixed time horizon, these equations contain the parameters c_i , $i = 1, ..., 8$, which can be specified by solving a system of 8 equations identical to the one of *Approach A-QA-SP*. This time, let us denote by t_{SP-2} the time when the EV reaches the traffic light position p_{SP} in *Problem 5*. The behavior of J_{SP} is the same as in the previous approach and to solve this constrained problem in presence of a traffic light at p_{SP} and switching time to green t_r, Algorithm 5 is applied and the following steps are taken:
1) Solve *Problem 5*; if $t_{SP-2} \ge t_r$, then the solution of the *Problem 5* does not violate the green-light constraint and *Problem 9* is solved as well; else
2) Solve *Problem 9* with $t_{SP} = t_r$ to obtain the Stop Point problem solution.

Control Algorithm 5 Algorithm applied to solve the stop point problem

1: Solve *Problem 5* and compute t_{SP-2} - Go to Step 2
2: Compare t_{SP-2} to t_r. If $t_{SP-2} \geq t_r$, go to Step 3, otherwise go to Step 4
3: Apply the optimal solution from Step 1
4: Solve *Problem 9* - go to Step 5
5: Apply the optimal solution from Step 4

The solutions are obtained analytically using symbolic differentiation tools, as *Problems 4* and *5* require solving a system of four algebraic equations and *Problems 8* and *9* require solving a system of eight equations. The numerical execution of those analytical formulas to obtain the solution of these problems takes less than a second of computation time and so may be done locally in the EV once the system receives the next switching time. That being said, the vehicle trajectory can be updated periodically (using MPC) to take into consideration unpredicted disruptions to its speed, like slower traffic ahead for example.

Approach N-SM-SP

As in *Approach N-SM*, the cost function to be minimized is a discrete time formulation of the problem, using the smooth version $\tilde{P}_b^{SM}(v(k), a(k))$ of the power function, as shown in the following:

Problem 10 *Given the system initial conditions* $p(0) = p_0$ *and* $v(0) = v_0$, *find the optimal control* $a(k)$, $k = 0, ..., K-1$, *that minimizes*

$$\begin{aligned} & J_{SP}[v(k), a(k)] \\ & = \sum_{k=0}^{K-1} \left(p_1 \cdot \tilde{P}_b^{SM}(v(k), a(k)) \; + \; \frac{1}{2} p_2 \cdot \min[0, v(k) + \epsilon]^2 \right) \\ & + \; \frac{1}{2} p_3 \cdot [p_e - p(K)]^2 \; + \; \frac{1}{2} p_4 \cdot [v_e - v(K)]^2 \\ & + \; p_5 \sum_{k=0}^{k_r - 1} \left(\min(p_{SP} - p(k), 0)^2 \right). \end{aligned} \tag{4.56}$$

subject to the state equations (4.43) and (4.42) and the final conditions (4.13) and (4.14).

The objective function of *Problem 10* has an additional penalty term for the stop point constraint compared to (4.44) from *Problem 6*, which is the fifth term representing a penalty term that prevents position values greater than the traffic signal position, p_{SP}, as long as $k < k_r$ where k_r is the signal switching time step, with p_5 as the corresponding weight. In this approach, FDA is used to solve *Problem 10*, like for *Approach N-SM*.

4.6 Results and Comparisons

In order to address the energy consumption problem, several scenarios are considered using the previously explained approaches: *Approaches A-QA* and *A-SA* consist of getting an analytical solution using an approximation of the power-based energy model (quadratic approximation for *A-QA* and the square-of-acceleration for *A-SA*) while *Approach N-SM* consists of getting a numerical solution using a smoothed form of the model and the feasible direction algorithm. More specifically, three scenarios are explored where an EV has to go from an initial state to a final one during a fixed time horizon: scenarios 1 and 2 address the problem without a stop point while scenario 3 represents a traffic light case. The conditions of each scenario are the initial and final positions in m, p_0 and p_e respectively, the initial and final speeds in m/s, v_0 and v_e respectively, and the time horizon T in s. For scenario 3, two additional conditions are the position of the traffic signal p_{SP} in m and the switching time from red to green of the signal t_r in s (non existent for scenarios 1 and 2). The quadratic approximation in *approaches A-QA* and *A-QA-SP* was effectuated for $v_1 = 0\ m/s, v_2 = 25\ m/s, a_1 = -2\ m/s^2, a_2 = 2\ m/s^2$ (check (4.16)) and $0.2m/s$ and $0.1m/s^2$ as counting steps for speed and acceleration respectively. Details about each scenario are shown in Table 4.1.

As shown in Table 4.1, the initial speed is higher than the final one in Scenario 1 so it is an example of a negative acceleration trajectory where the EV needs to decelerate. On the contrary in Scenario 2, a positive acceleration is presented by an initial speed that is less than the final speed, so the vehicle needs to accelerate in order to reach the final position within the time horizon. Scenario 3 has again an initial speed greater than the final one but this time there is a traffic light, so the EV should adjust its speed to cross the signal after it switches from red to green and then arrive to its final state. For each scenario, the obtained speed and acceleration profiles from all approaches are fed into the original energy consumption model (4.9) and the resulting

TABLE 4.1: The conditions of each scenario and the approaches used to solve the optimal control problem

Scenario	1	2	3
p_0	0	0	0
p_e	320	420	320
v_0	20	15	10
v_e	15	20	15
T	19	25	30
p_{SP}	-	-	85
t_r	-	-	12
Approaches	A-QA, A-SA, N-SM	A-QA, A-SA, N-SM	A-QA-SP, A-SA-SP, N-SM-SP

energy consumption values are used to compare these approaches. The most exact values are the ones obtained from the numerical solutions, and they are compared to the other values in order to evaluate the effectiveness of the analytical approaches of giving close results. As an extension to Scenario 3, section 4.6.4 includes comparisons of the energy consumption between the three approaches for multiple stop point scenarios. In fact, 6 initial speeds of the EV, 8 positions of the traffic light and 2 switching times are considered, while all other conditions are the same as Scenario 3. The values of the EV parameters used in this work are the ones of the Nissan Leaf [50]: m = 1521 kg, A_f = 2.3316 m^2, C_d = 0.28, f=0.015, $\eta_m = \eta_b$ = 0.9, η = 0.7, P_a = 700 w, g=9.8066 m/s^2, ρ=1.2256 kg/m^3.

4.6.1 Scenario 1

The optimal trajectories of acceleration, speed and position of the vehicle in Scenario 1, resulting from *Approaches A-QA, A-SA* and *N-SM*, are presented in Figure 4.3. It is evident that the derived results from all approaches are close to each other; and that the final speed v_e and position x_e are achieved at the final time T as requested. The speed and acceleration profiles are fed into the original model (4.9) and the energy consumption values obtained for Scenario 1 are: 2.155 *Wh* for *Approach A-QA*, 2.156 *Wh* for *Approach N-SM* (0.046% difference) and 2.5 *Wh* for *Approach A-SA* (16% difference). Note that in this scenario, the vehicle decelerates continuously to reach the final speed of 15 m/s, and despite that, the minimization of the square-of-acceleration does a decent job of giving very close speed profile as the other approaches but the energy consumption for this approach is higher than the others. The

trends for the power consumption from all approaches are presented in Figure 4.2.

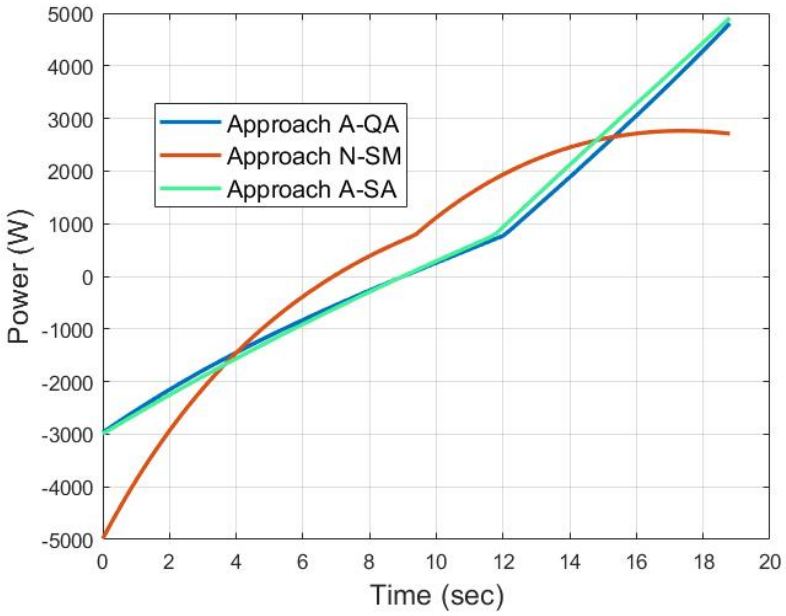

FIGURE 4.2: Power profiles from *Approaches A-QA, A-SA and N-SM* for Scenario 1

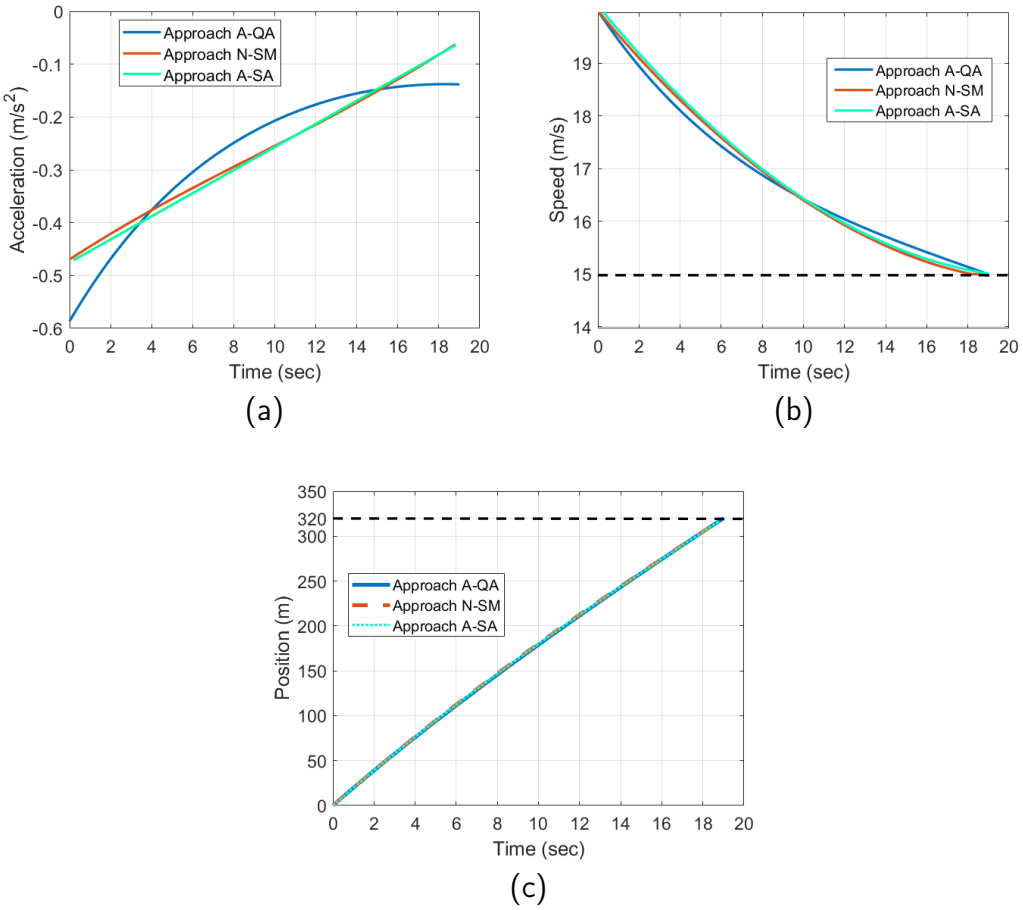

FIGURE 4.3: Acceleration (4.3a), speed (4.3b) and position (4.3c) profiles from approaches A-QA, A-SA and N-SM for Scenario 1

4.6.2 Scenario 2

The optimal trajectories of acceleration, speed and position of the vehicle in Scenario 2 resulting from *Approaches A-QA, A-SA* and *N-SM* are presented in Figure 4.5 . As in the first scenario, the results from all approaches are very close and the final conditions are satisfied. The energy consumption values obtained from using the speed and acceleration profiles in the original model (4.9) for Scenario 2 are: 99.3 *Wh* for *Approach A-QA*, 98.74 *Wh* for *Approach N-SM* (0.56% difference) and 99.91 *Wh* for *Approach A-SA* (0.6% difference from *Approach A-QA* and 1.18% difference from *Approach N-SM*). Note that, for this scenario, the vehicle needs to accelerate continuously in order to reach the required final speed of 20 m/s, and as expected, the square-of-acceleration works better than the previous scenario as an approximation for the minimization of the energy consumption. The trends for the power consumption from all approaches are presented in Figure 4.4.

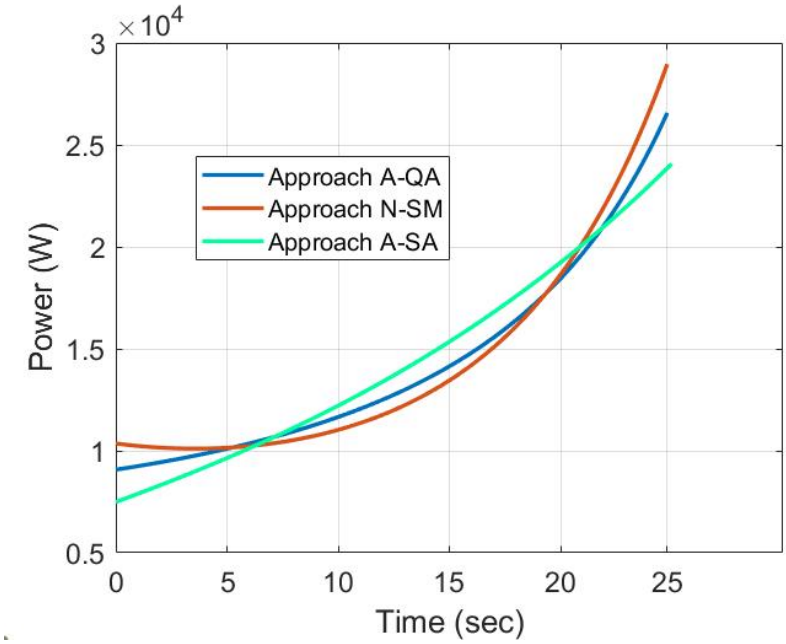

FIGURE 4.4: Power profiles from *Approaches A-QA, A-SA* and *N-SM* for Scenario 2

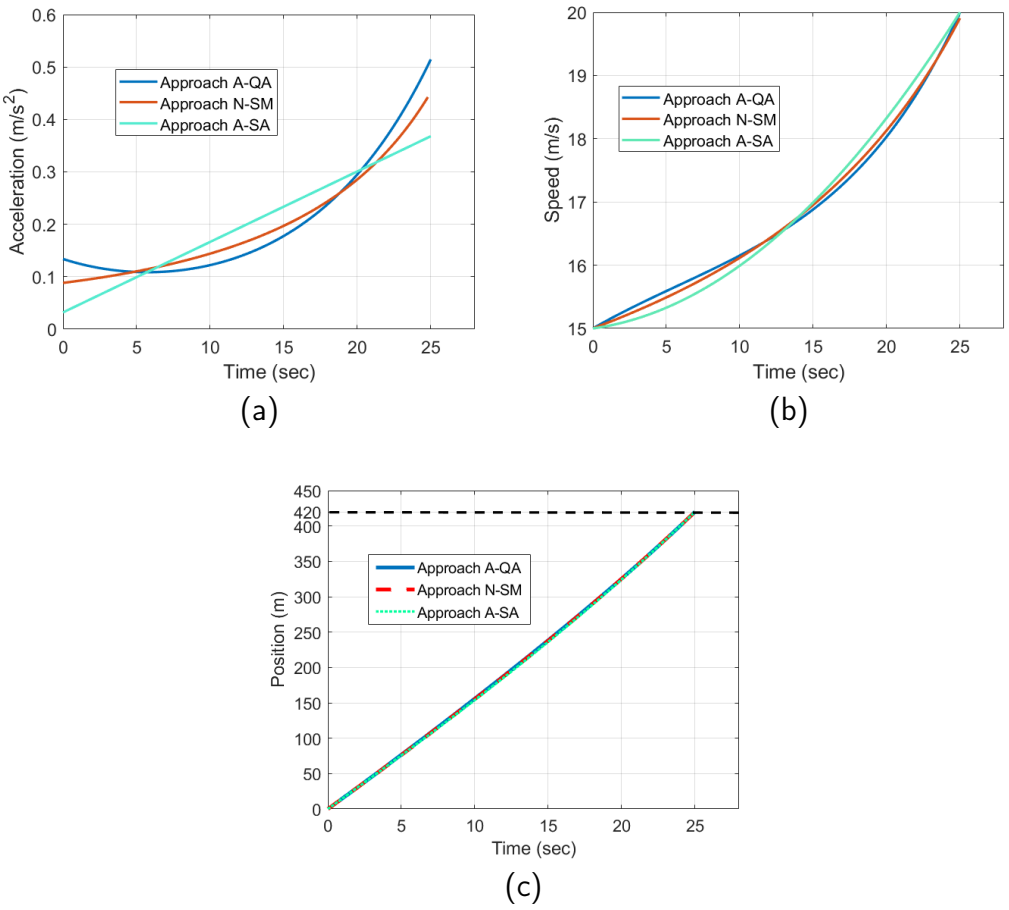

FIGURE 4.5: Acceleration (4.5a), speed (4.5b) and position (4.5c) profiles from approaches A-QA, A-SA and N-SM for Scenario 2

4.6.3 Scenario 3

The optimal trajectories of acceleration, speed and position of the vehicle from *Approaches A-QA-SP, A-SA-SP* and *N-SM-SP* for Scenario 3 are presented in Figure 4.7, and the power trends are shown in Figure 4.6. It is obvious from the trajectories that the vehicle reduces its speed in order to pass the traffic signal just after switching from red to green. The energy consumption values obtained from the original model (4.9) by using the speed and acceleration profiles for Scenario 3 are: 76.99 *Wh* for *Approach A-QA-SP*, 77.02 *Wh* for *Approach N-SM-SP* (0.039% difference) and 76.97 *Wh* for *Approach A-SA-SP* (0.026% difference from *Approach A-QA-SP* and 0.065% difference from *Approach N-SM-SP*). This scenario represents the stop point case, and although the initial speed is lower than the final one, the EV has to first decrease its speed in order to reach the traffic signal after the switching time, so in fact it is a case of both deceleration and acceleration. As the previous scenarios, *Approach A-QA-SP* gave very close results to *Approach N-SM-SP*,

which again shows that the quadratic approximation performs very well. As the deceleration period is short, *Approach A-SA-SP* gives satisfactory results and is able to compete with the other approaches.

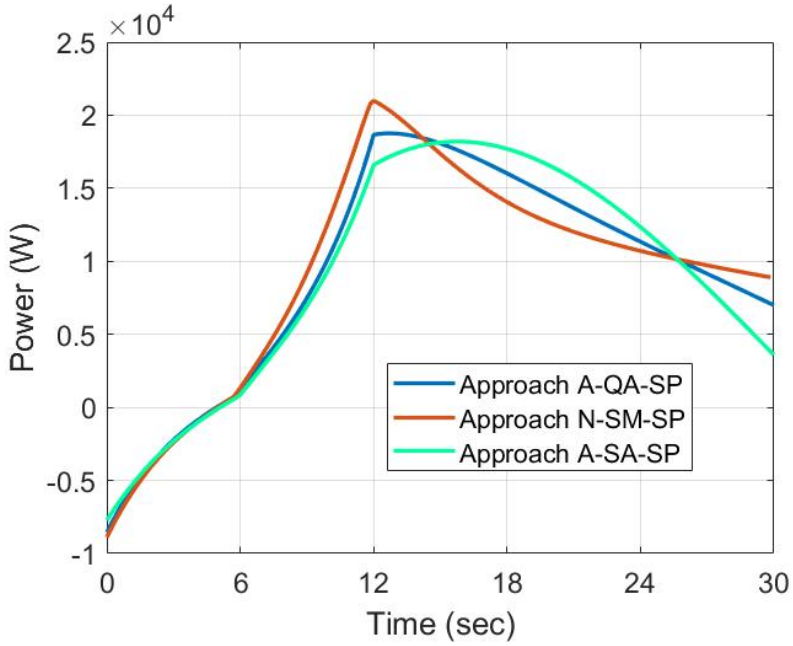

FIGURE 4.6: Power profiles from *Approaches A-QA-SP, A-SA-SP* and *N-SM-SP* for Scenario 3

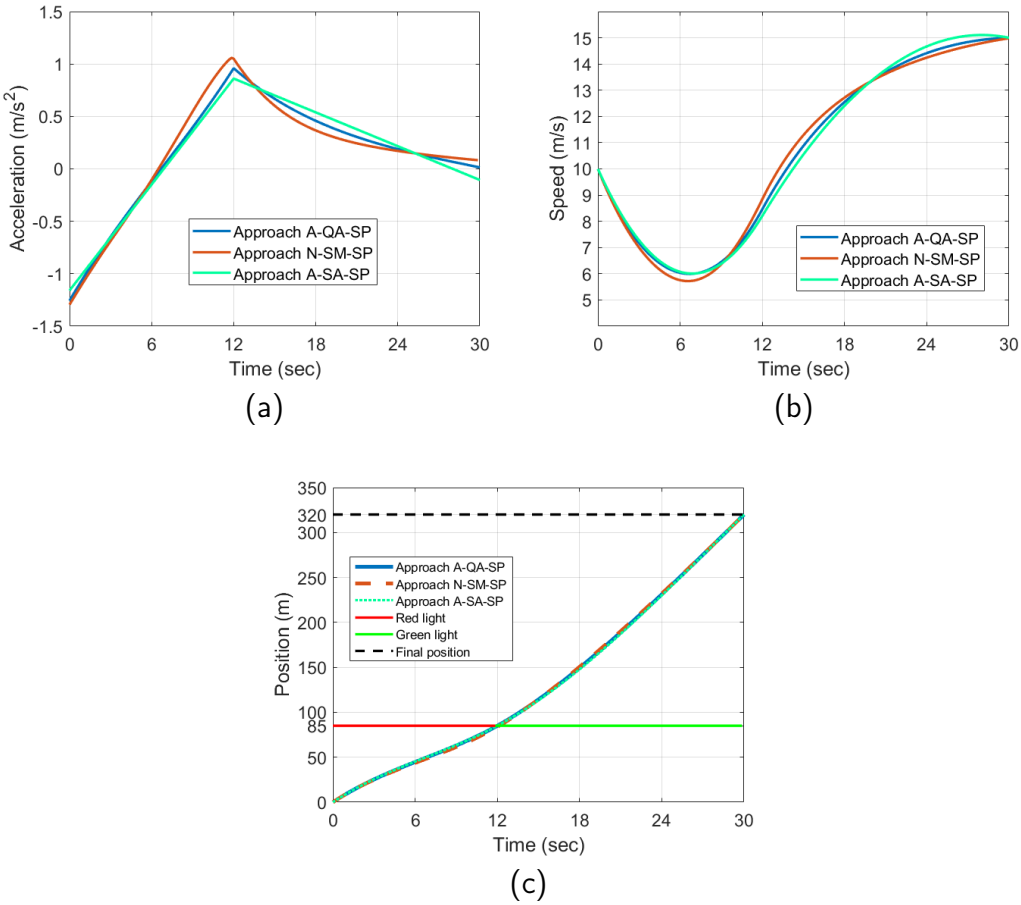

FIGURE 4.7: Acceleration (4.7a), speed (4.7b) and position (4.7c) profiles from approaches A-QA-SP, A-SA-SP and N-SM-SP for Scenario 3

4.6.4 More stop point scenarios

In this section, comparisons of the energy consumption values obtained from the original model (4.9) between the 3 different approaches to solve the stop point problem are shown. More specifically, 6 initial speeds of the EV, from 5 m/s to 12 m/s, 8 positions of the traffic signal, from 50 m to 105 m, and 2 switching times of the traffic light, 9 s and 12 s, are considered, which brings the total number of scenarios to 96. Figures 4.8, 4.9 and 4.10 show the relative difference in consumed energy between *Approaches A-QA-SP* and *A-SA-SP*, *Approaches A-QA-SP and N-SM-SP* and *Approaches A-SA-SP* and *N-SM-SP* respectively for a switching time of 9 s, while Figures 4.11, 4.12 and 4.13 show the relative difference in consumed energy between *Approaches A-QA-SP* and *A-SA-SP*, *Approaches A-QA-SP and N-SM-SP* and *Approaches A-SA-SP* and *N-SM-SP* respectively for a switching time of 12 s. As it is demonstrated in these figures, almost all relative differences between energy consumption values

from *Approaches A-QA-SP* and *N-SM-SP* are under 1%. This shows that the analytic solution using the quadratic approximation can be a very good approach for energy minimization of a trip of an EV. As for *Approach A-SA-SP* compared to the others, we can see that the energy consumption difference is high for extreme values of initial speed and traffic signal position. This is due to the fact that more deceleration is done by the EV in these cases, and like previously mentioned, the square-of-acceleration approximation is not a good fit for prolonged periods of negative acceleration.

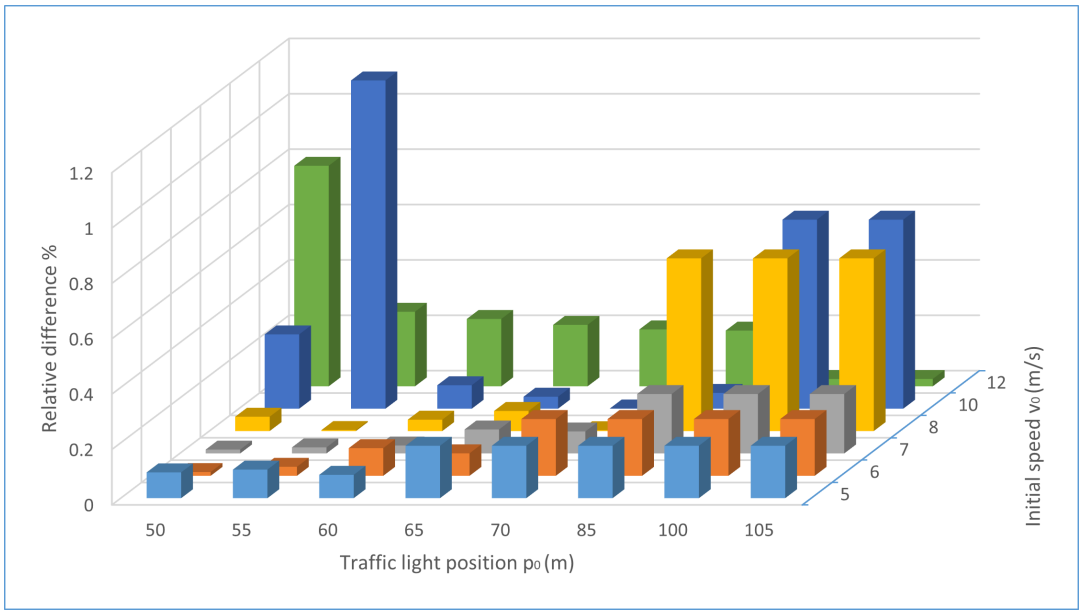

FIGURE 4.8: Relative difference of energy consumption between *Approaches A-QA-SP* and *A-SA-SP* for a switching time of 9 *s*

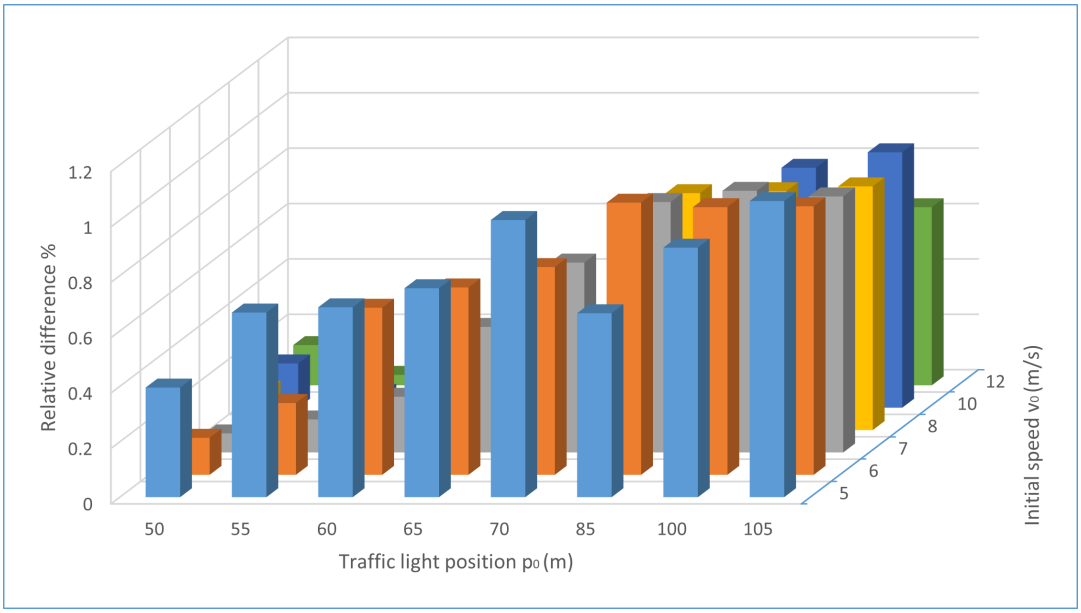

FIGURE 4.9: Relative difference of energy consumption between *Approaches A-QA-SP* and *N-SM-SP* for a switching time of 9 *s*

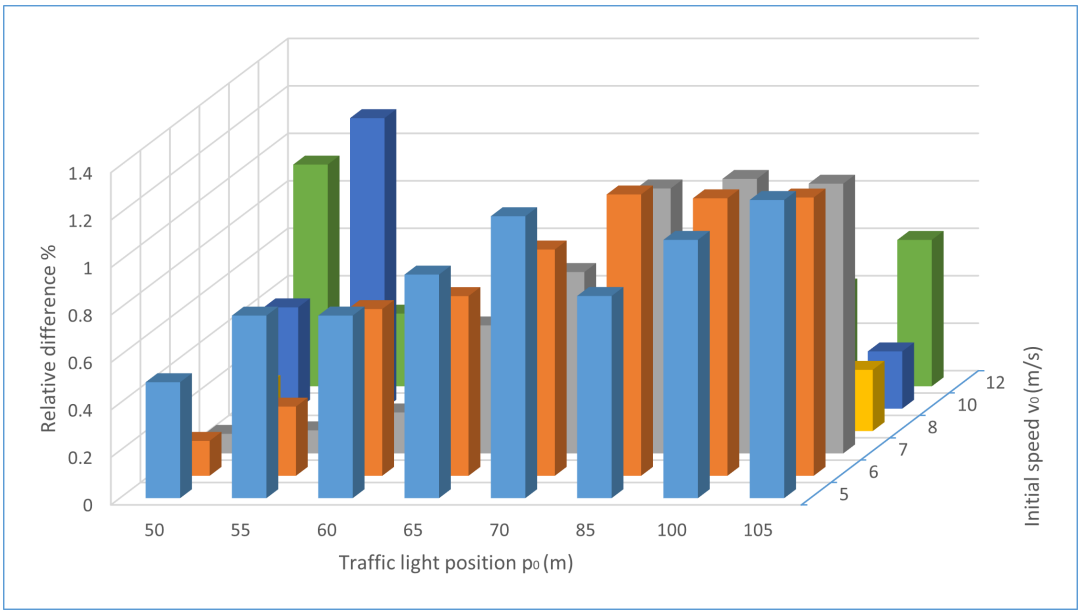

FIGURE 4.10: Relative difference of energy consumption between *Approaches A-SA-SP* and *N-SM-SP* for a switching time of 9 *s*

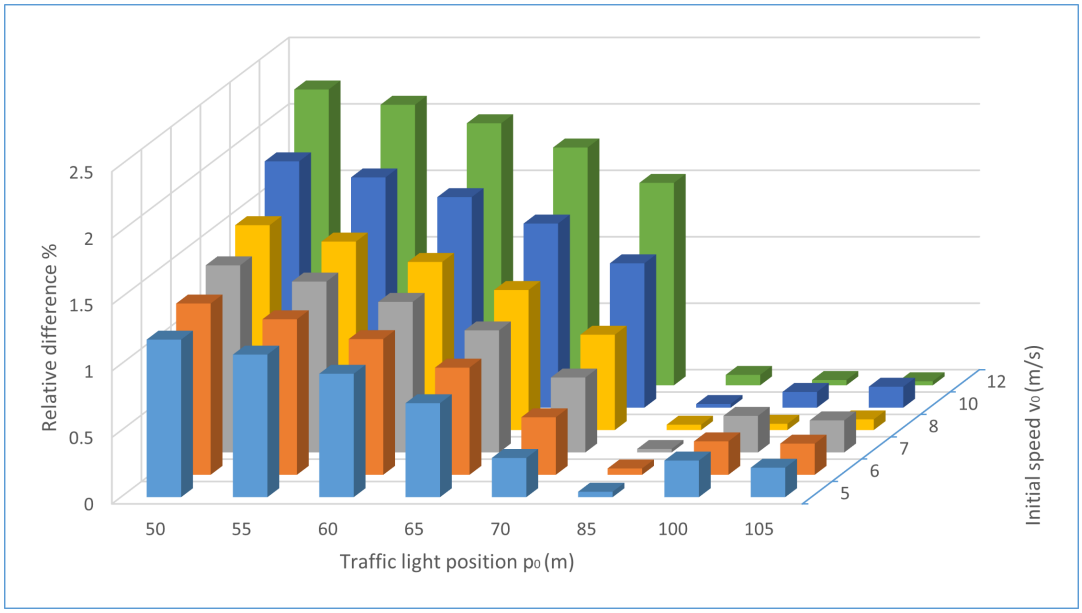

FIGURE 4.11: Relative difference of energy consumption between *Approaches A-QA-SP* and *A-SA-SP* for a switching time of 12 *s*

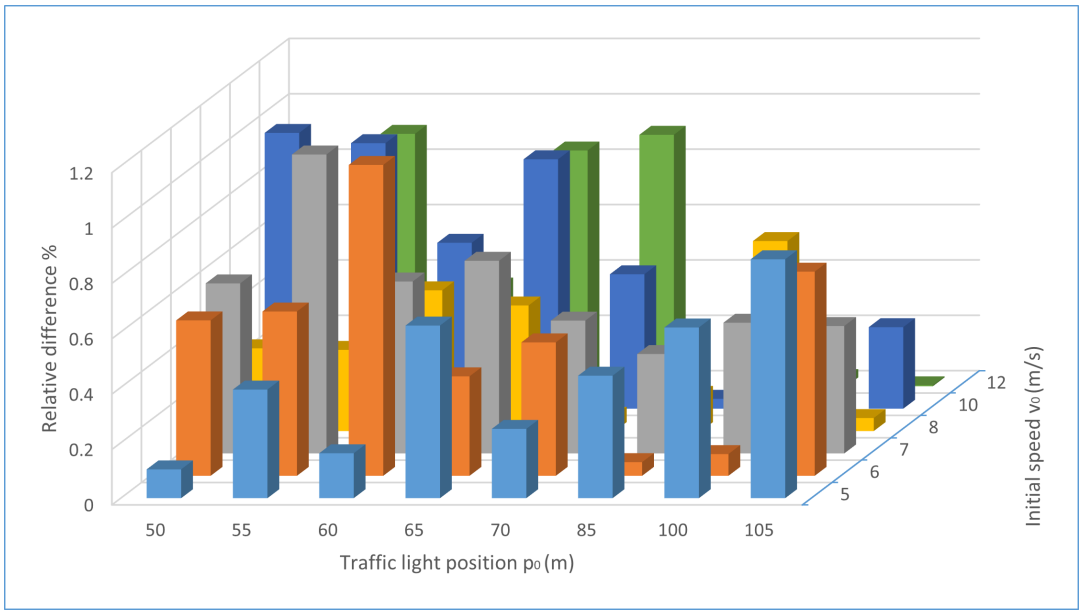

FIGURE 4.12: Relative difference of energy consumption between *Approaches A-QA-SP* and *N-SM-SP* for a switching time of 12 *s*

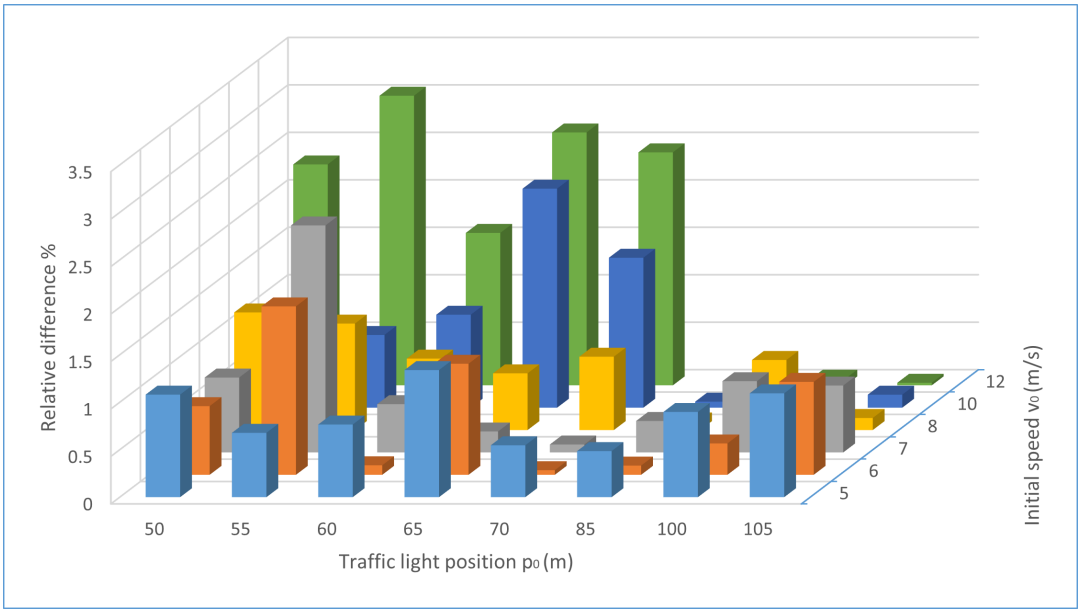

FIGURE 4.13: Relative difference of energy consumption between *Approaches A-SA-SP* and *N-SM-SP* for a switching time of 12 s

4.6.5 Discussion

As *Approaches N-SM* and *N-SM-SP* minimize a smoothed version of the original energy model, the resulting solutions are exact and superior to the solutions from *Approaches A-QA*, *A-SA*, *A-QA-SP* and *A-SA-SP*. But as shown previously in this section, using an approximation of the model and solving for a minimum analytically gives satisfactory results as they are very close to the numerical solutions. In fact, the states and control profiles and energy consumption are almost similar using the quadratic approximation $\tilde{P}_b^{QA}(v,a)$. This opens the way for the use of these analytical solutions in real life systems for finding optimal speeds of a trajectory, like GLOSA, as *Approaches N-SM* and *N-SM-SP* can be heavy computationally and time consuming for the real applications. Concerning the square-of-acceleration, the results show that it can be a very good approximation for energy consumption minimization over a short time horizon in positive acceleration cases, as it does not take into consideration the regeneration of energy from the brakes and the absence of consumption in negative accelerations.

4.7 Conclusions

This chapter focuses on the concept of Eco-driving and its applications, falling under the theme of sustainability in mobility and transportation. At first, a

literature review on Eco-driving techniques was presented, showcasing the innovations in this domain and the advancements achieved since decades ago. Then an overview of energy/fuel consumption models used for improving efficiency and optimizing vehicle performance was shown and in particular, a power-based energy consumption model was detailed, specifically for EVs with regenerative brakes, allowing to recover some of the energy lost while braking.

A particular part of the state of the art talks about GLOSA systems and their effectiveness in making traffic flow smoother and reducing congestion and fuel consumption. The work of the thesis presented in this chapter focuses on the algorithms that find the optimal kinematic trajectory of an EV traveling from an initial state of position and speed to a final one. The objective is to provide a replacement for the computationally heavy algorithms with simpler ones that give very close results. To this end, an optimal control problem was formulated and three approaches were used: the first approach is to solve it analytically using a quadratic approximation calculated by the least square method (*Approach A-QA*), the second one consists as well of solving it analytically but using the square-of-acceleration (*Approach A-SA*), while the third approach consists of solving it numerically, using an FDA and a smoothed version of the original energy model that has discontinuous first-order derivative (*Approach N-SM*).

Then another optimal control problem was presented, which is similar to the previous one, but this time there is a traffic signal on the way of vehicle, so the crossing must be done after the switching time of the traffic light from red to green. This problem is solved using *Approaches A-QA-SP*, *A-SA-SP* and *N-SM-SP*, which are analogous to *Approaches A-QA*, *A-SA* and *N-SM* respectively but with taking into consideration the new constraint of the traffic signal. In order to test the ability of *Approaches A-QA* and *A-SA* to give close results to *Approach N-SM*, and *Approaches A-QA-SP* and *A-SA-SP* to give close results to *Approach N-SM-SP*, three scenarios were considered, with one of them including a traffic signal. The respective approaches were compared, in terms of acceleration, speed, position and power profiles, along with energy consumption. Then the relative difference of energy consumption calculated for all the stop point problem approaches were shown for a sizable number of scenarios.

The results show that analytical solutions using a quadratic approximation of the energy model are very similar to numerical exact solutions, which allows

them to be used in real life applications for them being less costly and time consuming. The square-of-acceleration also appears to be a good approximation for energy minimization of EVs for short time horizons and positive acceleration cases.

Chapter 5

Conclusion

The transportation sector is at the forefront of addressing critical challenges related to sustainability, efficiency, and technological advancement. Freeway networks, as vital components of modern infrastructure, are increasingly strained by growing traffic volumes, leading to significant issues such as congestion, greenhouse gas emissions, and energy inefficiency. This thesis has addressed these challenges by focusing on mixed traffic systems, comprising both human-driven and autonomous vehicles, and exploring innovative solutions to enhance traffic flow, reduce energy consumption, and improve system sustainability. Central to this research is the recognition that sustainable transportation solutions must integrate advanced modeling, control strategies, and technological innovations. By considering the dynamics of freeway traffic, the complexities of mixed traffic scenarios, and the potential of autonomous vehicle technologies, this work contributes to a broader effort to create smarter, more sustainable transportation systems. The methodologies and models developed herein not only advance theoretical understanding but also provide practical tools for optimizing traffic flow and minimizing environmental impact in real-world applications.

Chapter 2 of this thesis addresses traffic modeling, which has long been a cornerstone of transportation research, offering valuable tools to analyze, simulate, and optimize traffic systems. The literature review on this topic focuses on the fact that traffic models are traditionally categorized into three types: macroscopic, mesoscopic, and microscopic, each with distinct advantages. Microscopic models focus on individual vehicle dynamics, providing detailed insights into driver behavior and vehicle interactions. Macroscopic models, on the other hand, capture aggregate traffic flow characteristics such as density, flow, and speed, offering scalability and computational efficiency. Mesoscopic models bridge these two extremes, modeling traffic at

an intermediate level of detail, while retaining computational feasibility. Two specific macroscopic models, METANET and the Cell Transmission Model (CTM), have been studied in detail and used in this work. METANET, a second-order traffic flow model, is utilized in Chapter 3 due to its capability to accurately model traffic speed dynamics, which is critical for the analysis presented in that chapter. Its ability to capture the acceleration and deceleration of vehicles with greater precision makes it a robust choice for tasks requiring detailed speed profiles. Conversely, CTM is explored in Chapter 2 as the foundation for the proposed traffic modeling framework. Its simplicity and the advantage of discretizing roadways into cells make it a suitable choice for modeling mixed traffic systems.

The state-of-the-art in mixed traffic modeling addresses the complexities introduced by the heterogeneity of vehicle types, driving behaviors, and interactions. Recent advancements incorporate autonomous vehicle technologies into established modeling frameworks to better predict traffic dynamics and explore control strategies. This thesis contributes to this growing body of knowledge by employing advanced traffic models to analyze and optimize mixed traffic scenarios. Specifically, the CTM-based mixed traffic model developed in this thesis incorporates CAVs as control actuators in a traffic stream with HVs. The core innovation lies in modeling CAVs as clusters—groups of closely spaced vehicles acting as moving bottlenecks, dividing each cell into upstream and downstream segments. This division allows for a more nuanced representation of the impact of CAVs on traffic flow, enhancing the accuracy and applicability of the model to real-world scenarios. When properly controlled, these clusters can mitigate congestion, leading to shorter travel times, or even preventing congestion altogether. Two forms of the model were developed. The single-lane version simplifies the highway stretch by ignoring lane distinctions, focusing on controlling cluster speeds to smooth traffic flow and reduce congestion ahead. The multi-lane version extends this capability, incorporating lane-changing dynamics to allow clusters to block or influence specific lanes, enhancing control of HV traffic.

The promising results highlight the potential of this model, particularly when applied to real-time traffic control scenarios. Future works include testing more case studies of real highways and complicated traffic scenarios, while applying more complex control schemes to the clusters. CAV speeds would be determined using machine learning techniques to reduce congestion more effectively. Strategies might also consider the cluster to change lanes during

its trip, variable time gap between the CAVs and the optimal number of CAVs that form a cluster.

In line with the goals of this thesis, the subsequent chapter shifts focus to another promising sustainable solution in traffic systems: platooning. Specifically, it examines truck platooning, a concept with the potential to transform freight transportation by enabling groups of trucks to travel in tightly coordinated formations. The benefits of truck platooning are multifaceted, including reduced fuel consumption through aerodynamic drag reduction, lower greenhouse gas emissions, improved road utilization, and enhanced safety due to CACC. The chapter explores the complexities and innovations underpinning platooning, including the processes of platoon formation, control, and scheduling at both low and high levels. The importance of inter-carrier cooperation is highlighted, demonstrating its ability to maximize the economic and environmental benefits of platooning. Additionally, the chapter delves into the challenges and limitations of platooning, such as ensuring robust communication, managing platoon merging and splitting, addressing regulatory and infrastructure constraints, and securing broad adoption among carriers. The state-of-the-art research activities aimed at overcoming these obstacles are presented, showcasing innovative methodologies and technologies that pave the way for widespread implementation of this sustainable solution. The state-of-the-art literature also reveals a significant gap: limited consideration of real-time traffic conditions in platoon coordination. Unpredicted congestion can disrupt platoon schedules, reducing the overall efficiency of the system and diminishing stakeholder trust in its reliability.

To address this, the work presented in Chapter 3 integrates traffic predictions, derived using the METANET model detailed in Chapter 2, into the platoon coordination framework. This novel approach enhances the operational reliability of truck platooning, further demonstrating its viability as a sustainable solution in modern traffic systems. This work contributes to the field of platoon coordination by bridging strategic and tactical levels of planning through a centralized, off-board control scheme. The proposed approach re-plans coordination decisions made at the strategic level by incorporating real-time traffic predictions, an essential consideration given the impact of traffic conditions on high-level planning. By doing so, the method addresses situations where pre-defined platoon merging decisions may become suboptimal or unfeasible due to unforeseen traffic dynamics. Unlike

existing studies, this work defines platoon speed profiles online using a predictive control scheme. A central coordinator periodically forecasts traffic conditions along the platoons' routes, evaluates the feasibility and benefits of planned rendezvous points, and determines the optimal speeds to maintain schedule adherence. This study specifically focuses on the coordination of two platoons, predetermined to meet at a hub on their shared route. The inclusion of priority constraints, where one platoon (the "priority platoon") has strict time requirements, while the other (the "non-priority platoon") has greater flexibility, adds a practical dimension to the model.

By incorporating real-time traffic considerations and addressing practical constraints, this work highlights the importance of adaptability in platoon coordination and underscores the potential for predictive control to improve the reliability and efficiency of truck platooning systems. The results of a case study show that and open the door for future works that consider the presence of multiple platoons and meeting points, as well as equal priority levels of platoons.

Another essential element of sustainability is eco-driving, which is explored in Chapter 4, addressing its potential to significantly enhance energy efficiency and reduce emissions in modern transportation systems. Eco-driving strategies represent a critical shift toward more sustainable mobility, emphasizing the importance of optimizing driving behaviors and vehicle operations to minimize environmental impact. A comprehensive review of the literature highlights a wide range of techniques, innovations, and algorithms developed to improve fuel consumption efficiency, including GLOSA systems. Collectively, these approaches showcase the progress made in promoting more sustainable driving practices while underscoring the challenges that remain. Moreover, electric vehicles, with their lower environmental impact and energy-efficient design, represent a key component in sustainable mobility. The integration of EVs in mixed traffic scenarios presents new opportunities for reducing the carbon footprint and improving air quality, aligning with the broader goals of sustainability in the transportation sector. The discussion further delved into the significance of fuel and energy consumption models, which are crucial for evaluating and improving vehicle efficiency. These models provide the necessary framework to assess the impact of various driving strategies and technologies on energy consumption. In particular, this chapter detailed a consumption model specifically tailored for electric vehicles equipped with regenerative braking systems. This model

accounts for the unique energy recovery capabilities of regenerative braking, enabling a more accurate representation of energy usage and potential savings. The findings presented in this chapter emphasize the growing relevance of eco-driving in achieving sustainable transportation goals, demonstrating how advancements in modeling and technology can drive progress toward greener mobility solutions.

The work presented in Chapter 4 has successfully explored the optimization of the trajectory of an electric vehicle equipped with regenerative braking, focusing on minimizing energy consumption while transitioning from an initial state to a fixed final state, within fixed time horizons. The core of this research involved the formulation of an optimal control problem that minimizes energy consumption using the dynamic power-based model mentioned earlier. Despite the complexities in the energy consumption model, including discontinuities and non-smooth parts, a smoothened version was employed to derive a quasi-exact numerical solution using an efficient feasible direction algorithm. Furthermore, two simpler approximations were explored to assess their effectiveness in determining vehicle trajectories. The first approach utilized an analytical solution based on the Pontryagin's Maximum Principle with a quadratic approximation of the power-based model, while the second approach is based on the square-of-acceleration criterion. Both approaches demonstrated their potential for generating eco-driving control trajectories with remarkable accuracy. Additionally, the problem was extended to include a stop point, simulating a traffic signal along the EV's route. The solutions to this extended problem, incorporating new constraints based on fixed traffic light timings, further demonstrated the robustness of the proposed methodologies.

This outcome holds practical significance, suggesting that the proposed approach could be applied in GLOSA systems guiding EVs, contributing to improved energy efficiency and sustainability in real-world transportation systems. Future works would consider a free time horizon of the EV's trajectory and a stochastic switching time of the traffic light, which takes into account more real-life systems. Moreover, realistic traffic scenarios, like congestion, can be taken into consideration where the vehicles in front of the EV are slower and not following the recommended speed, so the EV's trajectory could be updated periodically using model predictive control.

Bibliography

[1] M. Abdolmaleki, M. Shahabi, Y. Yin, and N. Masoud. "Itinerary Planning for Cooperative Truck Platooning". In: *Transportation Research Part B: Methodological* (2021), pp. 91–110.

[2] International Energy Agency. Accessed: 2024-11-18. n.d. URL: https://www.iea.org/.

[3] K. Ahmed. "Modeling drivers' acceleration and lane-changing behavior". PhD thesis. Massachusetts Institute of Technology (MIT), 1999.

[4] C. Ngo et al. "Real-time eco-driving for connected electric vehicles". In: *IFAC-PapersOnLine*. Vol. 54. 10. 2021, pp. 126–131.

[5] M. Muratori et al. "The rise of electric vehicles—2020 status and future expectations". In: *Progress in Energy* 3 (2021).

[6] A. Alam, B. Besselink, V. Turri, J. Må rtensson, and K. H. Johansson. "Heavy-duty vehicle platooning for sustainable freight transportation: a cooperative method to enhance safety and efficiency". In: *IEEE Control Systems* 35 (2015), pp. 34–56.

[7] A. Alam, A. Gattami, and K. H. Johansson. "An Experimental Study on the Fuel Reduction Potential of Heavy Duty Vehicle Platooning". In: *IEEE Intelligent Transportation Systems*. 2010, pp. 119–124. DOI: \\10.1109/ITSC.2010.5625209.

[8] American Transportation Research Institute. *The Economic Costs of Congestion in the U.S.* Accessed: 2024-11-18. 2023. URL: https://trucking-research.org/2023/10/truckings-annual-congestion-costs-top-94-6-billion/.

[9] American Transportation Research Institute (ATRI). *Operational and Economic Considerations of Truck Platooning in the US*. Tech. rep. Available at: https://truckingresearch.org/. American Transportation Research Institute, 2020.

[10] E. Aria, J. Olstam, and C. Schwietering. "Investigation of Automated Vehicle Effects on the Capacity of a Highway Link Using Microscopic Traffic Simulation". In: *Transportation Research Procedia* 15 (2016), 761–770. DOI: 10.1016/j.trpro.2016.06.070.

[11] A. Aw and M. Rascle. "Resurrection of "Second Order" Models of Traffic Flow". In: *SIAM Journal on Applied Mathematics* 60.3 (2000), 916–938.

[12] J. Axelsson, T. Bergh, A. Johansson, B. Mårdberg, P. Svenson, and V. Åkesson. *Truck platooning business case analysis*. Sweden4Platooning. 2020.

[13] J. Barceló and J. L. Ferrer. *AIMSUN2: Advanced interactive microscopic simulator for urban networks, user's manual*. Rapport Technique. Universitat Politècnica de Catalunya, 1997.

[14] J. N. Barkenbus. "Eco-driving: An overlooked climate change initiative". In: *Energy Policy* 38.2 (2010), pp. 762–769.

[15] A. Bayuwindra, J. Ploeg, E. Lefeber, and H. Nijmeijer. "Combined longitudinal and lateral control of car-like vehicle platooning with extended look-ahead". In: *IEEE Transactions on Control Systems Technology* 28.3 (2019), pp. 790–803.

[16] A. L. C. Bazzan and F. Klügl. "Agent-Based Modeling and Simulation of Transportation Systems". In: *Autonomous Vehicles in Mixed Traffic*. Springer, 2013, pp. 463–487. DOI: 10.1007/978-3-642-35850-0_20.

[17] B. Besselink and K. H. Johansson. "String Stability and a Delay-Based Spacing Policy for Vehicle Platoons Subject to Disturbances". In: *IEEE Transactions on Automatic Control* 62.9 (2017), pp. 4376–4391.

[18] A. K. Bhoopalam, N. Agatz, and R. Zuidwijk. "Planning of truck platoons: A literature review and directions for future research". In: *Transportation Research Part B* 107 (2018), pp. 212–228.

[19] Sneha S. Bhurse and A.A. Bhole. "A Review of Regenerative Braking in Electric Vehicles". In: *2018 International Conference on Computation of Power, Energy, Information and Communication (ICCPEIC)*. 2018, pp. 363–367. DOI: 10.1109/ICCPEIC.2018.8525157.

[20] O. Biham, A. A. Middleton, and D. Levine. "Self-organization and a dynamical transition in traffic-flow models". In: *Physical Review A* 46.10 (1992), R6124–R6127. DOI: 10.1103/PhysRevA.46.R6124.

[21] K. Biswas, S. Kumar, S. Banerjee, and A. K. Pandey. "SMU: Smooth activation function for deep networks using smoothing maximum technique". In: *ArXiv* (2021).

[22] A. Boretti. "Comparison of regenerative braking efficiencies of MY2012 and MY2013 nissan Leaf". In: *Int J Eng Technol Innovat* (2016).

[23] A. Bozzi, S. Graffione, C. Pasquale, R. Sacile, S. Sacone, and S. Siri. "A hierarchical control scheme to improve the travel performance of

truck platoons in freeways". In: *Proc. of the ITSC 2022, 25st International Conference on Intelligent Transportation Systems*. 2022, pp. 2063–2068.

[24] M. Brackstone and M. McDonald. "Car-following: a historical review". In: *Transportation Research Part F: Traffic Psychology and Behaviour* 2.4 (1999), pp. 181–196. DOI: 10.1016/S1369-8478(99)00022-7.

[25] F. Browand, J. McArthur, and C. Radovich. *Fuel saving achieved in the field test of two tandem trucks*. Tech. rep. Tech. Rep. UCB-ITS-PRR-2004-20. University of Southern California, Berkeley, CA, USA, 2004.

[26] C. Caballini, S. Sacone, and M. Saeednia. "Cooperation among truck carriers in seaport containerized transportation". In: *Transportation Research Part E* 93 (2016), pp. 38–56.

[27] S. C. Calvert and B. Van Arem. "Cooperative adaptive cruise control and intelligent traffic signal interaction: a field operational test with platooning on a suburban arterial in real traffic". In: *Transportation Research Part C: Emerging Technologies* 120 (2020), p. 102781. DOI: 10.1016/j.trc.2020.102781.

[28] G. Cameron, B. J. N. Wylie, and D. McArthur. "PARAMICS: Moving vehicles on the connection machine". In: *Proceedings of the 1994 ACM/IEEE Conference on Supercomputing*. 1994, pp. 291–300. DOI: \\ 10.1109/SUPERC.1994.336209.

[29] R. C. Carlson, Ioannis Papamichail, Markos Papageorgiou, and Andreas Messmer. "Optimal dynamic speed limits for motorway traffic control". In: *Transportation Research Part C: Emerging Technologies* 18.5 (2010), pp. 584–594.

[30] M. J. Cassidy and J. P. Windover. "Methodology for assessing dynamics of freeway traffic flow". In: *Transportation Research Part A: Policy and Practice* 28.4 (1994), pp. 273–285. DOI: 10.1016/0965-8564(94)90001-3.

[31] T. Chaanine, A. Ferrando, C. Pasquale, V. P. Pastore, M. Sadeghi Garjan, and S. Siri. "A Control-Oriented Highway Traffic Model with Multiple Clusters of CAVs". In: *2023 IEEE 26th International Conference on Intelligent Transportation Systems (ITSC)*. 2023, pp. 5198–5203. DOI: 10.1109/ITSC57777.2023.10421830.

[32] T. Chaanine, C. Pasquale, S. Siri, and S. Sacone. "Real-Time Planning of Platoons Coordination Decisions Based on Traffic Prediction". In: *2024 European Control Conference (ECC)*. 2024, pp. 1423–1428. DOI: 10.23919/ECC64448.2024.10591111.

[33] T. Chaanine, S. Siri, C. Pasquale, P. Typaldos, M. Papageorgiou, and I. Papamichail. *Optimal Control Methodologies for Eco-Driving of Electric Vehicles with Regenerative Braking*. Preprint, accessed 2025-01-06. 2024. DOI: 10.2139/ssrn.5015302. URL: https://papers.ssrn.com/sol3/papers.cfm?abstract_id=5015302.

[34] R. E. Chandler, R. Herman, and E. W. Montroll. "Traffic dynamics: Studies in car following". In: *Operations Research* 6.2 (1958), pp. 165–184. DOI: 10.1287/opre.6.2.165.

[35] D. Chen, S. Ahn, M. Chitturi, and Z. Zheng. "Optimal Control of Automated Vehicles at Intersections: Theory and Experiments". In: *Transportation Research Part C: Emerging Technologies* 82 (2017), pp. 161–179. DOI: 10.1016/j.trc.2017.06.008.

[36] B. Chopard and M. Droz. *Cellular Automata Modeling of Physical Systems*. Cambridge University Press, 1998.

[37] International Council on Clean Transportation. *A Global Comparison of the Life-Cycle Greenhouse Gas Emissions of Combustion Engine and Electric Passenger Cars*. Accessed: 2024-11-18. 2021. URL: https://theicct.org/publication/a-global-comparison-of-the-life-cycle-greenhouse-gas-emissions-of-combustion-engine-and-electric-passenger-cars/.

[38] C. F. Daganzo. "A finite difference approximation of the kinematic wave model of traffic flow". In: *Transportation Research Part B: Methodological* 28.4 (1994), pp. 269–287. DOI: 10.1016/0191-2615(94)90002-X.

[39] C. F. Daganzo. "The cell transmission model: A dynamic representation of highway traffic consistent with the hydrodynamic theory". In: *Transportation Research Part B: Methodological* 28.4 (1994), 269–287.

[40] C. F. Daganzo. "The Cell Transmission Model, Part II: Network Traffic". In: *Transportation Research Part B* 29.2 (1995), pp. 79–93. DOI: 10.1016/0191-2615(94)00022-R.

[41] Z. Deng, K. Yang, W. Shen, and Y. Shi. "Cooperative Platoon Formation of Connected and Autonomous Vehicles: Toward Efficient Merging Coordination at Unsignalized Intersections". In: *IEEE Transactions on Vehicular Technology* 72.8 (2023), pp. 9355–9366. DOI: 10.1109/TVT.2023.3269653.

[42] J. Devore. *A modern introduction to probability and statistics: understanding why and how*. Vol. 101. 473. 2012, pp. 393–394.

[43] R. A. Dollar, A. Vahidi, B. Pattel, and H. Borhan. "A linear programming formulation for eco-driving over road slopes". In: *Automatica* 161 (2024).

[44] European Truck Platooning Challenge (ETPC). *Truck Platooning: A Practical Perspective*. Tech. rep. Available at: https://www.eutruck - platooning.com/. European Commission, 2017.

[45] F. Farokhi, K. Liang, and K.H. Johansson. "Cooperation Patterns between Fleet Owners for Transport Assignments". In: *2015 IEEE Conference on Control Applications (CCA)*. 2015.

[46] F. Farokhi et al. "Cooperation Patterns between Fleet Owners for Transport Assignments". In: *IEEE Conference on Control Applications (CCA)*. 2015, pp. 423–428. DOI: 10.1109/CCA.2015.7320705.

[47] F. Farokhi et al. "Private and secure coordination of match-making for heavy-duty vehicle platooning". In: *IFAC Proceedings*. 2017, pp. 232–239. DOI: 10.1016/j.ifacol.2017.10.067.

[48] M. Fellendorf and P. Vortisch. "Microscopic Traffic Flow Simulator VISSIM". In: *Fundamentals of Traffic Simulation*. Ed. by Jaime Barceló. Vol. 145. International Series in Operations Research Management Science. New York, NY: Springer, 2010, pp. 63–93.

[49] S. Feng, Y. Zhang, S. E. Li, Z. Cao, H. X. Liu, and L. Li. "String stability for vehicular platoon control: Definitions and analysis methods". In: *Annual Reviews in Control* 47 (2019), pp. 81–97.

[50] C. Fiori, K. Ahn, and H. A. Rakha. "Power-based electric vehicle energy consumption model: Model development and validation". In: *Applied Energy* 168 (2016), pp. 257–268.

[51] H. Fritz, A. Gern, H. Schiemenz, and C. Bonnet. "CHAUFFEUR Assistant: a driver assistance system for commercial vehicles based on fusion of advanced ACC and lane keeping". In: *IEEE Intelligent Vehicles Symposium*. 2004, pp. 495–500. DOI: 10.1109/IVS.2004.1336532.

[52] M. Fukui and Y. Ishibashi. "Traffic flow in 1D cellular automaton model including cars moving with high speed". In: *Journal of the Physical Society of Japan* 65.6 (1996), pp. 1868–1870. DOI: 10.1143/JPSJ.65.1868.

[53] Y. Gao, L. Chu, and M. Ehsani. "Design and control principles of hybrid braking system for EV, HEV and FCV". In: *IEEE Vehicle Power and Propulsion Conference*. 2007.

[54] D. C. Gazis. "The origins of traffic theory". In: *Operations Research* 50.1 (2002), pp. 69–77. DOI: 10.1287/opre.50.1.69.15189.

[55] D. C. Gazis, R. Herman, and R. W. Rothery. "Nonlinear follow-the-leader models of traffic flow". In: *Operations Research* 9.4 (1961), 545–567. DOI: 10.1287/opre.9.4.545.

[56] A. Ghosal, S.U. Sagong, S. Halder, K. Sahabandu, M. Conti, R. Poovendran, and L. Bushnell. "Truck platoon security: State-of-the-art and road ahead". In: *Computer Networks* (2021).

[57] P. G. Gipps. "A behavioural car-following model for computer simulation". In: *Transportation Research Part B: Methodological* 15.2 (1981), pp. 105–111. DOI: 10.1016/0191-2615(81)90037-X.

[58] P. G. Gipps. "A model for the structure of lane-changing decisions". In: *Transportation Research Part B: Methodological* 20.5 (1986), pp. 403–414. DOI: 10.1016/0191-2615(86)90026-4.

[59] A. Gühnemann, P. Wagner, and N. Eissfeldt. "Intelligent transport management by integrated dynamic traffic simulation and impact assessment". In: *Proceedings of the International Conference on Transportation and Traffic Engineering*. 2001, Page range.

[60] J. Han, A. Vahidi, and A. Sciarretta. "Fundamentals of energy efficient driving for combustion engine and electric vehicles: An optimal control perspective". In: *Automatica* 103 (2019), pp. 558–572.

[61] A. Hegyi, B. De Schutter, and H. Hellendoorn. "Model predictive control for optimal coordination of ramp metering and variable speed limits". In: *Transportation Research Part C: Emerging Technologies* 13.3 (2005), pp. 185–209.

[62] W. Helly. "Simulation of traffic flow". In: *Transportation Science* 3.1 (1959), pp. 1–26. DOI: 10.1287/trsc.3.1.1.

[63] S. van de Hoef, K. H. Johansson, and D. V. Dimarogonas. "Fuel-efficient en route formation of truck platoons". In: *IEEE Transactions on Intelligent Transportation Systems* 19 (2018), pp. 102–112.

[64] S. van de Hoef, K.H. Johansson, and D.V. Dimarogonas. "Fuel-Optimal Centralized Coordination of Truck Platooning Based on Shortest Paths". In: *American Control Conference (ACC)*. 2015.

[65] S. van de Hoef, J. Må rtensson, D. V. Dimarogonas, and K. H. Johansson. "A predictive framework for dynamic heavy-duty vehicle platoon coordination". In: *ACM Transactions on Cyber-Physical Systems* 4.1 (2019), pp. 1–25.

[66] S. Hong, A. A. Malikopoulos, J. Lee, and B. B. Park. "Development and evaluation of speed harmonization using optimal control theory:

A simulation-based case study at a speed reduction zone 2". In: *Proc. 96th Annu. Meeting Transp. Res. Board (TRB)*. 2017.

[67] S. P. Hoogendoorn. "Multiclass continuum modelling of multilane traffic flow". PhD thesis. Delft University of Technology, 1999.

[68] S. P. Hoogendoorn and P. H. Bovy. "State-of-the-art of vehicular traffic flow modelling". In: *Proceedings of the Institution of Mechanical Engineers, Part I: Journal of Systems and Control Engineering* 215.4 (2001), pp. 283–303. DOI: 10.1243/09596510175026959 7.

[69] J. Hooker. "Optimal driving for single-vehicle fuel economy". In: *Transp. Res. A, Gen.* 22.3 (1988), pp. 183–201.

[70] INRIX. *2018 U.S. Traffic Scorecard*. Accessed: 2024-11-18. 2018. URL: https://inrix.com/press-releases/scorecard-2018-us/.

[71] Y. Jiang, H. Cong, H. Chen, and Z. Yao. "Safety evaluation for mixed traffic flow of CAVs with different automation and connection levels". In: *Expert Systems with Applications* 261 (2025), p. 125561. ISSN: 0957-4174. DOI: https://doi.org/10.1016/j.eswa.2024.125561. URL: https://www.sciencedirect.com/science/article/pii/S095741742402428X.

[72] Wen-Long Jin. "A kinematic wave theory of multi-commodity network traffic flow". In: *Transportation Research Part B: Methodological* 46.8 (2012), pp. 1000–1022. ISSN: 0191-2615. DOI: https://doi.org/10.1016/j.trb.2012.02.009. URL: https://www.sciencedirect.com/science/article/pii/S0191261512000343.

[73] A. Johansson, T. Bai, K. H. Johansson, and J. Må rtensson. "Platoon Cooperation Across Carriers: From System Architecture to Coordination". In: *IEEE Intelligent Transportation Systems Magazine* (2022).

[74] A. Johansson, E. Nekouei, K. H. Johansson, and J. Må rtensson . "Strategic hub-based platoon coordination under uncertain travel times". In: *IEEE Transactions on Intelligent Transportation Systems* 23.7 (2021), pp. 8277–8287.

[75] R. K. Kamalanathsharma and H. A. Rakha. "Multi-stage dynamic programming algorithm for eco-speed control at traffic signalized intersections". In: *Proc. 16th Int. IEEE Conf. Intell. Transp. Syst. (ITSC)*. 2013, pp. 2094–2099.

[76] B. S. Kerner and P. Konhäuser. "Cluster effect in initially homogeneous traffic flow". In: *Physical Review E* 48.4 (1993), R2335–R2338. DOI: 10.1103/PhysRevE.48.R2335.

[77] A. Kesting and M. Treiber. "How Reaction Time, Update Time, and Adaptation Time Influence the Stability of Traffic Flow". In: *Computer-Aided Civil and Infrastructure Engineering* 23.2 (2008), pp. 125–137. DOI: 10.1111/j.1467-8667.2007.00537.x.

[78] A. Kesting, M. Treiber, and D. Helbing. "General Lane-Changing Model MOBIL for Car-Following Models". In: *Transportation Research Record: Journal of the Transportation Research Board* 1999.1 (2007), pp. 86–94.

[79] A. Kotsialos, M. Papageorgiou, C. Diakaki, Y. Pavlis, and F. Middelham. "Traffic flow modeling of large-scale motorway networks using the macroscopic modeling tool METANET". In: *IEEE Transactions on Intelligent Transportation Systems* 3.4 (2002), pp. 282–292.

[80] D. Krajzewicz, J. Erdmann, M. Behrisch, and L. Bieker. "Recent Development and Applications of SUMO - Simulation of Urban MObility". In: *International Journal on Advances in Systems and Measurements* 5.3&4 (2012), pp. 128–138.

[81] M. Lammert, A. Duran, J. Diaz, K. Burton, and A. Nicholson. "Effect of Platooning on Fuel Consumption of Class 8 Vehicles Over a Range of Speeds, Following Distances, and Mass". In: *SAE 2014 Commercial Vehicle Engineering Congress (COMVEC)*. 2014. DOI: 10.4271/2014-01-2451.

[82] R. Larsen, J. Rich, and T. K. Rasmussen. "Hub-based truck platooning: Potentials and profitability". In: *Transportation Research Part E* (2019), pp. 249–264.

[83] E. Larsson, G. Sennton, and J. Larson. "The Vehicle Platooning Problem: Computational Complexity and Heuristics". In: *Transportation Research Part C: Emerging Technologies* 60 (2015), pp. 258–277. DOI: 10.1016/j.trc.2015.08.003.

[84] J. Li, A. Fotouhi, W. Pan, Y. Liu, Y. Zhang, and Z. Chen. "Deep reinforcement learning-based eco-driving control for connected electric vehicles at signalized intersections considering traffic uncertainties". In: *Energy* 279 (2023).

[85] Kun Li and P. Ioannou. "Modeling of traffic flow of automated vehicles". In: *IEEE Transactions on Intelligent Transportation Systems* 5.2 (2004), pp. 99–113. DOI: 10.1109/TITS.2004.828170.

[86] K. Liang, J. Mårtensson, and K.H. Johansson. "Heavy-Duty Vehicle Platoon Formation for Fuel Efficiency". In: *IEEE Transactions on Intelligent Transportation Systems* 17 (2016), pp. 1051–1061.

[87] K.-Y. Liang, S. van de Hoef, H. Terelius, V. Turri, B. Besselink, J. Må rtensson, and K.H. Johansson. "Networked control challenges in collaborative road freight transport". In: *European Journal of Control* 30 (2016), pp. 2–14.

[88] M. J. Lighthill and G. B. Whitham. "On kinematic waves II. A theory of traffic flow on long crowded roads". In: *Proceedings of the Royal Society of London. Series A* 229.1178 (1955), pp. 317–345.

[89] P. A. Lopez, M. Behrisch, L. Bieker-Walz, J. Erdmann, D. Krajzewicz, P. Wagner, and E. Wießner. "Microscopic Traffic Simulation using SUMO". In: *2018 21st International Conference on Intelligent Transportation Systems (ITSC)*. IEEE, 2018, pp. 2575–2582. DOI: 10.1109/ITSC.2018.8569938.

[90] B. Luin, S. Petelin, and F. Al-Mansour. "Microsimulation of electric vehicle energy consumption". In: *Energy* 174 (2019), pp. 24–32.

[91] A. A. Malikopoulos, C. G. Cassandras, and Y. J. Zhang. "A decentralized energy-optimal control framework for connected automated vehicles at signal-free intersections". In: *Automatica* 93 (2018), pp. 244–256.

[92] V. Marzano, F. Tinessa, C. Fiori, D. Tocchi, A. Papola, D. Aponte, E. Cascetta, and F. Simonelli. "Impacts of truck platooning on the multimodal freight transport market: An exploratory assessment on a case study in Italy". In: *Transportation Research Part A* 163 (2022), pp. 100–125.

[93] H. R. Mehrabani, C. C. Chen, and W. Y. Szeto. "Mesoscopic Traffic Assignment Model for Mixed Traffic with Connected Autonomous and Human-Driven Vehicles". In: *Transportation Research Part C: Emerging Technologies* 145 (2023), p. 103853.

[94] F. Mensing, R. Trigui, and E. Bideaux. "Vehicle trajectory optimization for application in eco-driving". In: *Proc. IEEE Vehicle Power Propuls. Conf. (VPPC)*. 2011, pp. 1–6.

[95] A. Messmer and M. Papageorgiou. "METANET: A macroscopic simulation program for motorway networks". In: *Proceedings of the 1990 IEEE International Conference on Systems, Man, and Cybernetics*. IEEE. 1990, pp. 390–395.

[96] J. Van Mierlo, G. Maggetto, E. Van De Burgwal, and R. Gense. "Driving style and traffic measures-influence on vehicle emissions and fuel consumption". In: *Proc. Inst. Mech. Eng. D, J. Automobile Eng.* 218.1 (2004), pp. 43–50.

[97] V. Milanés and S. E. Shladover. "Modeling cooperative and autonomous adaptive cruise control dynamic responses using experimental data". In: *Transportation Research Part C: Emerging Technologies* 43 (2014),
42–54. DOI: 10.1016/j.trc.2014.01.003.

[98] Clarity Air Monitor. *A Deep Dive into the Economic Impacts of Air Pollution*. Accessed: 2024-11-18. 2023. URL: https://www.clarity.io/blog/a-deep-dive-economic-impacts-of-air-pollution.

[99] M. M. Morando, Q. Tian, L. T. Truong, and H. L. Vu. "Studying the Safety Impact of Autonomous Vehicles Using Simulation-Based Surrogate Safety Measures". In: *Journal of Advanced Transportation* 2018 (2018), pp. 1–11. DOI: 10.1155/2018/6135183.

[100] K. Nagel and M. Schreckenberg. "A cellular automaton model for freeway traffic". In: *Journal de Physique I* 2.12 (1992), pp. 2221–2229. DOI: 10.1051/jp1:1992163.

[101] G. F. Newell. "A simplified car-following theory: a lower order model". In: *Transportation Research Part B: Methodological* 36.3 (2022), pp. 195–205. DOI: 10.1287/opre.9.2.209.

[102] G. F. Newell. "Nonlinear effects in the dynamics of car following". In: *Operations Research* 9.2 (1961), pp. 209–229. DOI: 10.1287/opre.9.2.209.

[103] Z. Nie and H. Farzaneh. "Real-time dynamic predictive cruise control for enhancing eco-driving of electric vehicles, considering traffic constraints and signal phase and timing (SPaT) information, using artificial-neural-network-based energy consumption model". In: *Energy* 241
(2022).

[104] I. A. Ntousakis, I. K. Nikolos, and M. Papageorgiou. "Optimal vehicle trajectory planning in the context of cooperative merging on highways". In: *Transp. Res. C, Emerg. Technol.* 71 (2016), pp. 464–488.

[105] H. Zhang K. Bian P. Wang B. Di and L. Song. "Joint Platoon Formation and Resource Allocation for Connected Vehicles by Cellular V2X

Communication". In: *2019 IEEE International Conference on Communications (ICC)*. IEEE, 2019, pp. 1–6. DOI: 10.1109/GLOBECOM38437.2019.9013613. URL: https://ieeexplore.ieee.org/document/8761878.

[106] S. Pan, D. Trentesaux, E. Ballot, and G. Q. Huang. "Horizontal collaborative transport: survey of solutions and practical implementation issues". In: *International Journal of Production Research* 57.15–16 (2019), pp. 5340–5361.

[107] M. Papageorgiou and A. Kotsialos. "Freeway ramp metering: an overview". In: *IEEE Transactions on Intelligent Transportation Systems* (2002), pp. 271–281. DOI: 10.1109/TITS.2002.1010174.

[108] M. Papageorgiou, A. Kotsialos, and J. Tsitsiklis. "Traffic Flow Modeling and Control: A Review". In: *Transportation Research Part C: Emerging Technologies* 11.5-6 (2003), pp. 223–240. DOI: \\10.1016/S0968-090X(03)00024-5.

[109] M. Papageorgiou, M. Leibold, and M. Buss. *Optimierung*. Berlin, Germany: Springer, 1991.

[110] M. Papageorgiou, M. Marinaki, P. Typaldos, and K. Makantasis. *A feasible direction algorithm for the numerical solution of optimal control problems–extended version*. Tech. rep. Tech. Univ. Crete, Dyn. Syst. Simul. Lab., Chania, Greece, 2016.

[111] C. Pasquale, S. Sacone, S. Siri, and A. Ferrara. "A New Micro-Macro METANET Model for Platoon Control in Freeway Traffic Networks". In: *Proceedings of the 21st IEEE Intelligent Transportation Systems Conference (ITSC)*. IEEE, 2018, pp. 1481–1486.

[112] C. Pasquale, S. Sacone, S. Siri, and A. Ferrara. "A new Micro-Macro METANET model for platoon control in freeway traffic networks". In: *Proc. of the 21th IEEE Intelligent Transportation Systems Conference*. 2018, pp. 1481–1486.

[113] H. J. Payne. "Models of Freeway Traffic and Control". In: *Mathematical Models of Public Systems* 1 (1971), pp. 51–61.

[114] G. Piacentini, C. Pasquale, S. Sacone, S. Siri, and A. Ferrara. "Multiple Moving Bottlenecks for Traffic Control in Freeway Systems". In: *2019 18th European Control Conference (ECC)*. Napoli, Italy: IEEE, 2019, pp. 2623–2628.

[115] L. A. Pipes. "An operational analysis of traffic dynamics". In: *Journal of Applied Physics* 24.3 (1953), pp. 274–281. DOI: 10.1063/1.1721475.

[116] *Platooning together*. ENSEMBLE Project. Available: https://platooningensemble.eu/.

[117] L. S. Pontryagin. *Mathematical Theory of Optimal Processes*. Boca Raton, FL, USA: CRC Press, 1987.

[118] Y. Qin and H. Wang. "Cell Transmission Model for Mixed Traffic Flow with Connected and Autonomous Vehicles". In: *Journal of Transportation Engineering Part A: Systems* 145 (May 2019). DOI: 10.1061/JTEPBS.0000238.

[119] M. Rahman M.and Chowdhury, Y. Xie, and Y. He. "Review of Microscopic Traffic Simulation Models and Software Tools for Connected and Automated Vehicle Research". In: *IEEE Intelligent Transportation Systems Magazine* 11.4 (2019), pp. 19–32. DOI: 10.1109/MITS.2019.2930512.

[120] R. Ramakers, K. Henning, S. Gies, D. Abel, and H. M. Max. "Electronically coupled truck platoons on German highways". In: *IEEE International Conference on Systems, Man and Cybernetics*. 2009, pp. 2409–2414. DOI: 10.1109/ICSMC.2009.5346135.

[121] A. Reuschel. "Vehicle movements in a platoon". In: *Oesterreichisches Ingenieur-Archiv* 4 (1950), pp. 193–215.

[122] P. I. Richards. "Shock Waves on the Highway". In: *Operations Research* 4.1 (1956), pp. 42–51.

[123] C. Roncoli, M. Papageorgiou, and I. Papamichail. "Traffic Flow Optimisation in Presence of Vehicle Automation and Communication Systems – Part I: A First-Order Multi-Lane Model for Motorway Traffic". In: *Transportation Research Part C: Emerging Technologies* 57 (2015), pp. 241–259. DOI: 10.1016/j.trc.2015.05.017.

[124] S. Sacone, C. Pasquale, S. Siri, and A. Ferrara. "Centralized and Decentralized Schemes for Platoon Control in Freeway Traffic Systems". In: *60th IEEE Conference on Decision and Control (CDC)*. Austin, USA: IEEE, 2021, pp. 2665–2670.

[125] M. Sadeghi Garjan, T. Chaanine, C. Pasquale, V. Paolo Pastore, and A. Ferrando. "AGAMAS: A New Agent-Oriented Traffic Simulation Framework for SUMO". In: *Multi-Agent Systems*. Springer Nature Switzerland, 2023, pp. 396–405. ISBN: 978-3-031-43264-4.

[126] SAE International. *Taxonomy and Definitions for Terms Related to On-Road Motor Vehicle Automated Driving Systems*. https://www.sae.org/-standards/content/j3016_202104/. Accessed: 2024-11-18. 2021.

[127] W. Schakel, V. Knoop, and B. Van Arem. "Integrated lane change model with relaxation and synchronization". In: *Transportation Research Record* 2316.1 (2012), pp. 47–57. DOI: 10.3141/2316-06.

[128] J. Schindler, M. Löchl, B. Ciuffo, and F. Viti. "Modelling Driver Behaviour and Traffic Performance in Mixed Traffic Conditions with SUMO". In: *2018 21st International Conference on Intelligent Transportation Systems (ITSC)*. IEEE, 2018, pp. 3937–3942. DOI: 10.1109/ITSC.2018.8569931.

[129] Steven E. Shladover et al. "Benefits and challenges of automated vehicle platooning". In: *Transportation Research Record* 2672.1 (2018), pp. 1–11. DOI: 10.1177/0361198118758613.

[130] F. Shokouhi and A. H. Davaie Markazi. "A new continuous approximation of sign function for sliding mode control". In: *International Conference on Robotics and Mechantronics (ICRoM)*. Tehran, Iran, 2018.

[131] L. Simchon and R. Rabinovici. "Real-Time Implementation of Green Light Optimal Speed Advisory for Electric Vehicles". In: *Vehicles* 2.1 (2020), pp. 35–54.

[132] Abhinav Srivastava, W.-L. Jin, and J.-P. Lebacque. "A Modified Cell Transmission Model with Realistic Queue Discharge Features at Signalized Intersections". In: *Transportation Research Part B: Methodological* 81.P1 (2015), pp. 302–315. DOI: 10.1016/j.trb.2015.05.013.

[133] R. Stahlmann, M. Möller, A. Brauer, R. German, and D. Eckhoff. "Technical evaluation of glosa systems and results from the field". In: *Proc. IEEE Veh. Netw. Conf. (VNC)*. 2016, pp. 1–8.

[134] A. Stevanovic, J. Stevanovic, and C. Kergaye. "Green Light Optimized Speed Advisory Systems: Impact of Signal Phasing Information Accuracy". In: *Transportation Research Record* 2390.1 (2013), pp. 53–59.

[135] A. Sumalee T. Pan W. H. K. Lam and R. Zhong. "Multiclass multilane model for freeway traffic mixed with connected automated vehicles and regular human-piloted vehicles". In: *Transportmetrica A: Transport Science* 17.1 (2021), pp. 5–33. DOI: 10.1080/23249935.2019.1573858. eprint: https://doi.org/10.1080/23249935.2019.1573858. URL: https://doi.org/10.1080/23249935.2019.1573858.

[136] F. Tajdari, C. Roncoli, and M. Papageorgiou. "Feedback-Based Ramp Metering and Lane-Changing Control With Connected and Automated Vehicles". In: *IEEE Transactions on Intelligent Transportation Systems* 23.2 (2022), pp. 939–951.

[137] A. Talebpour and H. S. Mahmassani. "Influence of Connected and Autonomous Vehicles on Traffic Flow Stability and Throughput". In: *Transportation Research Part C: Emerging Technologies* 71 (2016), pp. 143–163. DOI: 10.1016/j.trc.2016.07.007.

[138] S. Taylor, F. Ahmad, H. Nguyen, S. Shaikh, D. Evans, and D. Price. "Vehicular Platoon Communication: Cybersecurity Threats and Open Challenges". In: *51st Annual IEEE/IFIP International Conference on Dependable Systems and Networks Workshops (DSN-W)*. 2021.

[139] The SUMO Team. *SUMO - Simulation of Urban MObility*. https://www.eclipse.org/sumo/. Accessed: 2024-11-18. 2024.

[140] M. Treiber, A. Hennecke, and D. Helbing. "Congested Traffic States in Empirical Observations and Microscopic Simulations". In: *Physical Review E* 62.2 (2000), pp. 1805–1824.

[141] M. Treiber and A. Kesting. *Traffic Flow Dynamics: Data, Models and Simulation*. Springer, 2013. ISBN: 978-3-642-31939-3.

[142] M. Treiber, A. Kesting, and D. Helbing. "Delays, inaccuracies and anticipation in microscopic traffic models". In: *Physica A: Statistical Mechanics and its Applications* 360.1 (2006), pp. 71–88. DOI: 10.1016/j.physa.2005.07.066.

[143] P. Typaldos, I. Papamichail, and M. Papageorgiou. "Minimization of fuel consumption for vehicle trajectories". In: *IEEE Transactions on Intelligent Transportation Systems* 21.4 (2020), pp. 1716–1727.

[144] UPI News. *Study: Boston, D.C., Chicago worst U.S. cities for traffic congestion*. Accessed: 2024-11-18. 2019. URL: https://www.upi.com/Top_News/US/2019/02/12/Study-Boston-DC-Chicago-worst-US-cities-for-traffic-congestion/7251549987226/.

[145] M. Van Aerde and H. Rakha. "Multivariate Calibration of Single-Regime Speed-Flow-Density Relationships". In: *Proceedings of the 6th Vehicle Navigation and Information Systems Conference*. 1995, Page range.

[146] B. Van Arem, J. Hogema, and M. Vanderschuren. *An assessment of the impact of Autonomous Intelligent Cruise Control*. Tech. rep. Report Number (if available). Institution Name, 1995.

[147] R. Wiedemann. *Simulation of Road Traffic Flow*. Karlsruhe, Germany: Technical University Karlsruhe, 1974.

[148] Y. Wu, Y. Lin, R. Hu, Z. Wang, B. Zhao, and Z. Yao. "Modeling and Simulation of Traffic Congestion for Mixed Traffic Flow with Connected Automated Vehicles: A Cell Transmission Model Approach". In: *Journal of Advanced Transportation* 2022.1 (2022), p. 8348726. DOI:

https://doi.org/10.1155/2022/8348726. eprint: https://onlinelibrary.wiley.com/doi/pdf/10.1155/2022/8348726. URL: https://onlinelibrary.wiley.com/doi/abs/10.1155/2022/8348726.

[149] S. Xu, K. Deng, S. E. Li, S. Li, and B. Cheng. "Legendre pseudospectral computation of optimal speed profiles for vehicle eco-driving system". In: *Proc. IEEE Intell. Vehicles Symp.* 2014, pp. 1103–1108.

[150] J. Yan, M. Xiong, and L. Zhang. "A Cooperative Control Strategy of Connected and Autonomous Vehicles in Ramp Merging Areas with Mixed-Autonomy Traffic". In: *2021 IEEE Conference on Telecommunications, Optics and Computer Science (TOCS)*. Shenyang, China: IEEE, 2021, pp. 214–218.

[151] H. Yang, H. Rakha, and M. V. Ala. "Eco-cooperative adaptive cruise control at signalized intersections considering queue effects". In: *IEEE Trans. Intell. Transp. Syst.* 18.6 (2016), pp. 1575–1585.

[152] Z. Yang, Yiheng Feng, and Henry X. L. "A cooperative driving framework for urban arterials in mixed traffic conditions". In: *Transportation Research Part C: Emerging Technologies* 124 (2021), p. 102905. DOI: 10.1016/j.trc.2020.102905.

[153] L. Ye and T. Yamamoto. "Evaluating the impact of connected and autonomous vehicles on traffic safety". In: *Physica A: Statistical Mechanics and its Applications* 526 (2019), p. 121145. DOI: 10.1016/j.physa.2019.121145.

[154] K. Yeom. "Model predictive control and deep reinforcement learning based energy efficient eco-driving for battery electric vehicles". In: *Energy Reports* 8.12 (2022), pp. 34–42.

[155] H. Zhai, H. C. Frey, and N. M. Rouphail. "A vehicle-specific power approach to speed and facility-specific emissions estimates for diesel transit buses". In: *Environ. Sci. Technol.* (2008).

[156] H. M. Zhang. "A non-equilibrium traffic model devoid of gas-like behavior". In: *Transportation Research Part B: Methodological* 36.3 (2002), pp. 375–380. DOI: 10.1016/S0191-2615(01)00081-2.

[157] H. M. Zhang. "A theory of nonequilibrium traffic flow". In: *Transportation Research Part B: Methodological* 36.3 (2002), pp. 275–292. DOI: 10.1016/S0191-2615(01)00069-3.

[158] J. Zhang, Y. Yuan, C. Lv, and Y. Li. "Modeling and analysis of regenerative braking system for electric vehicle based on AMESim". In: *2015 IEEE International Conference on Mechatronics and Automation (ICMA)*. 2015, pp. 1307–1312. DOI: 10.1109/ICMA.2015.7237674.

[159] S. Zhang, S. Zhu, W. Zhuang, Y. Zhang, and K. Yang. "SFO: An Adaptive Task Scheduling Based on Incentive Fleet Formation and Metrizable Resource Orchestration for Autonomous Vehicle Platooning". In: *IEEE Transactions on Intelligent Transportation Systems* 24.4 (2023), 1221–1233. DOI: 10.1109/TITS.2023.3272569. URL: https://ieeexplore.ieee.org/document/10330714.

[160] Z. Zhang, Y. Zou, X. Zhang, and T. Zhang. "Green Light Optimal Speed Advisory System Designed for Electric Vehicles Considering Queuing Effect and Driver's Speed Tracking Error". In: *IEEE Access* 8 (2020), pp. 208796–208808.

[161] M. Zhou, X. Qu, and S. Jin. "On the Impact of Cooperative Autonomous Vehicles in Improving Freeway Merging: A Modified Intelligent Driver Model-Based Approach". In: *IEEE Transactions on Intelligent Transportation Systems* 18.6 (2017), pp. 1422–1428. DOI: 10.1109/TITS.2016.2606496.

[162] Y. Zhu, Z. Xu, Y. Zhang, X. Wu, and Z. Li. "Dynamic Event-Triggered Scheduling and Platooning Control Co-Design for Automated Vehicles Over Vehicular Ad-Hoc Networks". In: *IEEE Transactions on Vehicular Technology* 70.11 (2021), pp. 11545–11556. DOI: 10.1109/TVT.2021.3053484.